NASA Technical Memorandum 4112

Static Internal Performance of Convergent Single-Expansion-Ramp Nozzles With Various Combinations of Internal Geometric Parameters

E. Ann Bare and Francis J. Capone
Langley Research Center
Hampton, Virginia

National Aeronautics and
Space Administration
Office of Management
Scientific and Technical
Information Division

1989

Summary

An investigation has been conducted in the static test facility of the Langley 16-Foot Transonic Tunnel to determine the effects of five geometric design parameters on the internal performance of convergent single-expansion-ramp nozzles. The effects of ramp chordal angle, initial ramp angle, flap angle, flap length, and ramp length were determined. All nozzles tested had a nominally constant throat area and aspect ratio. Static pressure distributions along the centerlines of the ramp and flap were also obtained for each configuration. Nozzle pressure ratio was varied up to 10.0 for all configurations.

Results show that nozzle discharge coefficient is reduced when actual nozzle throat is skewed downstream from the geometric nozzle throat. Thrust performance remained constant throughout the nozzle pressure ratio range. The most significant parameter affecting thrust performance was flap length.

Introduction

A number of studies of fighter aircraft configurations have shown potential benefits in the installation of two-dimensional nozzles (refs. 1–7). It was indicated in some of these studies that integration of the nonaxisymmetric nozzle could provide a level of installed performance comparable to, and in some cases better than, the traditional axisymmetric nozzle design. An important phase of the development of these nozzles for practical use on a production aircraft is the establishment of a documented data base of the internal nozzle performance and how that performance is affected by geometry changes.

One of the most promising nonaxisymmetric nozzles that has been investigated is the single-expansion-ramp nozzle (SERN) (refs. 8–16). The SERN was originally designed to use a hood-type jet deflector to provide high angles of thrust vectoring required for vertical takeoff and landing (VTOL) operation (refs. 8 and 9). Requirements by conventional high-performance fighter aircraft for angles of thrust vectoring that could be achieved by varying the angle of the expansion ramp (refs. 9–11) led to the removal of the deflector which, in turn, reduced the weight of the nozzle. Some investigations have been done for specific configurations (ref. 6) or for variations of the SERN design such as the augmented deflector exhaust nozzle (ADEN) (refs. 5 and 11). Data are available for the SERN on the effect of variations in expansion ratio, flap length, and flap angle. (See ref. 13.) Configurations with thrust vectoring (refs. 13 and 15) and with thrust reversing (ref. 13) have been tested, and data are available showing the effect of varying expansion-ramp length and expansion-ramp initial and chordal angles as well as flap length and flap angle (ref. 14).

This paper adds to the experimental data base of SERN configurations by presenting static internal performance data for convergent SERN configurations. This type of nozzle could be used for an all-subsonic-mission aircraft that does not require a means for controlling internal expansion ratio, thus allowing the use of this simpler, lighter, fixed-geometry nozzle. Investigations have been conducted on convergent SERN nozzles to show the effect of flap length, flap angle, expansion-ramp initial angle, expansion-ramp chordal angle, and expansion-ramp length. All nozzles had the same nominal throat area and aspect ratio. The nozzle external expansion ratios varied from 1.17 to 2.05. This investigation was conducted in the static test facility adjacent to the Langley 16-Foot Transonic Tunnel.

Symbols and Abbreviations

A_e	vertical displacement between end of nozzle ramp and flap multiplied by nozzle width, in^2
$(A_e/A_t)_e$	external geometric nozzle expansion ratio
A_t	measured nozzle throat area (table 1), in^2
C_m	pitching-moment coefficient, $M/p_a A_t h_{t,n}$
C_N	normal-force coefficient, $N/p_a A_t$
F	measured thrust along body axis, lbf
F_i	ideal isentropic gross thrust, $w_p\sqrt{\frac{RT_{t,j}}{g}\frac{2\gamma}{\gamma-1}\left[1-\left(\frac{p_a}{p_{t,j}}\right)^{\frac{\gamma-1}{\gamma}}\right]}$, lbf
F_r	resultant gross thrust, $\sqrt{F^2+N^2}$, lbf
g	gravitational constant, 32.17 ft/sec^2
$h_{t,n}$	nominal nozzle-throat height, 1.00 in.
l_f	length of flap (see fig. 2), in.
l_r	length of expansion ramp (see fig. 2), in.
M	measured pitching moment (about point on model centerline at station 29.39), in-lb

N	measured normal force, lbf
NPR	nozzle pressure ratio, $p_{t,j}/p_a$
p	local static pressure, psi
p_a	ambient pressure, psi
$p_{t,j}$	jet total pressure, psi
R	specific gas constant, 53.364 ft-lbf/lbm-°R
$T_{t,j}$	jet total temperature, °R
w_i	ideal weight-flow rate, lbf/sec
w_p	measured weight-flow rate, lbf/sec
x	axial coordinate measured from nozzle connect at station 41.13 (positive downstream), in.
y	vertical coordinate measured from horizontal model centerline (positive upward), in.
β	flap angle (see fig. 2), deg
γ	ratio of specific heats, 1.3997 for air
δ	resultant thrust-vector angle, $\tan^{-1}$ (N/F), deg
θ	expansion-ramp chordal angle (see fig. 2), deg
ρ	expansion-ramp initial angle (see fig. 2), deg

Abbreviation:

SERN	single-expansion-ramp nozzle

Nozzle and nozzle component designations:

First character in nozzle configuration designation:

A–H	expansion-ramp designation (see table A1)

Second character in nozzle configuration designation:

I–W	flap designation (see table A2)

Number in nozzle configuration designation:

1–4	sidewall designation (see fig. 3)

Apparatus and Methods

Static Test Facility

This investigation was conducted in the static test facility of the Langley 16-Foot Transonic Tunnel. All tests were conducted with the jet exhausting to the atmosphere. This facility utilizes the same clean, dry-air supply used in the 16-Foot Transonic Tunnel (ref. 17) and an air-control system that includes valving, filters, and a heat exchanger (to operate the jet flow at constant stagnation temperature).

Single-Engine, Propulsion-Simulation System

A sketch of the single-engine, air-powered nacelle model (described in ref. 17) on which the various nozzles were mounted is presented in figure 1 with a typical SERN configuration attached. An external high-pressure air system provided a continuous flow of clean, dry air at a controlled temperature of about 530°R (measured at the instrumentation section). This high-pressure air was brought through a dolly-mounted support strut by six tubes that were connected to a high-pressure plenum chamber. In order to minimize any forces imposed by the transfer of axial momentum as the air passed from the nonmetric high-pressure plenum to the metric low-pressure plenum (attached to the force balance), the air was discharged radially into the model low-pressure plenum through eight multiholed sonic nozzles equally spaced around the high-pressure plenum as shown in figure 1(a). Two flexible metal bellows were used as seals and served to compensate for the forces caused by pressurization. Figure 1(b) shows a cross section of the flow transfer assembly.

The air was then passed from the model low-pressure plenum through a transition section that provided a smooth flow path for the airflow from the round low-pressure plenum to the rectangular choke plate and instrumentation section. The transition section, choke plate, and instrumentation section were common for all SERN configurations tested. The instrumentation section had a flow path width-to-height ratio of 1.437. All nozzle configurations were attached to the instrumentation section at model station 41.13.

Nozzle Design and Models

There are two basic components in a single-expansion-ramp nozzle (SERN), a two-dimensional flap that is relatively short in comparison with the second component which is a two-dimensional ramp. In SERN designs the portion of the ramp downstream of the nozzle throat serves as an expansion

surface. The ramp can be fixed or have variable geometry by rotation of the entire external ramp downstream of the throat or by rotation of a small portion of the downstream ramp in order to control external expansion ratio (refs. 13 and 15). Rotating the entire ramp has been shown to be more efficient from a performance standpoint than rotating a small portion of the ramp. This is because deflection of the supersonic exhaust flow generally results in performance losses. The flap may vary to provide internal-expansion-ratio control.

Although the typical SERN nozzle is convergent-divergent, the nozzle models of the current investigation are convergent nozzles and do not have internal expansion. That is, the trailing edge of the flap is used to set the nozzle minimum area (the throat), and the only expansion surface is that portion of the ramp downstream of the throat.

The geometric parameters varied for the ramp and flap are shown in figure 2. The values of these parameters for each configuration are given in table 1. All configurations had a nominal throat width of 4.0 in. and a throat aspect ratio of nominally 4.0. The lengths of the two flat portions of the ramp were adjusted to obtain the variations in initial ramp angle ρ to produce the selected values of $\rho - \theta$. (See table 1.) The internal geometry of the ramps and flaps is given in appendix A. The nozzle sidewalls provided full containment of the flow for all configurations tested. Geometry details of the sidewalls are shown in figure 3.

Instrumentation

A six-component strain-gauge balance was used to measure the forces and moments on the model downstream of station 20.50. (See fig. 1(a).) Jet total pressure was measured by means of a four-probe rake through the upper surface, a three-probe rake through the side, and a three-probe rake through the corner of the instrumentation section (fig. 1). Jet total temperature was measured by a shielded thermocouple probe that was also located in the instrumentation section. Mass-flow rate of the high-pressure air was measured by a pair of critical-flow venturis. All ramps and flaps were instrumented with internal static pressure orifices located on the plan view centerline.

Data Reduction

All data were recorded on magnetic tape with 50 frames of data averaged at each data point for use in computations. With the exception of resultant gross thrust F_r, force and resultant thrust-vector-angle data are referenced to the model centerline. Nominal throat height $h_{t,n}$ and measured nozzle throat area A_t (see table 1) were selected as nondimensionalizing constants since conventional aircraft nondimensionalizing constants are not normally associated with isolated nozzle tests.

Data are presented in basic performance parameters of internal thrust ratio, resultant thrust ratio, resultant thrust-vector angle, and nozzle discharge coefficient, which is the ratio of measured weight-flow rate to ideal weight-flow rate. The ratios of nozzle internal static pressures and jet total pressure are presented as a function of NPR and nondimensionalized axial location for each configuration in appendix B (table B1). Presented in appendix C are normal-force and pitching-moment coefficients for each configuration. The balance axial-force measurement, from which actual nozzle thrust is obtained, is corrected for model weight tares and balance interactions as are all other forces and moments. Although the bellows arrangement previously described was designed to eliminate pressure and momentum interactions with the balance, small bellows tares still exist on all balance components. When the bellows are pressurized, there are small differences in the forward and aft spring constants; there are also small differences in the pressure between the ends of the bellows at high internal velocities. These differences result in the bellows tares. In order to determine the bellows tares, calibration nozzles were tested over a range of expected normal force and pitching moment as discussed in reference 10. To obtain actual nozzle thrust, normal force, and pitching moment, balance data were corrected in a manner similar to that discussed in reference 10.

Although six balance components were computed, none of the nozzle configurations were designed to produce any significant lateral forces or moments and none are presented. The corrected balance data are then used to determine the basic performance parameters. The ideal gross thrust F_r is computed based on measured weight-flow rate, jet total pressure, and jet total temperature. The computed ideal weight-flow rate w_i is based on jet total pressure, jet total temperature, and measured nozzle throat area. Nozzle discharge coefficient is the ratio of measured weight-flow rate w_p to the ideal weight-flow rate w_i and is a measure of the ability of a nozzle to pass mass flow. All the data-reduction equations and methods can be found in reference 18. The internal nozzle static pressures were nondimensionalized by dividing them by the jet total pressure.

Presentation of Results

Basic nozzle internal performance data for all configurations and internal static pressure distributions for selected configurations are presented graphically in figures 4–26. The basic nozzle internal performance data, which consist of thrust ratio F/F_i, resultant thrust ratio F_r/F_i, discharge coefficient w_p/w_i, and resultant thrust-vector angle δ, are presented as a function of nozzle pressure ratio (NPR). Pitching-moment coefficient C_m and normal-force coefficient C_N for each configuration are presented graphically as a function of nozzle pressure ratio in appendix C. The normal-force and pitching-moment coefficients are presented for information purposes only and will not be discussed separately. Variations in the nozzle geometry usually result in a change in external expansion ratio, which shifts the pressure ratio for optimum performance. Performance changes are expected when these geometric variations are made, but the change cannot always be described as beneficial or detrimental. All data were machine plotted and curves were faired with a spline curve fit.

The results are presented graphically in the following figures:

Results and Discussion

The convergent SERN nozzles of the current investigation do not have internal expansion. The exhaust-flow expansion process, which is totally external and occurs from the end of the flap, is bounded by the free (ambient/exhaust) boundary and by the expansion ramp. That is, these nozzles have only an external expansion ratio associated with them, and design NPR (see table 1) is based on this external expansion ratio. The expansion of the exhaust flow over the external ramp produces a resultant thrust force that does not act along the horizontal centerline of the nozzle. The direction of this force varies with nozzle pressure ratio and can be expressed in terms of resultant thrust-vector angle. At overexpanded conditions (NPR less than design for fully expanded external flow), the single-expansion-ramp nozzle generally produces negative resultant thrust-vector angles (nose-up pitching moment). At NPR greater than design (underexpanded flow), the resultant thrust-vector angles are generally positive (nose-down pitching moment). Near design NPR, the resultant thrust-vector angles, though generally close to zero, are dependent on specific nozzle geometry. When a single-expansion-ramp nozzle is integrated into a complete aircraft configuration, this vertical force exerted on the ramp can be a pitching-moment contribution and would have to be included for trim or control consideration.

Ramp Chordal Angle

As with many of the geometric parameters in the single-expansion-ramp nozzle, changing the ramp chordal angle θ causes a change in the nozzle expansion ratio. When θ is increased, external expansion ratio also increases. (See table 1.) Figures 4 and 5 show the effect of increasing θ and consequently ρ (initial ramp angle) to maintain a constant value of ρ–θ on the nozzle internal performance characteristics. In general, all configurations maintained a constant level of resultant thrust ratio F_r/F_i throughout the nozzle pressure ratio range. The configurations with the smaller ramp chordal angle provided better performance at the lower values of NPR and poorer performance at the higher nozzle pressure ratios than those configurations with the larger chordal angles. Those nozzles with smaller expansion ratios have higher underexpansion losses at the high nozzle pressure ratios, and conversely the nozzles with the larger expansion ratios (larger θ) had greater overexpansion losses at the low nozzle pressure ratios. Similar results for varying expansion ratio were noted in reference 13.

The pressure data presented graphically in figures 6 and 7 are for the configurations shown in figures 4 and 5. Although the geometric throat (which is also the exit for convergent SERN nozzles) for these configurations is at $x/h_{t,n} = 4.74$ in figure 6 and 5.14 in figure 7, the actual throat ($p/p_{t,j} = 0.528$) is positioned differently. The actual nozzle throat location on the ramp is downstream beyond the end of the flap for $\theta = 4.4°$ and results in a skewed sonic line. The actual nozzle throat for the configurations with $\theta = 8.9°$ is near the geometric throat. The discharge coefficient is lower for the nozzle with the skewed throat. Similar results were noted in reference 15.

Flow over the ramp for all four configurations expands to near-sonic speeds at a point slightly downstream of $x/h_{t,n} = 4.0$. When θ was increased to 8.9°, a supersonic bubble had formed on the ramp. This supersonic flow region inside the nozzle is likely caused by the "bump" created by the internal contour of the ramp. That is, flow that is subsonic upstream and downstream can cause a region of supersonic flow over a bump (ref. 19).

The data in figures 6 and 7 indicated that the ramp static pressures were generally higher for the $\theta = 4.4°$ cases than for the $\theta = 8.9°$ cases. The higher pressure levels exerted (for small values of θ) over the large normal area projected by the ramp would be expected to result in larger normal-force values (and consequently higher resultant thrust-vector angles). This is readily apparent in the resultant thrust-vector-angle data of figures 4 and 5 with a difference of 4.0° to 6.0° between the two ramp chordal angles for nozzle pressure ratios greater than 4.0.

The pressure data for the flap indicated a higher static pressure at $\theta = 4.4°$ over the entire flap length in both figures 6 and 7. Note that sonic flow is never detected on the flap by the available pressure taps;

however, sonic flow must exist very near the flap termination.

Initial Ramp Angle

Figures 8–11 show the effect of varying initial ramp angle ρ on the nozzle internal performance. As indicated in table 1, it was possible to vary the initial ramp angle while keeping nozzle external expansion ratio nominally the same. For this particular set of hardware, constant values of $\rho - \theta$ were maintained and initial ramp angle ρ and ramp chordal angle θ were varied together. It would be expected that the effect of varying initial ramp angle on internal nozzle performance would be very similar to that noted previously for varying ramp chordal angle, and this is true. The larger values of initial ramp angle showed lower performance at the smaller NPR's with equal or slightly better performance at higher nozzle pressure ratios. The point at which the performance curves crossed was always less than the design NPR. (See table 1.) Also, thrust ratio maintained a nearly constant level throughout the NPR range.

Figures 12, 13, and 14 present internal static pressure distributions for the configurations shown in figures 8, 10(a), and 11, respectively. In general, increasing $\rho - \theta$ decreased pressure on the flap and on the upstream portion of the ramp, and it increased pressure on the downstream portion of the ramp. Flow over the expansion ramp of a SERN nozzle is characterized by a series of expansion and compression waves reflecting from the ramp and the jet-free boundary (ref. 14). The compression waves can coalesce into a shock that causes a sharp pressure rise on the ramp. The positioning of these shocks on the ramp is a function of NPR, in which the frequency of the shocks increases with decreasing NPR. (See refs. 14 and 20.) The static pressure data at NPR = 4.0 in figures 12–14 show the presence of a shock on the ramp. At NPR = 10.0, the nozzle is at a "flow-full" condition with the shock system being effectively "blown out" of the nozzle. This phenomenon is discussed further in reference 20.

Figure 14 and the data for $\rho = 6.4°$ in figure 12 and $\rho = 10.9°$ in figure 13 show a supersonic bubble as was previously noted in the discussion on ramp chordal angle. It is likely that the supersonic bubble also exists for the configurations at $\rho = 9.4°$ and at $\rho = 13.9°$, but because of the position of the pressure taps it is not evident. Examination of these pressure data does not indicate the skewed sonic line as was seen for varying the ramp chordal angle. As would be expected, discharge coefficient is relatively unaffected by changes in the initial ramp angle.

Ramp Length

Increasing the length of the ramp increased the nozzle external expansion ratio from 1.2 for the shortest ramp to 2.0 for the longest ramp. (See table 1.) Static internal performance data for the three ramp lengths tested are shown in figure 15. The effects of increasing ramp length on the thrust ratio are predominantly due to the corresponding increase in nozzle external expansion ratio. The shortest ramp has essentially no overexpansion losses at the low nozzle pressure ratios with a performance peak near NPR = 4.0. As expected, a decrease in performance due to underexpansion losses occurs at the higher values of NPR. The 8.64 ramp shows initial underexpansion losses at the low nozzle pressure ratios followed by performance recovery at the higher nozzle pressure ratios. The longest ramp indicates initial overexpansion losses followed by a nearly constant value of thrust ratio to NPR = 10.0.

Figure 16 presents the nozzle internal static pressure distribution on the ramp and flap for the three different ramp lengths tested. As expected, increasing ramp length had no effect on the flap static pressure distribution at either NPR = 4.0 or NPR = 10.0. For the three configurations tested, the nozzle geometric throat (exit) was at $x/h_{t,n} = 4.74$. The flow on all three ramps expanded to supersonic speeds before the second pressure tap ($x/h_{t,n} = 4.14$) and remained supersonic over the length of the ramp. It is difficult to compare the flow on the three ramps directly because the pressure taps are at different positions, but as previously discussed, the flow on the ramp is a series of expansion and compression cycles. The pressure distribution on the longest ramp shows two expansion-compression reexpansion cycles at NPR = 4.0, which is much less than the design NPR. (See table 1.) This would be expected from the previous discussion. At NPR = 10.0, which is still less than the design NPR for the longest ramp, there is still a shock on the longest ramp and the nozzle is not at the "flow-full" condition described in reference 20.

The fact that the expansion-compression wave pattern changes with NPR is also evident in the nonlinearity of the resultant thrust-vector angle. The SERN configurations typically produce both negative resultant thrust-vector angles at overexpanded conditions on the ramp and positive values of δ at underexpanded conditions. This is obvious in figure 15; after the design NPR is passed on the short- and medium-length ramps, the resultant thrust angle increases steadily with increasing NPR. However, the longest ramp does not reach this condition.

Flap Angle

Figures 17–19 show the effect of varying lower flap angle on internal nozzle performance parameters. It was possible to vary flap angle while maintaining nearly the same nozzle external expansion ratio since nominal throat area remained constant and the change in β was all upstream of the throat. In general, where there is a discernible difference, the thrust ratios increase with increasing β. The greater the difference in β, the larger the increment in thrust ratio. (See fig. 18(c).) Variations in discharge coefficient due to changes in flap angle were generally small. Figure 17(a) showed the greatest change in discharge coefficient. The internal static pressure distributions for these configurations are presented graphically (FO1 in fig. 12 and FQ1 in fig. 6); and, as noted previously, the actual nozzle throat of configuration FQ1 is skewed downstream of the geometric nozzle throat, thus causing a decrease in the discharge coefficient.

Figure 20 presents the nozzle internal static pressure distributions for the configurations whose performance data are plotted in figure 18(c). These configurations have the largest β difference tested. Increasing flap angle increased the static pressure on both the flap and the first two-thirds of the ramp. As seen, pressure increases on the flap were much greater than on the ramp. This was true at both NPR = 4.0 and NPR = 10.0. There was no effect of changes in β evident on the last one-third of the ramp. As stated previously, the expansion of the flow over the ramp produces a normal force, and the configuration with the highest static pressure on the ramp often generates the larger resultant thrust-vector angles. However, there is also a normal force produced by the flow over the flap that opposes the normal force produced by the ramp. Even though the area of the flap is small as compared with that of the ramp, in this case the pressure differential between the two flaps is large enough to cancel the pressure differential on the ramp at NPR = 4.0. This can be seen in the data of figure 18(c) because the resultant thrust-vector angles at NPR = 4.0 are about equal; and at NPR greater than 4.0, the smaller flap angle shows a larger resultant thrust-vector angle.

Flap Length

Increasing the length of the flap slightly decreased the external expansion ratio for these nozzles (a difference of 0.2 or less between the longest and shortest flaps tested). Figures 21–25 present the effect of increasing flap length on the nozzle internal performance. In general, increasing flap length increased thrust ratio. The magnitude of the increase in thrust ratio was in part a function of the value of nozzle external expansion ratio and in part a function of ρ. As ρ increased, the difference in thrust between the 4.14 flap and the longer flaps also increased. (Compare fig. 23 with fig. 22(a).) In all cases where all three flap lengths were tested, there is only a slight increase in thrust ratio when flap length is increased from 4.74 to 5.14 as compared with the increase in going from 4.14 to 4.74. As has been true for the other configurations discussed, the resultant thrust ratio remained nearly constant throughout the NPR range. The effect of increasing flap length on nozzle discharge coefficient was generally small with the longer flap showing a slightly higher discharge coefficient. Figure 21, however, shows a much larger difference in discharge coefficient. This data comparison is made at the smallest value of ramp chordal angle tested ($\theta = 4.4°$), but it is not understood from the available data why this result occurs.

Figure 26 shows nozzle internal static pressure distribution for the configurations shown in figure 24. Direct comparison of the pressure distributions on the flaps is somewhat difficult in that all pressure taps on the shortest flap were at an axial location upstream of the first pressure tap on either of the longer flaps. However, increasing static pressure with increasing flap length is indicated. As the length of the flap increased from 4.14 to 5.14, the length of the expansion-ramp surface was being decreased. It therefore follows that the pressure data on the ramp in figure 26 should be very similar to the data in figure 16 showing the effect of varying ramp length, and this is the case. As flap length is increased (expansion surface decreased), static pressure is increased. The expansion-compression cycles at NPR = 4.0 indicated by the static pressures would also be expected because of the difference in expansion ratio previously discussed. At NPR = 10.0, all the nozzles appear to be at the "flow-full" condition.

Conclusions

An investigation of convergent single-expansion-ramp nozzle (SERN) configurations has presented the following conclusions:

1. The configurations tended to maintain a nearly constant level of thrust performance throughout the nozzle pressure ratio range.
2. The discharge coefficient decreased for configurations in which the actual nozzle throat was skewed downstream of the geometric nozzle throat.
3. Increasing the flap length from 4.14 to 4.74 resulted in a large increase in thrust ratio, but increasing the flap length to 5.14 yielded only a slight increase in performance over the 4.74 flap. Flap

length was the most significant parameter affecting performance.

NASA Langley Research Center
Hampton, VA 23665-5225
April 10, 1989

References

1. *F-15 2-D Nozzle System Integration Study. Volume I—Technical Report.* NASA CR-145295, 1978.
2. Hiley, P. E.; Wallace, H. W.; and Booz, D. E.: Nonaxisymmetric Nozzles Installed in Advanced Fighter Aircraft. *J. Aircr.*, vol. 13, no. 12, Dec. 1976, pp. 1000–1006.
3. Capone, Francis J.; and Reubush, David E.: *Effects of Varying Podded Nacelle-Nozzle Installations on Transonic Aeropropulsive Characteristics of a Supersonic Fighter Aircraft.* NASA TP-2120, 1983.
4. Hiley, P. E.; and Bowers, D. L.: Advanced Nozzle Integration for Supersonic Strike Fighter Application. AIAA-81-1441, July 1981.
5. Wasson, H. R.; Hall, G. R.; and Palcza, J. L.: Results of a Feasibility Study To Add Canards and ADEN Nozzle to the YF-17. AIAA Paper 77-1227, Aug. 1977.
6. Capone, Francis J.; and Berrier, Bobby L.: *Investigation of Axisymmetric and Nonaxisymmetric Nozzles Installed on a 0.10-Scale F-18 Prototype Airplane Model.* NASA TP-1638, 1980.
7. Capone, Francis J.: Summary of Propulsive-Lift Research in the Langley 16-Ft. Transonic Tunnel. *J. Aircr.*, vol. 13, no. 10, Oct. 1976, pp. 803–808.
8. Lander, J. A.; and Palcza, J. Lawrence: Exhaust Nozzle Deflector Systems for V/STOL Fighter Aircraft. AIAA Paper No. 74-1169, Oct. 1974.
9. Dusa, D. J.; and Wooten, W. H.: Single Expansion Ramp Nozzle Development Status. AIAA-84-2455, Oct.–Nov. 1984.
10. Capone, Francis J.: *Static Performance of Five Twin-Engine Nonaxisymmetric Nozzles With Vectoring and Reversing Capability.* NASA TP-1224, 1978.
11. Schnell, W. C.; and Grossman, R. L.: Vectoring Nonaxisymmetric Nozzle Jet Induced Effects on a V/STOL Fighter Model. AIAA Paper 78-1080, July 1978.
12. Berrier, Bobby L.; and Re, Richard J.: *Effect of Several Geometric Parameters on the Static Internal Performance of Three Nonaxisymmetric Nozzle Concepts.* NASA TP-1468, 1979.
13. Re, Richard J.; and Berrier, Bobby L.: *Static Internal Performance on Single Expansion-Ramp Nozzles With Thrust Vectoring and Reversing.* NASA TP-1962, 1982.
14. Re, Richard J.; and Leavitt, Laurence D.: *Static Internal Performance of Single-Expansion-Ramp Nozzles With Various Combinations of Internal Geometric Parameters.* NASA TM-86270, 1984.
15. Berrier, Bobby L.; and Leavitt, Laurence D.: *Static Internal Performance of Single-Expansion-Ramp Nozzles With Thrust-Vectoring Capability up to 60°.* NASA TP-2364, 1984.
16. Miller, E. H.: Performance of a Forward Swept Wing Fighter Utilizing Thrust Vectoring. AIAA-83-2482, Oct. 1983.
17. Peddrew, Kathryn H., compiler: *A User's Guide to the Langley 16-Foot Transonic Tunnel.* NASA TM-83186, 1981.
18. Mercer, Charles E.; Berrier, Bobby L.; Capone, Francis J.; Grayston, Alan M.; and Sherman, C. D.: *Computations for the 16-Foot Transonic Tunnel—NASA, Langley Research Center, Revision 1.* NASA TM-86319, 1987.
19. Kaplan, Carl: *The Flow of a Compressible Fluid Past a Curved Surface.* NACA Rep. 768, 1943. (Supersedes NACA WR L-320.)
20. Schnell, W. C.; Grossman, R. L.; and Hoff, G. E.: *Comparison of Non-Axisymmetric and Axisymmetric Nozzles Installed on a V/STOL Fighter Model.* [Preprint] 770983, Soc. of Automotive Engineers, Nov. 1977.

Table 1. Nozzle Parameters

Configuration	ρ, deg	θ, deg	$\rho-\theta$, deg	$l_r/h_{t,n}$	$l_f/h_{t,n}$	β, deg	$(A_e/A_t)_e$	A_t, in^2	Design NPR
AK1	13.9	8.9	5.0	8.64	4.14	15.0	1.70	4.056	7.9
AL1	↓	↓	↓	↓	4.14	18.0	1.70	4.045	7.9
AM1	↓	↓	↓	↓	4.14	21.0	1.70	4.055	7.9
AQ1	↓	↓	↓	↓	4.74	15.0	1.64	4.165	7.4
AR1	↓	↓	↓	↓	4.74	18.0	1.60	4.056	7.1
AS1	↓	↓	↓	↓	4.74	21.0	1.62	4.158	7.2
AU2	↓	↓	↓	↓	5.14	15.0	1.62	4.096	7.2
AV2	↓	↓	↓	↓	5.14	18.0	1.52	4.139	6.4
AW2	↓	↓	↓	↓	5.14	21.0	1.51	4.127	6.3
BJ1	9.4	4.4	↓	↓	4.14	13.5	1.34	4.066	4.9
BO1	↓	↓	↓	↓	4.74	10.5	1.28	4.107	4.5
BP1	↓	↓	↓	↓	4.74	13.5	1.30	4.180	4.7
BV2	↓	↓	↓	↓	5.14	18.0	1.17	3.975	3.6
CI1	16.9	8.9	8.0	↓	4.14	4.0	1.70	4.069	7.9
CM1	↓	↓	↓	↓	4.14	21.0	1.70	4.053	7.9
CS1	↓	↓	↓	↓	4.74	21.0	1.62	4.153	7.2
CW2	↓	↓	↓	↓	5.14	21.0	1.51	4.222	6.3
DI1	10.9	↓	2.0	↓	4.14	4.0	1.70	4.090	7.9
DK1	↓	↓	↓	↓	4.14	15.0	1.70	4.046	7.9
DQ1	↓	↓	↓	↓	4.74	15.0	1.64	4.156	7.4
DU2	↓	↓	↓	↓	5.14	15.0	1.62	4.302	7.2
EN1	18.4	13.4	5.0	↓	4.14	22.5	2.05	4.040	11.1
ET1	18.4	13.4	5.0	↓	4.74	22.5	1.96	4.107	10.3
FO1	6.4	4.4	2.0	↓	↓	10.5	1.24	4.010	4.1
FQ1	6.4	4.4	2.0	↓	↓	15.0	1.24	4.060	4.1
GR3	13.9	8.9	5.0	11.14	↓	18.0	1.99	4.122	10.5
HR4	13.9	8.9	5.0	6.14	↓	18.0	1.21	4.082	3.9

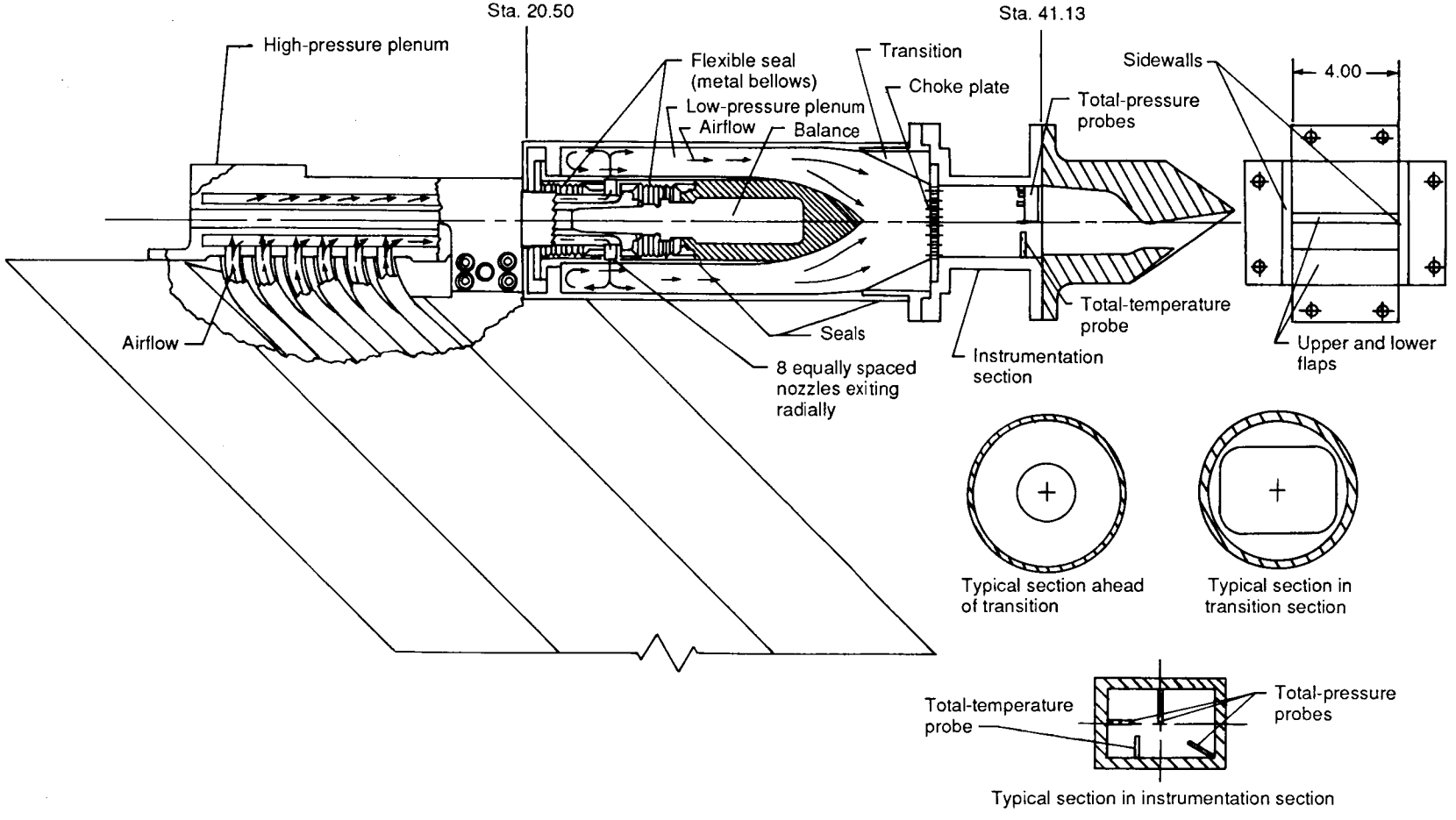

(a) Air-powered nacelle test apparatus.

Figure 1. Sketch of air-powered nacelle model with typical nozzle configuration installed. All dimensions are given in inches unless otherwise noted.

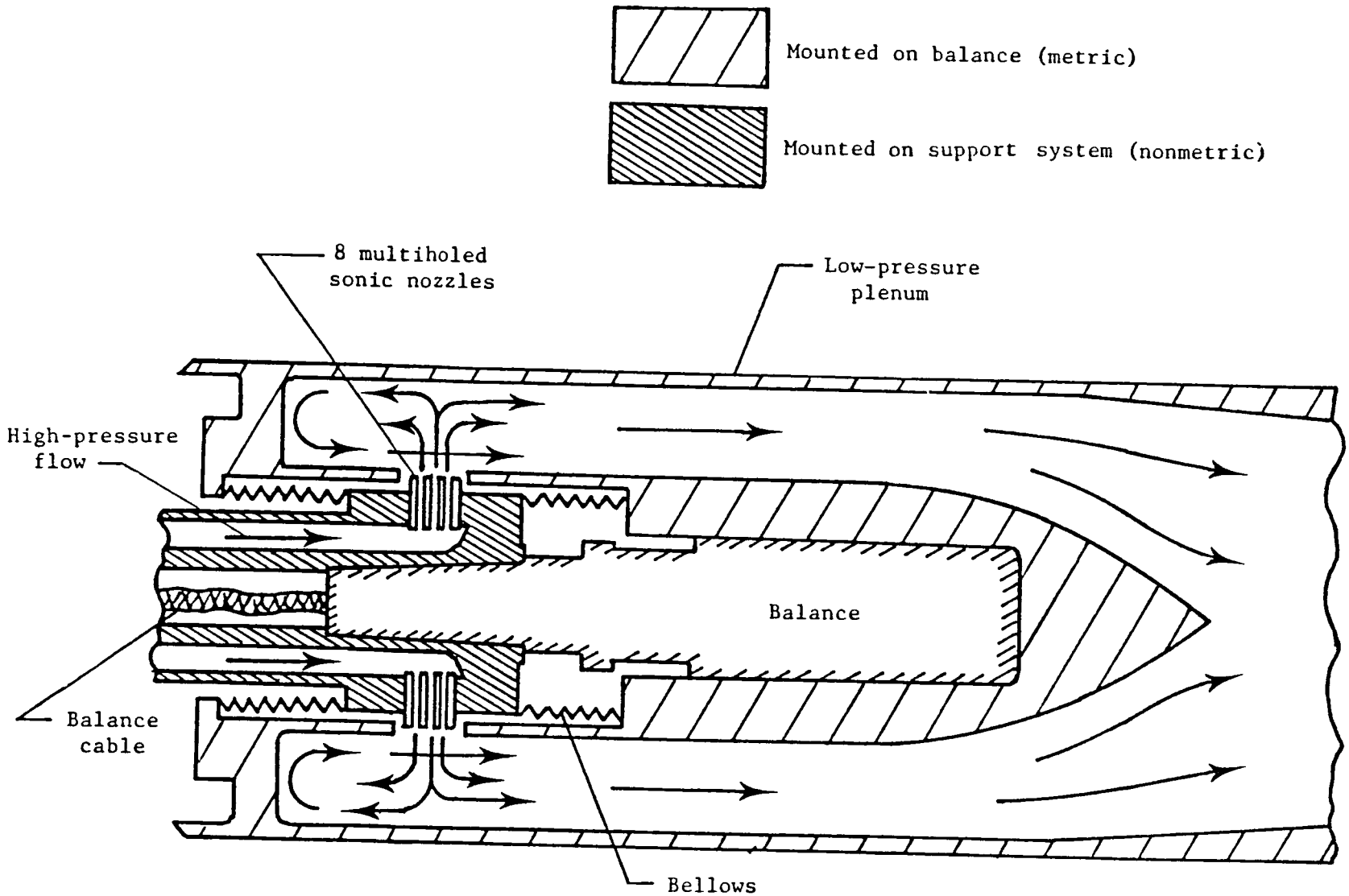

(b) Schematic cross section of flow transfer system.

Figure 1. Concluded.

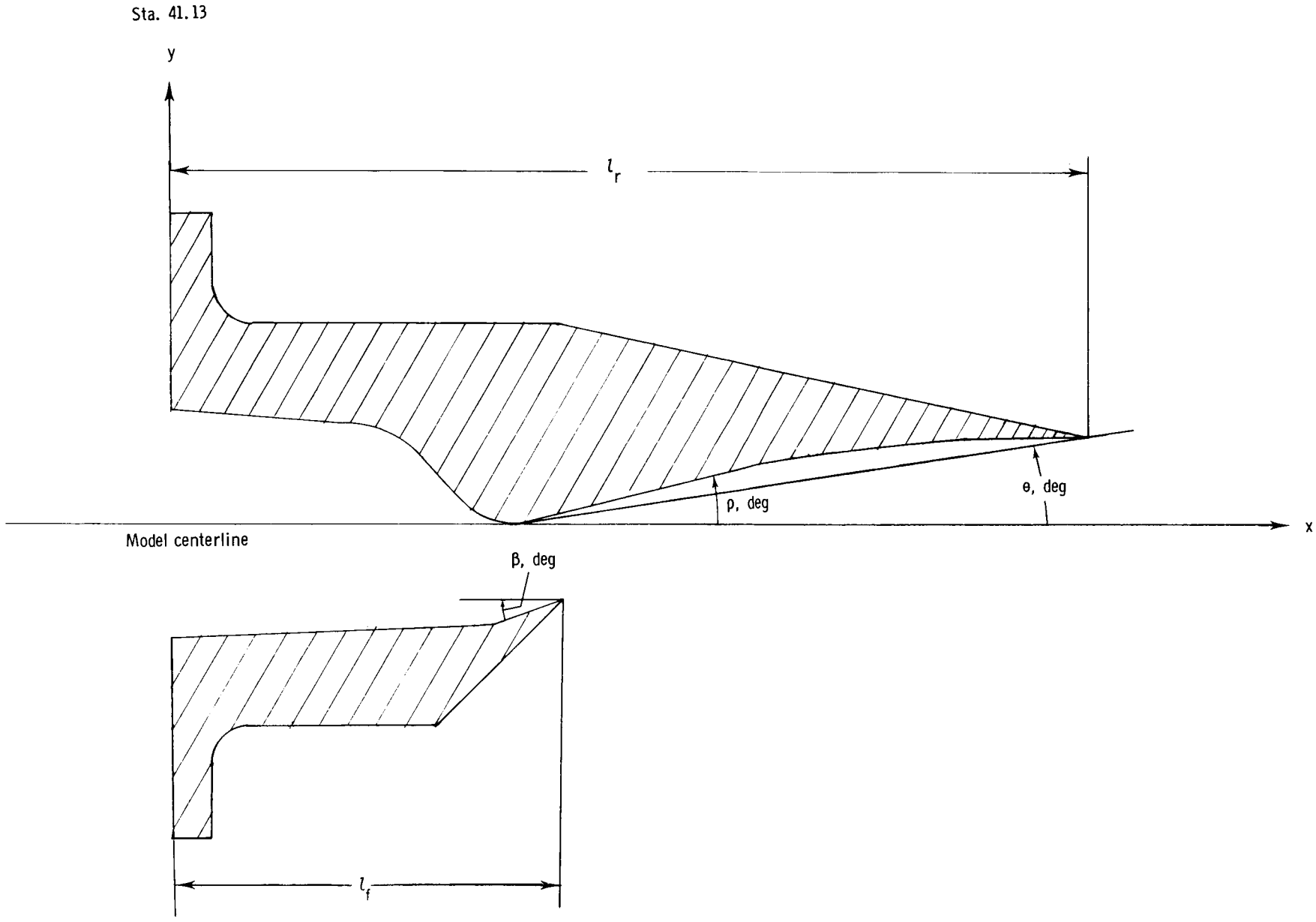

Figure 2. Sketch indicating the five geometric parameters varied for ramp and flap. All dimensions are given in inches unless otherwise noted.

Sidewall	x_1	y_1	x_2	y_2	x_3	y_3	x_4	y_4
1	8.640	2.374	8.640	0.696	4.570	-1.000	3.2-7	-2.375
2	8.640	↓	8.640	1.054	5.070	-1.000	3.217	↓
3	10.260	↓	10.260	1.267	4.745	-1.064	3.217	↓
4	6.140	↓	6.140	0.305	5.070	-1.000	3.942	↓

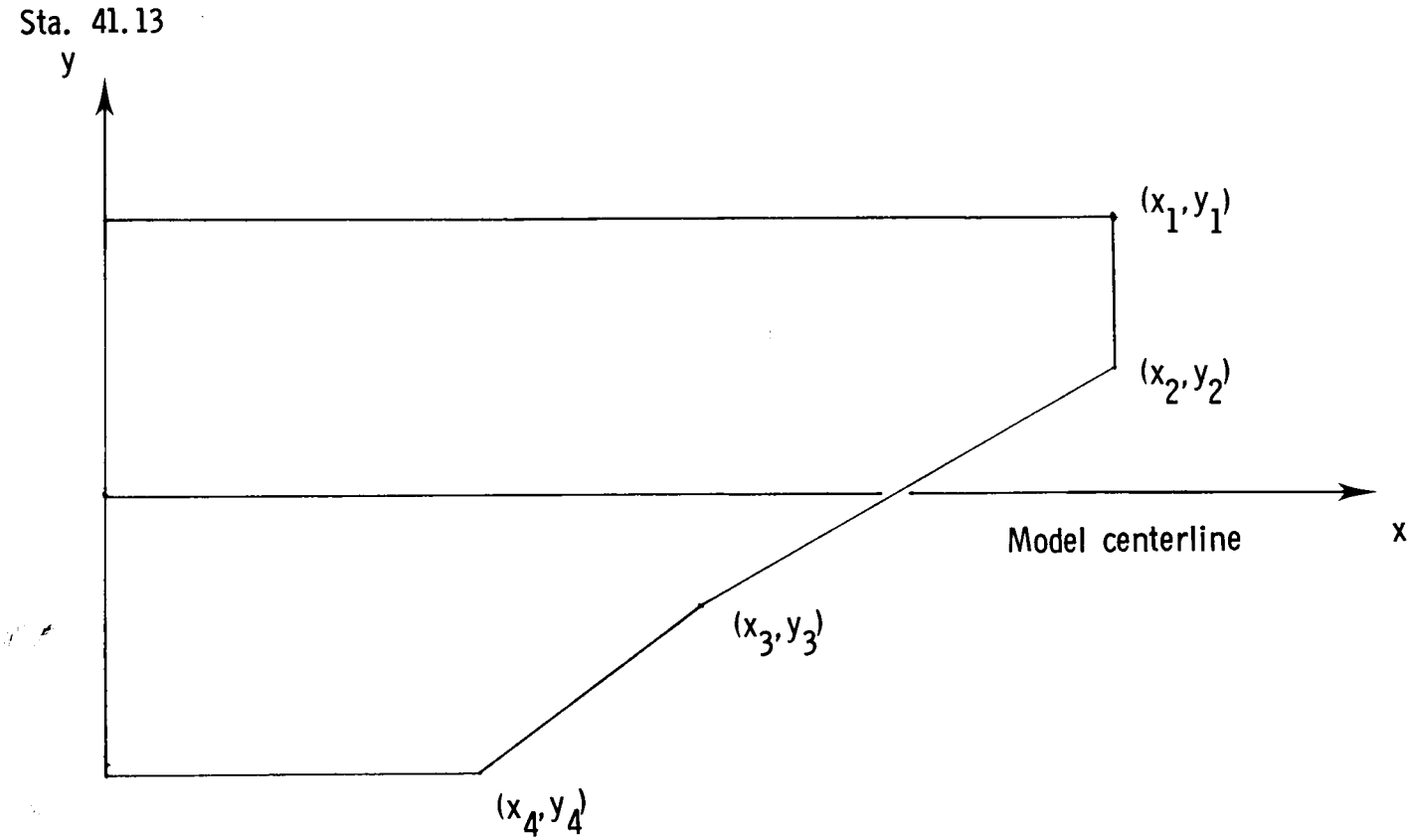

Figure 3. Planform of nozzle sidewall indicating coordinate axes and coordinates for downstream edge of sidewalls. All dimensions are given in inches.

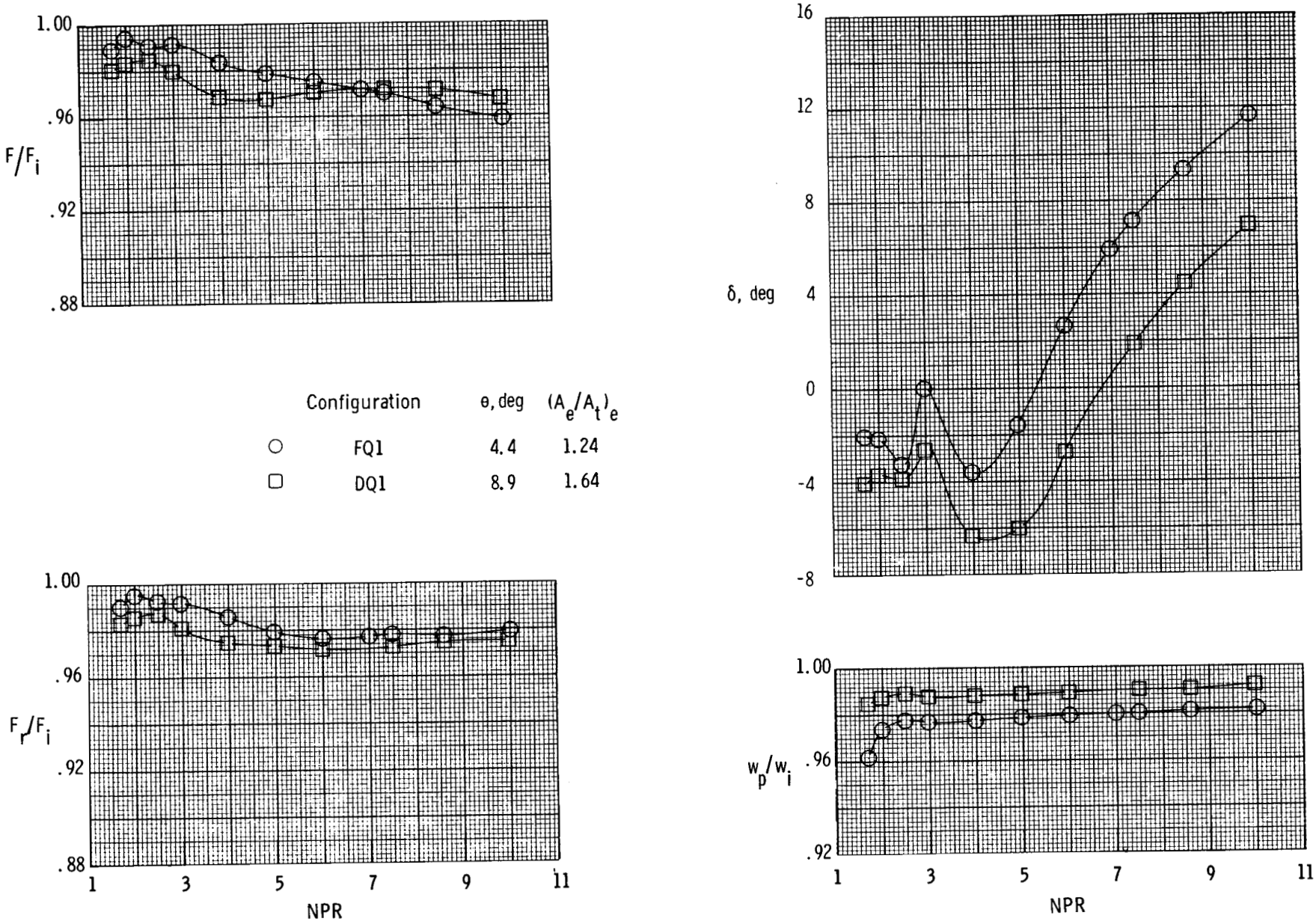

Figure 4. Effect of ramp chordal angle on nozzle performance parameters for $l_f/h_{t,n} = 4.74$, $\rho - \theta = 2.0°$, and $\beta = 15.0°$.

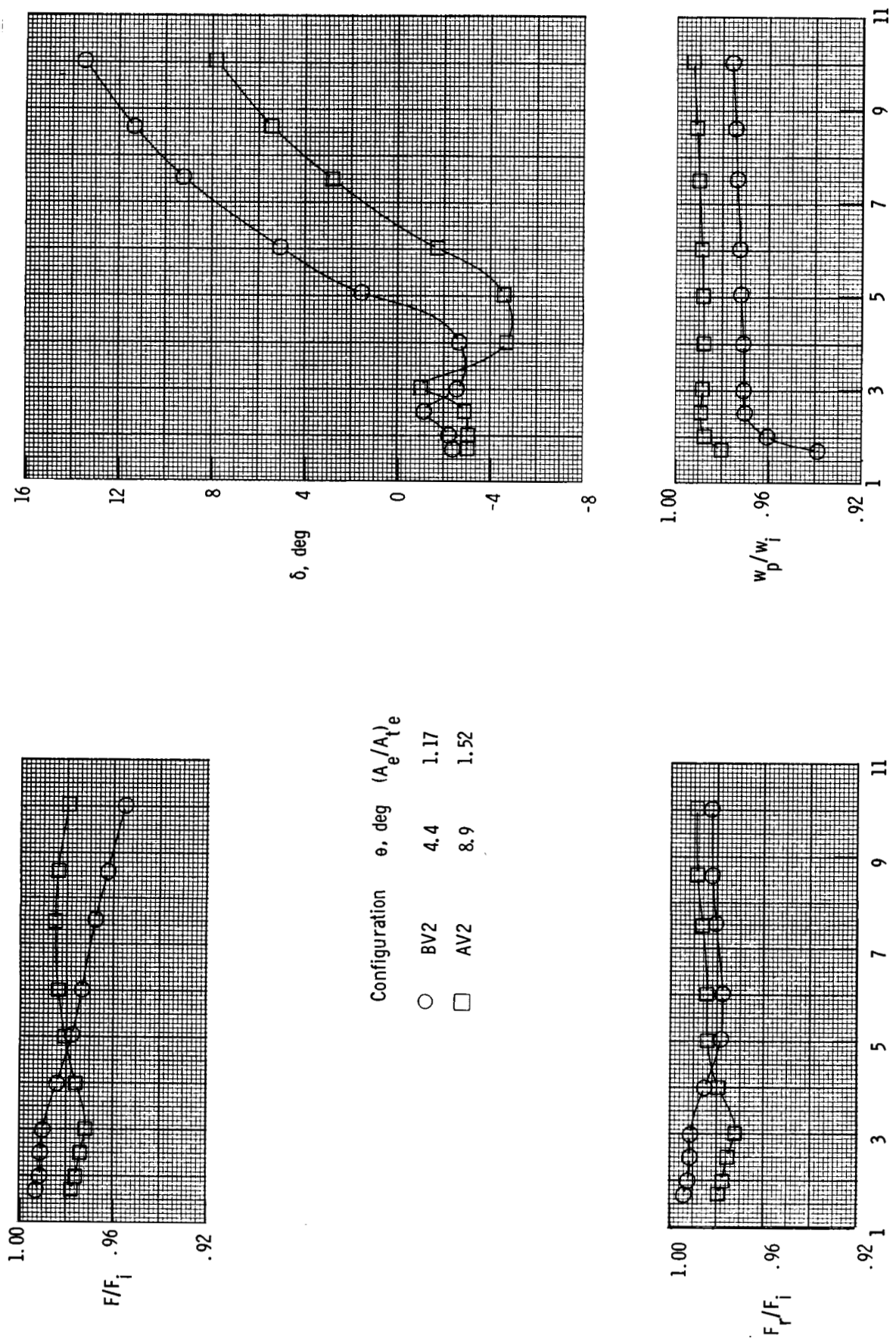

Figure 5. Effect of ramp chordal angle on nozzle performance parameters for $l_f/h_{t,n} = 5.14$, $\rho - \theta = 5.0°$, and $\beta = 18.0°$.

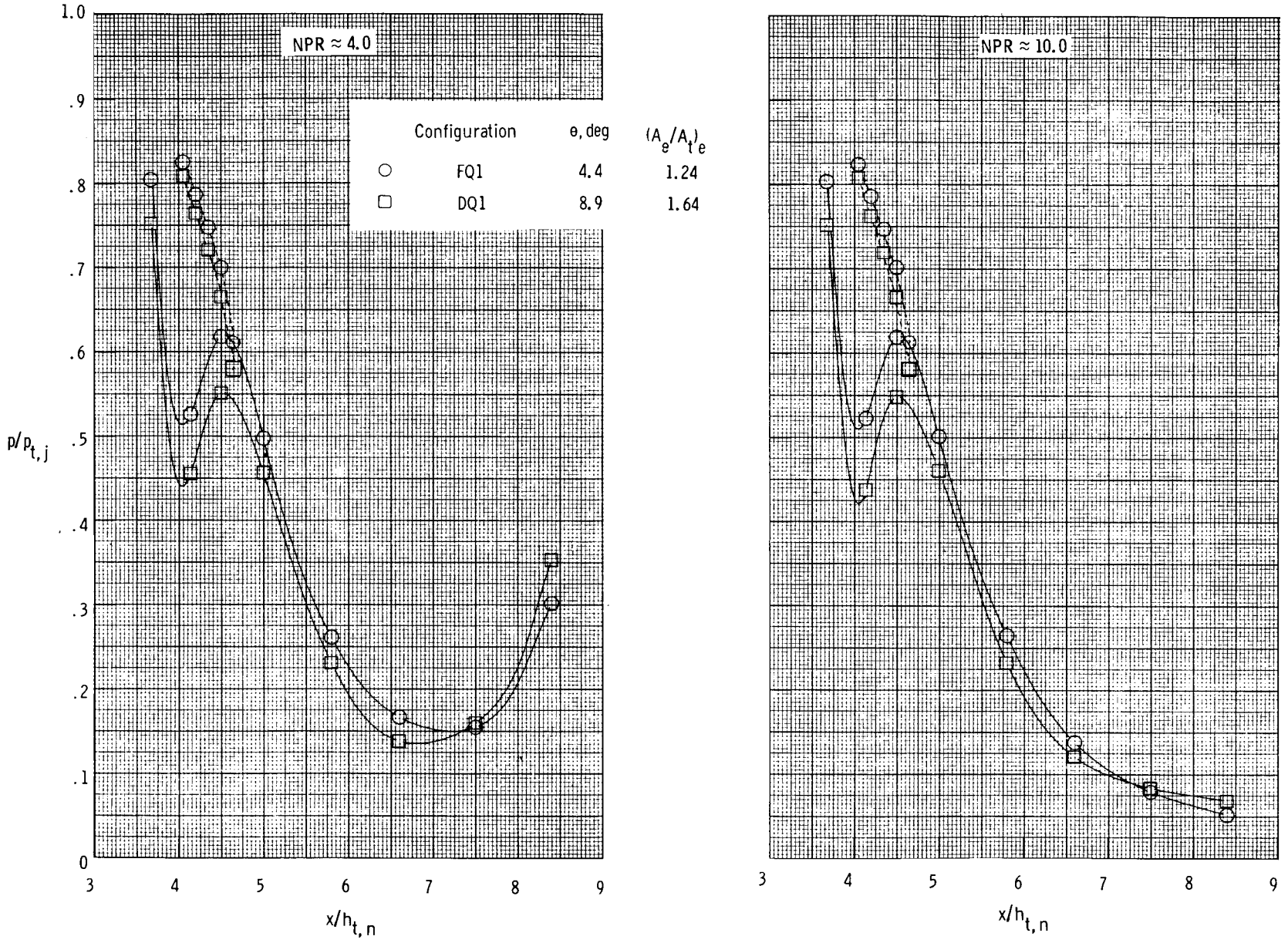

Figure 6. Effect of ramp chordal angle on nozzle internal static pressure distributions at two nozzle pressure ratios for $l_f/h_{t,n} = 4.74$, $\rho - \theta = 2.0°$, and $\beta = 15.0°$. Dashed lines indicate flap static pressures.

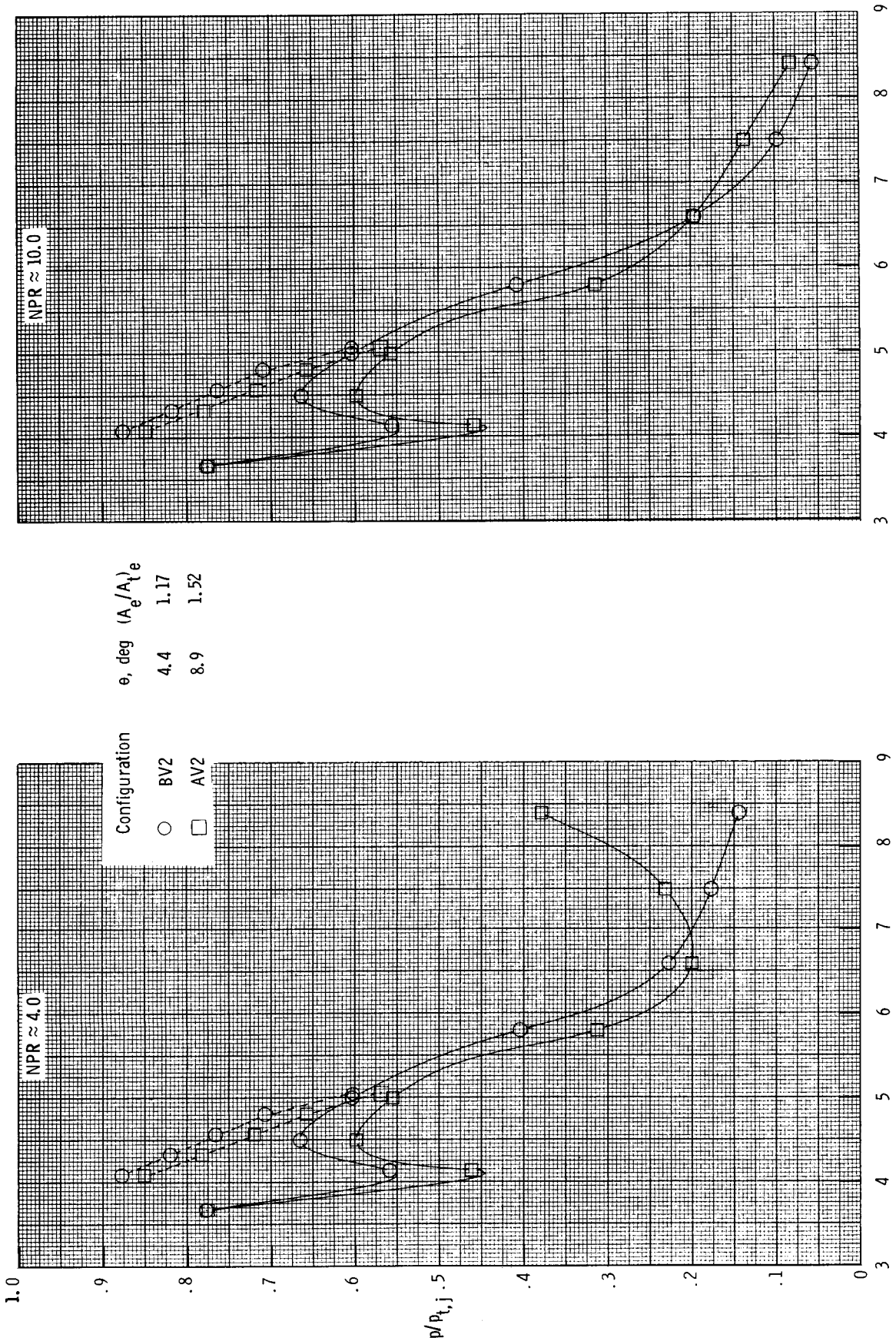

Figure 7. Effect of ramp chordal angle on nozzle static pressure distributions at two nozzle pressure ratios for $l_f/h_{t,n} = 5.14$, $\rho - \theta = 5.0°$, and $\beta = 18.0°$. Dashed lines indicate flap static pressures.

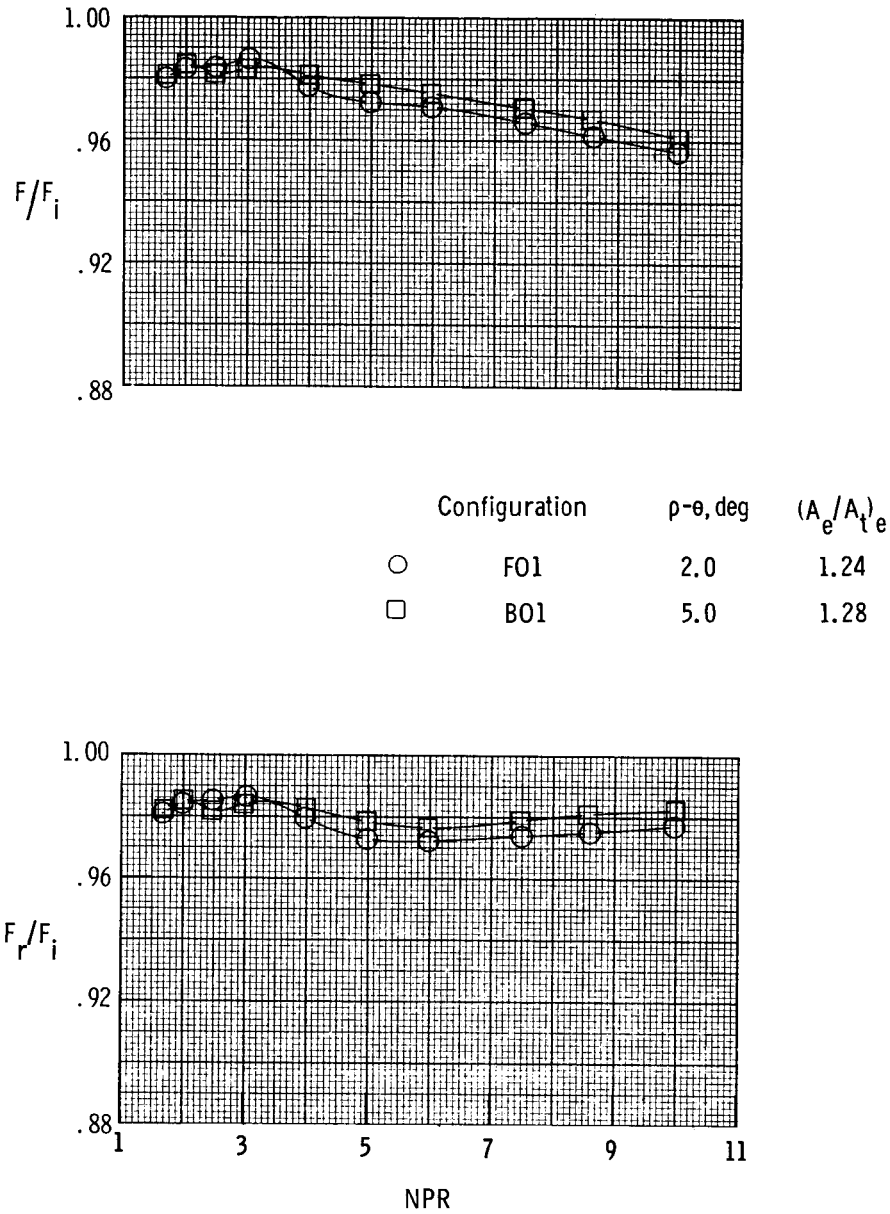

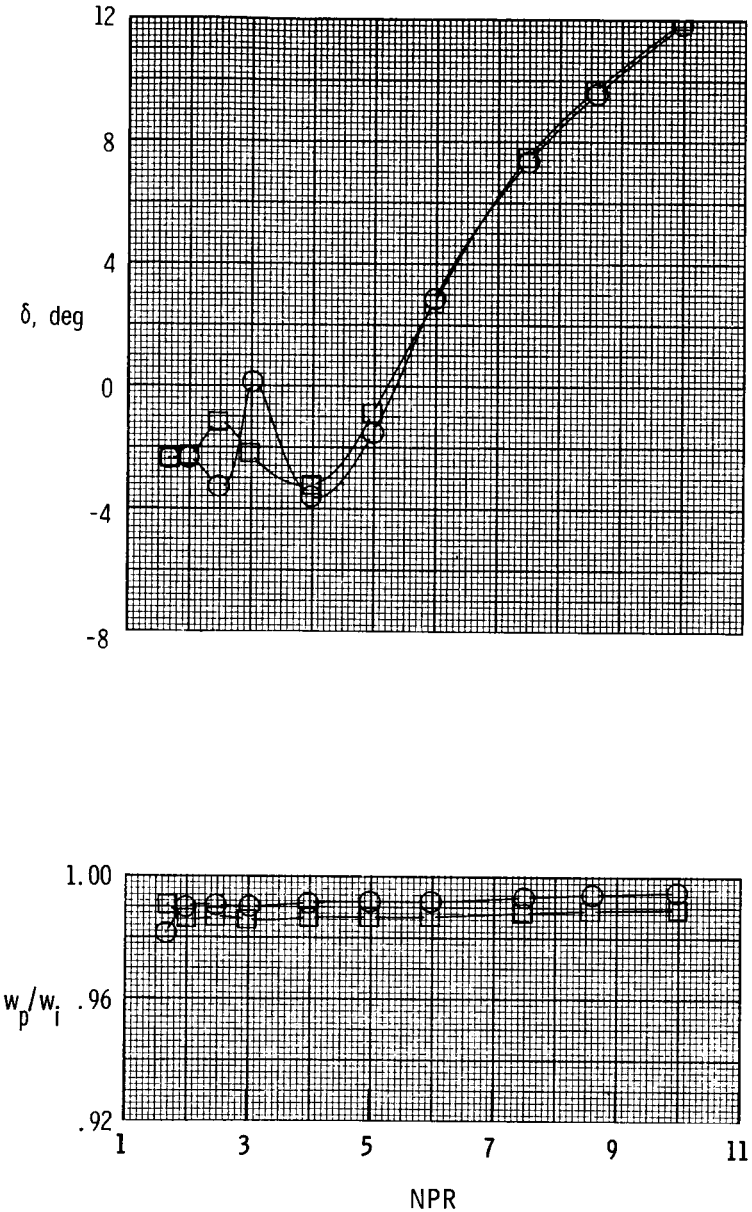

Figure 8. Effect of initial ramp angle on nozzle performance parameters for $\theta = 4.4°$, $l_f/h_{t,n} = 4.74$, and $\beta = 10.5°$.

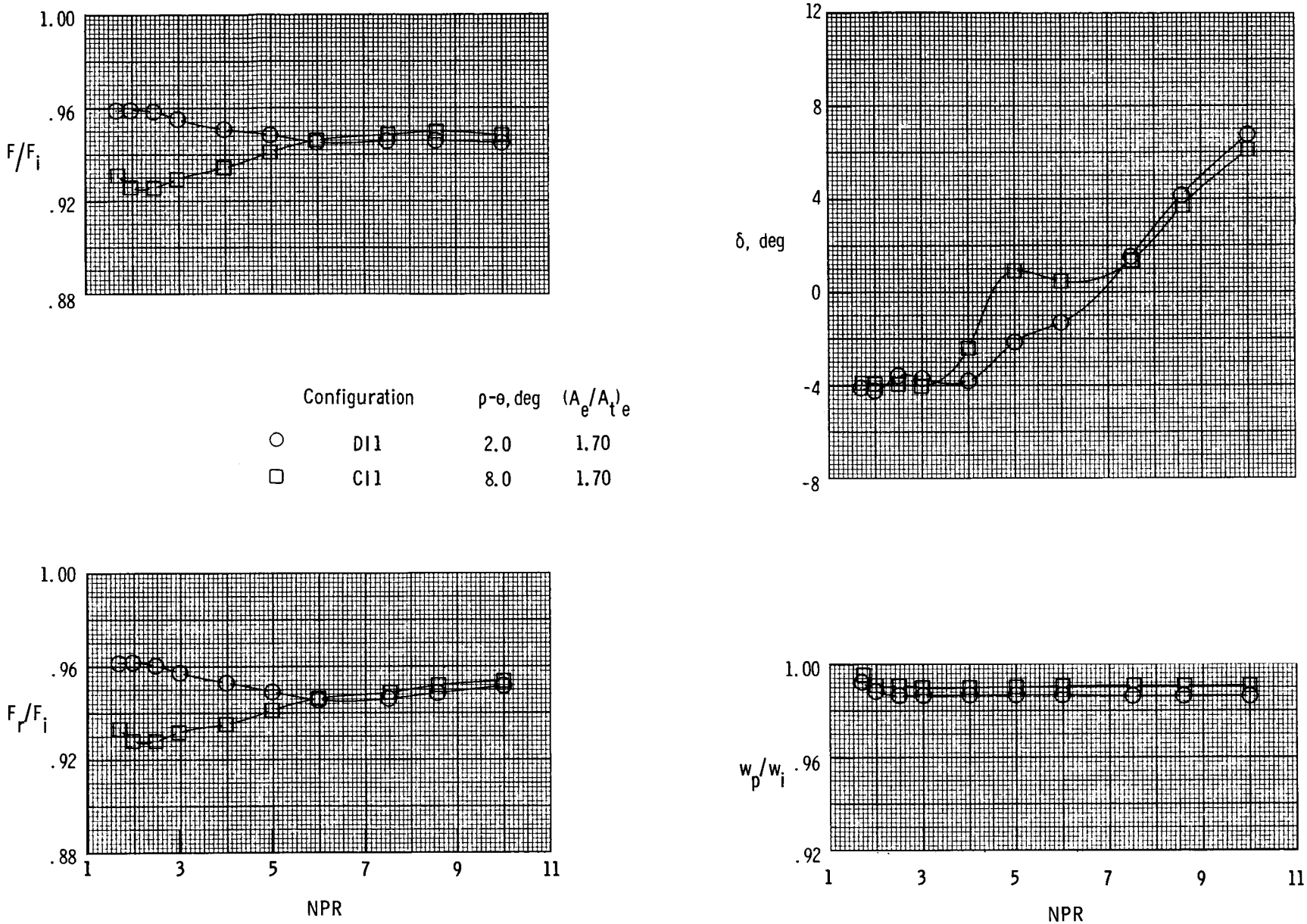

(a) $\beta = 4.0°$.

Figure 9. Effect of initial ramp angle on nozzle performance parameters for $\theta = 8.9°$ and $l_f/h_{t,n} = 4.14$.

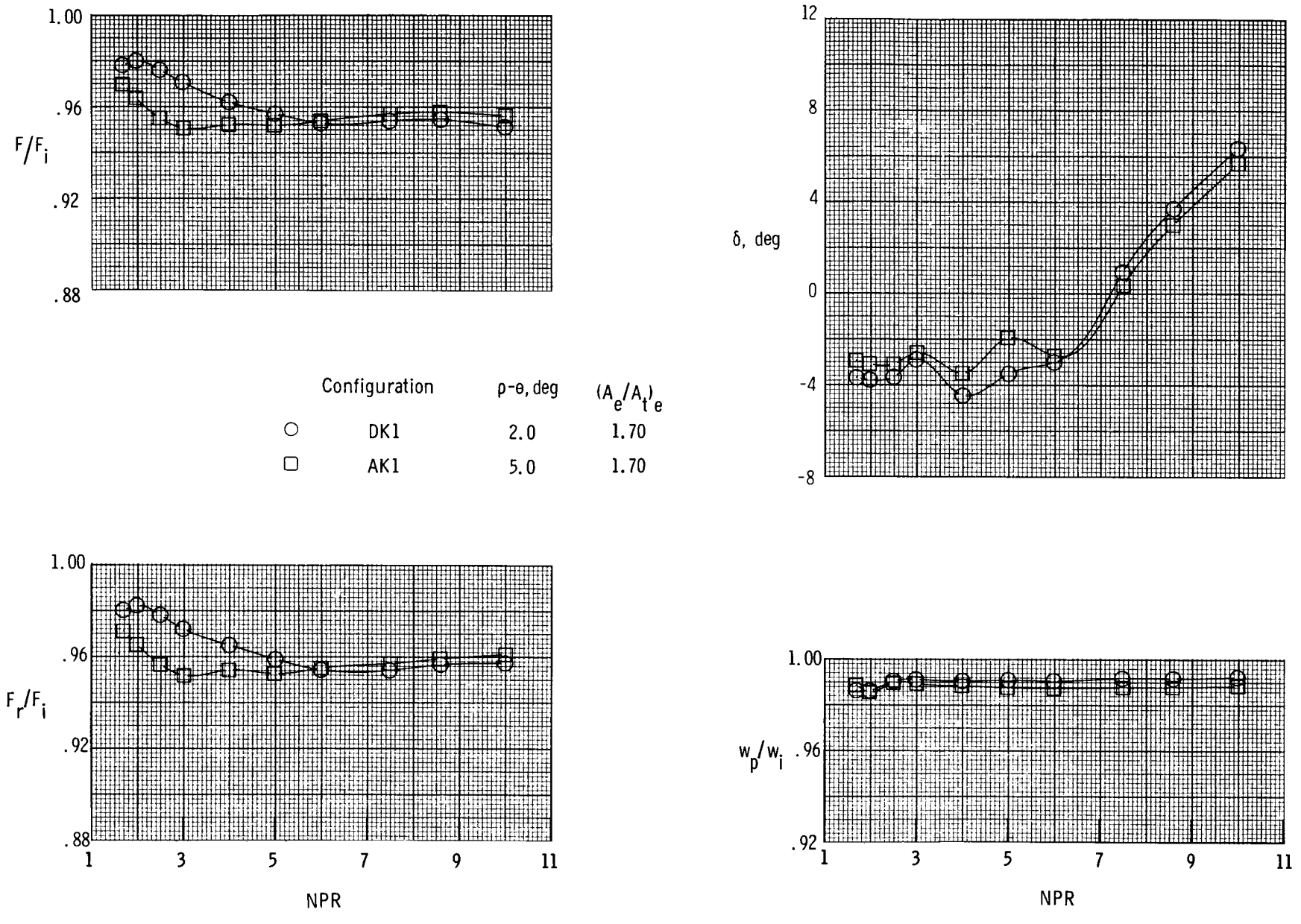

(b) $\beta = 15.0°$.

Figure 9. Continued.

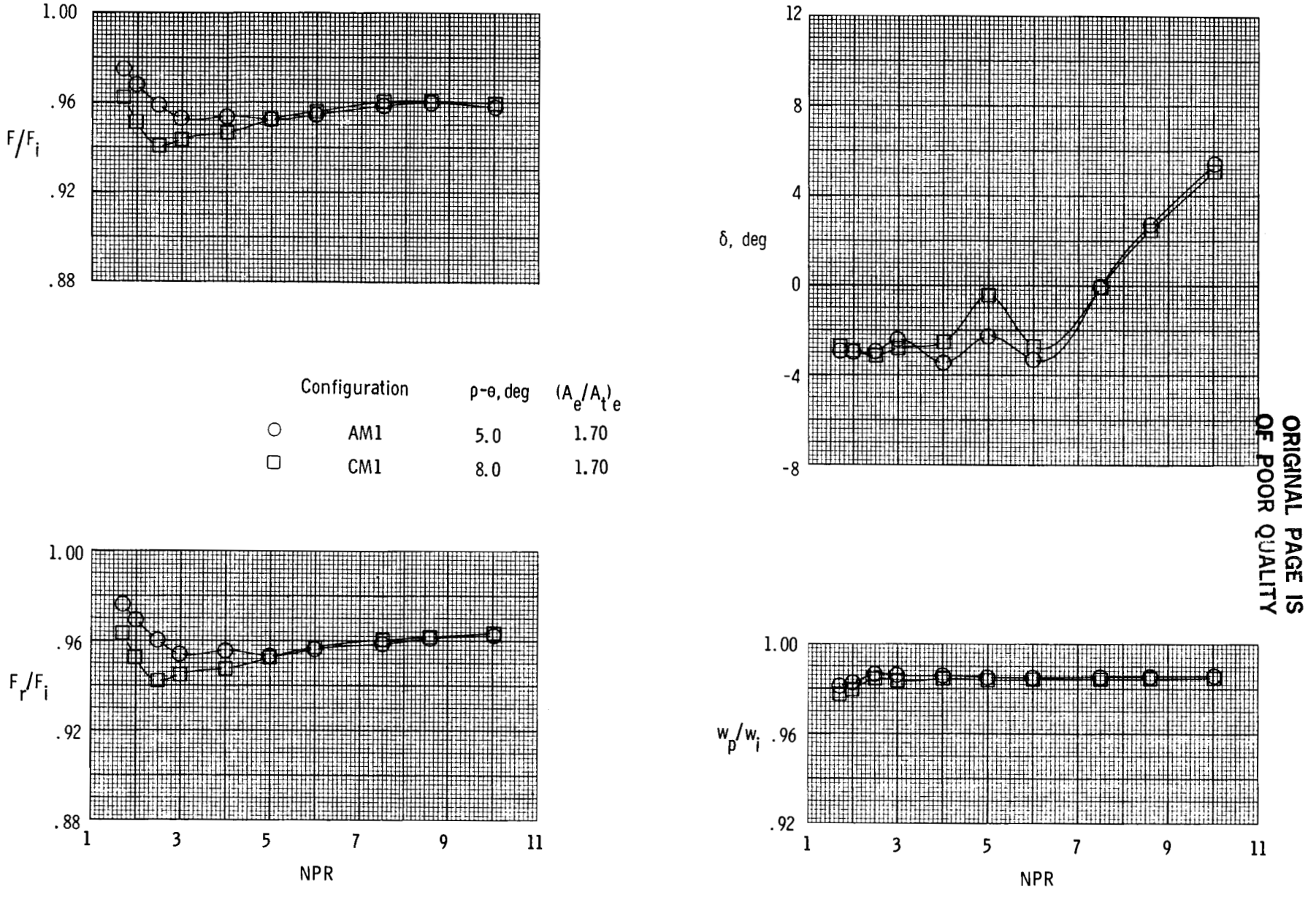

(c) $\beta = 21.0°$.

Figure 9. Concluded.

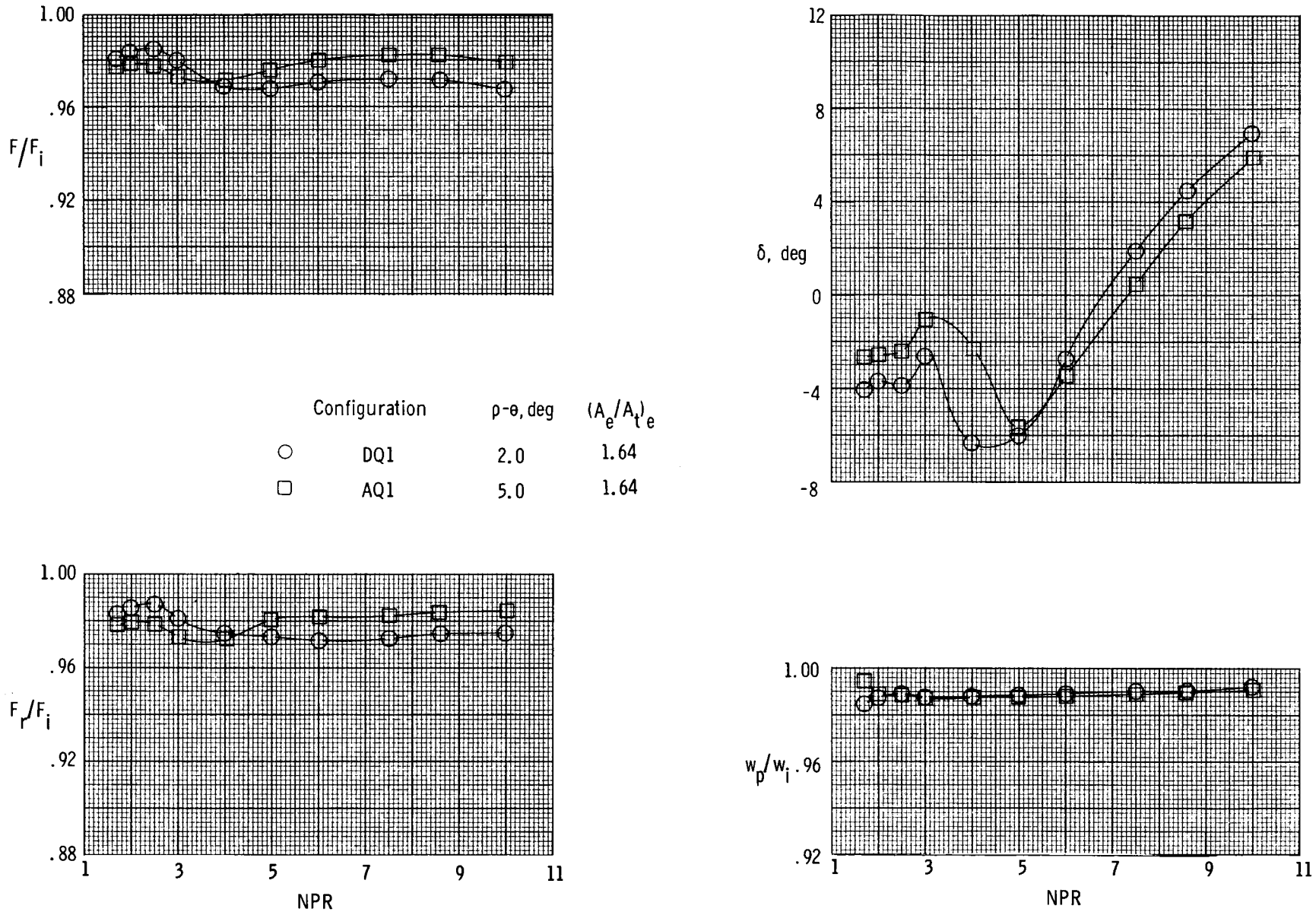

(a) $\beta = 15.0°$.

Figure 10. Effect of initial ramp angle on nozzle performance parameters for $\theta = 8.9°$ and $l_f/h_{t,n} = 4.74$.

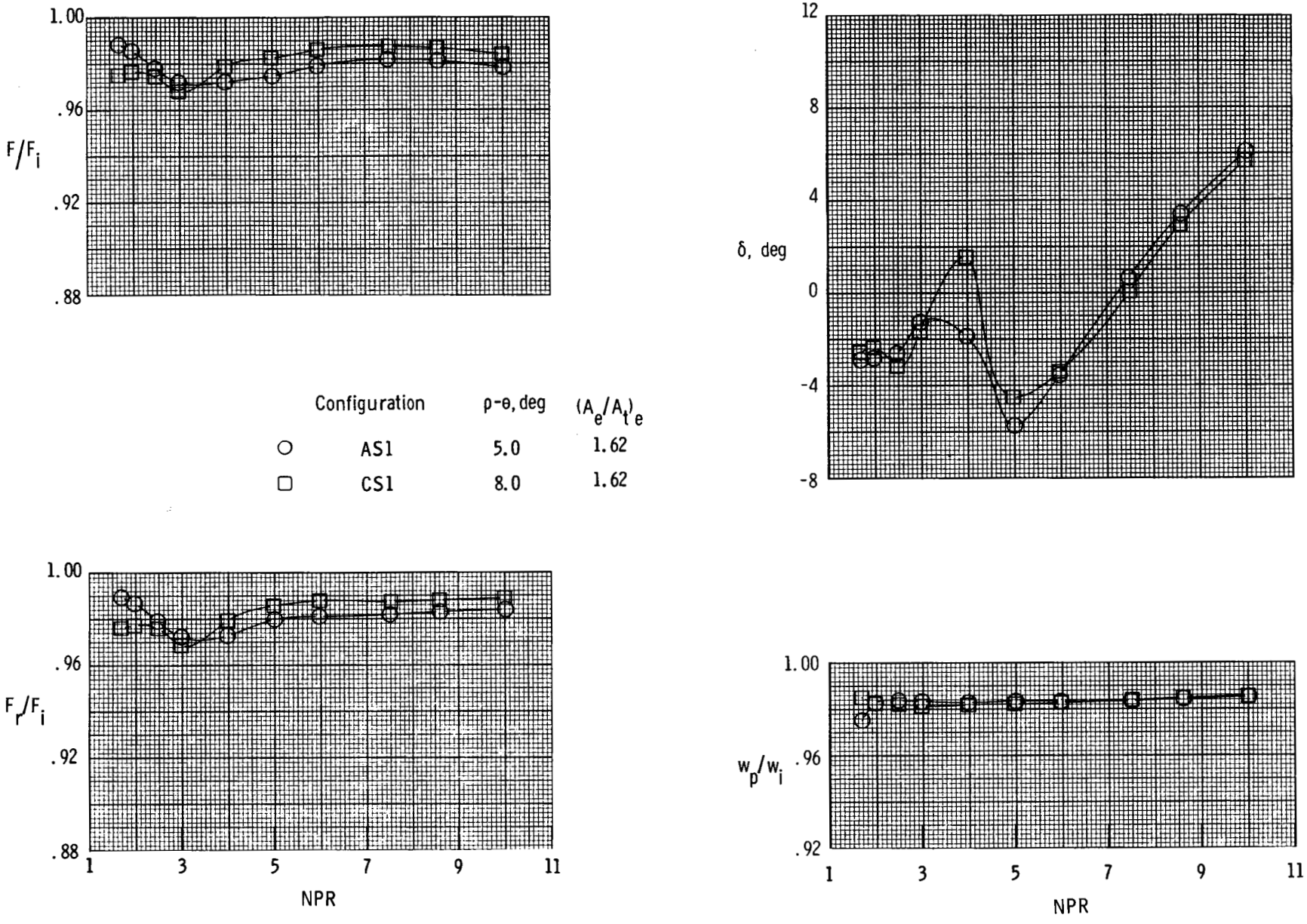

(b) $\beta = 21.0°$.

Figure 10. Concluded.

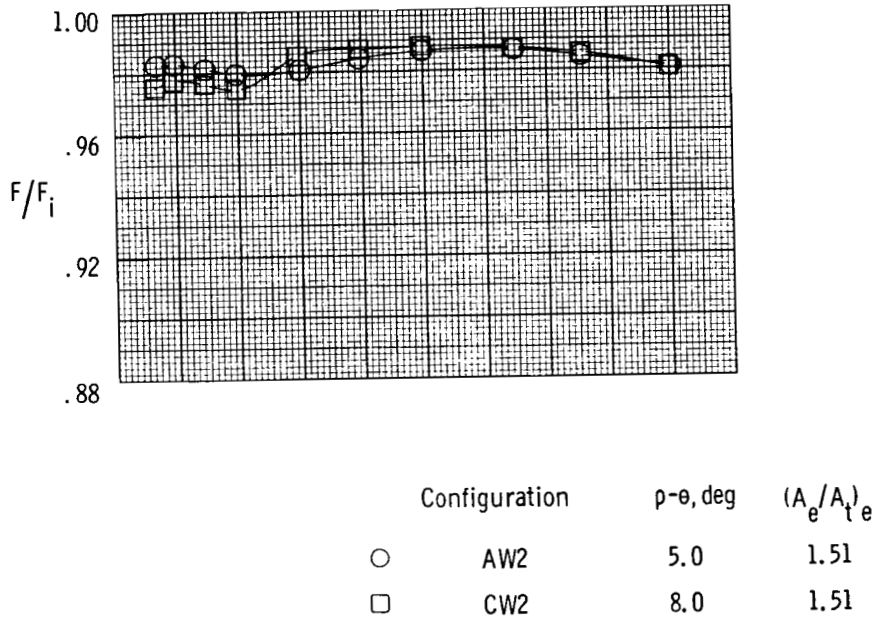

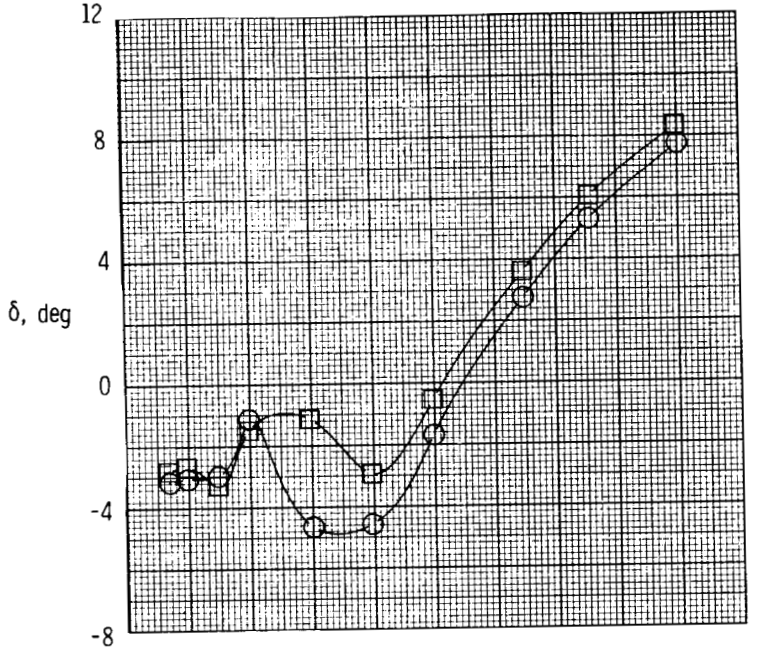

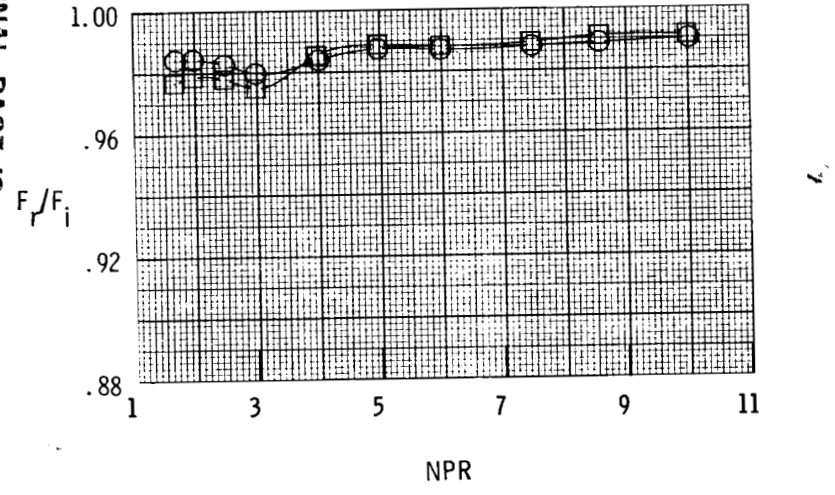

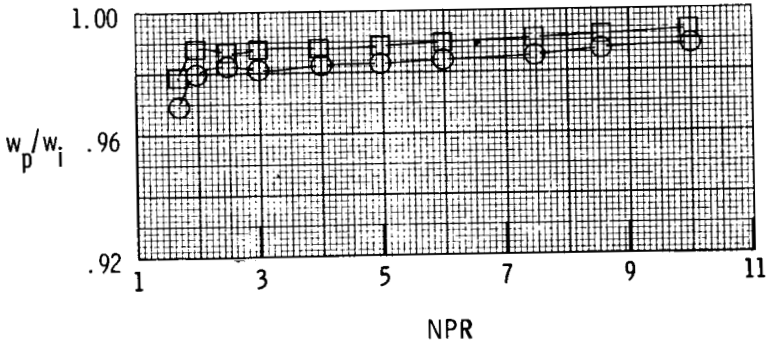

Figure 11. Effect of initial ramp angle on nozzle performance parameters for $\theta = 8.9°$, $l_f/h_{t,n} = 5.14$, and $\beta = 21.0°$.

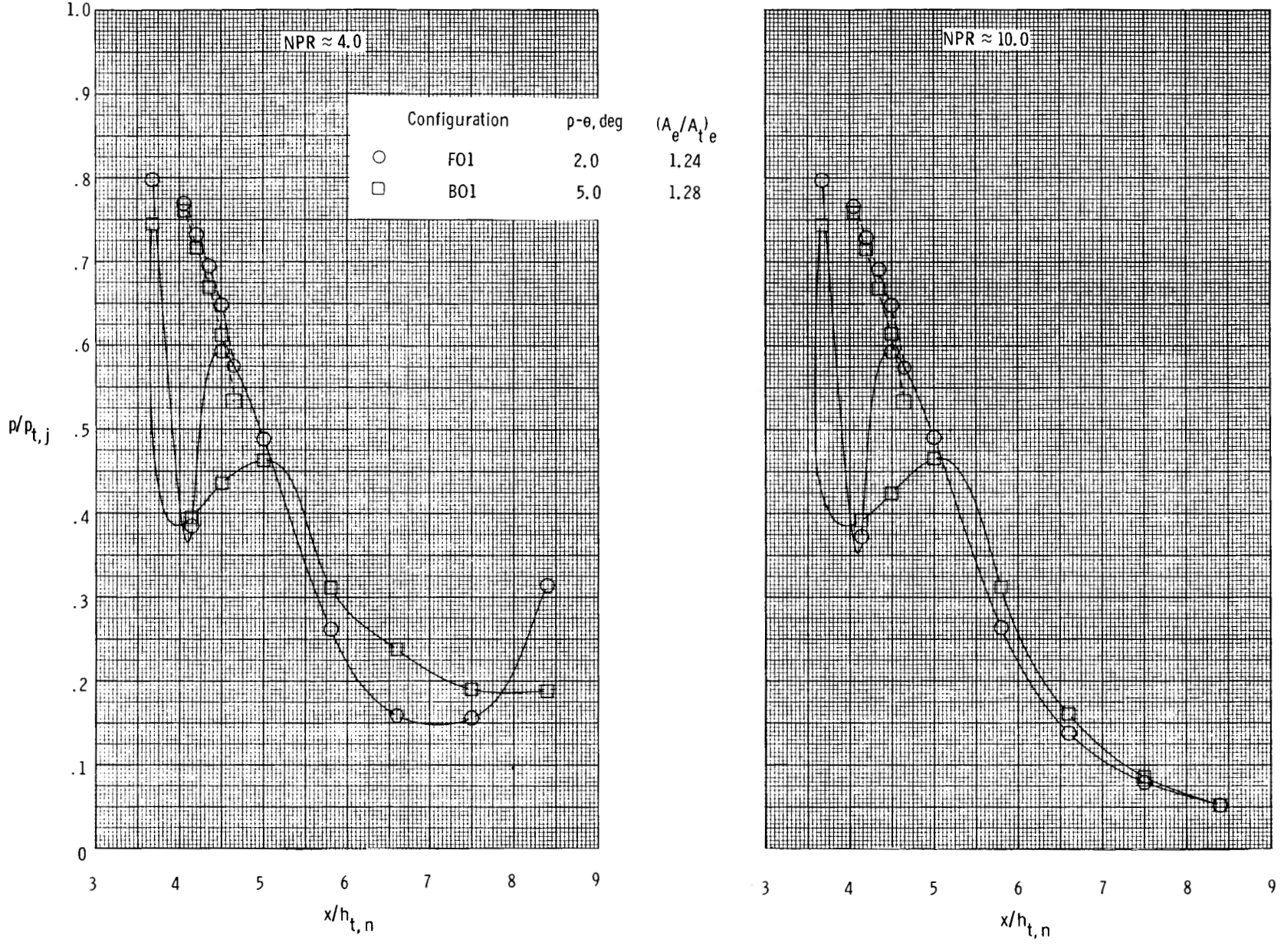

Figure 12. Effect of initial ramp angle on nozzle internal static pressure distributions at two nozzle pressure ratios for $\theta = 4.4°$, $l_f/h_{t,n} = 4.74$, and $\beta = 10.5°$. Dashed lines indicate flap static pressures.

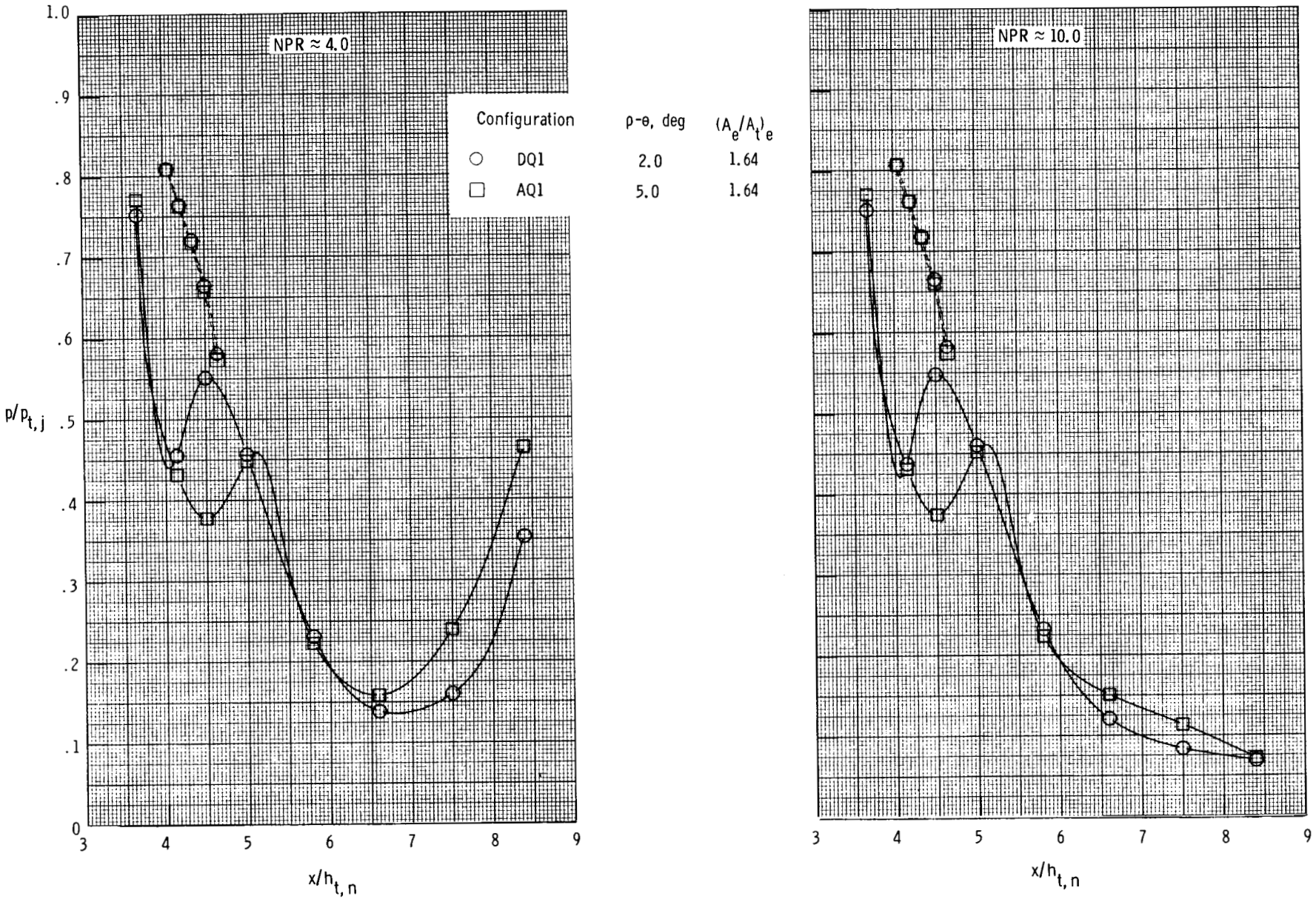

Figure 13. Effect of initial ramp angle on nozzle internal static pressure distributions at two nozzle pressure ratios for $\theta = 8.9°$, $l_f/h_{t,n} = 4.74$, and $\beta = 15.0°$. Dashed lines indicate flap static pressures.

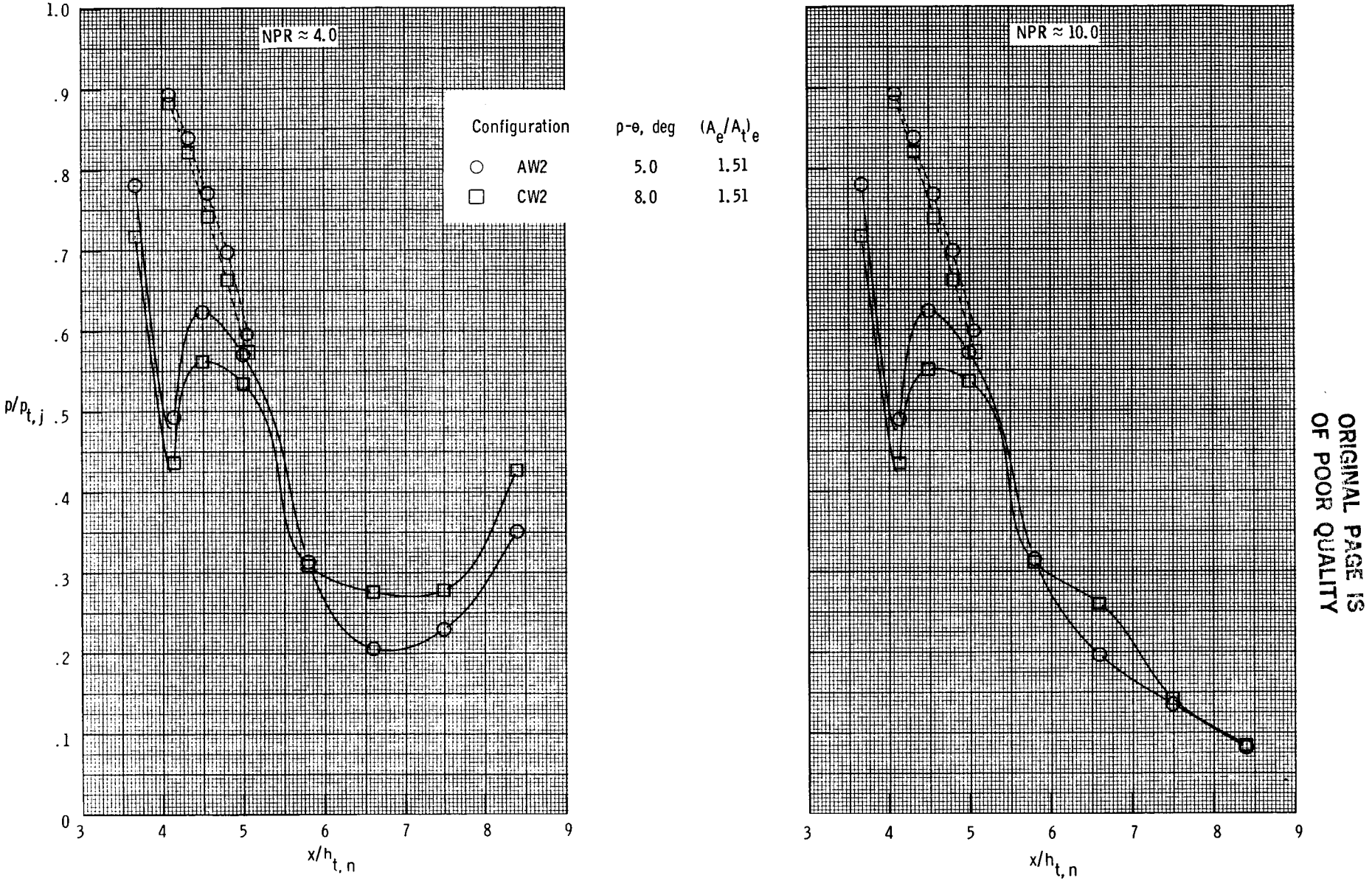

Figure 14. Effect of initial ramp angle on nozzle internal static pressure distributions at two nozzle pressure ratios for $\theta = 8.9°$, $l_f/h_{t,n} = 5.14$, and $\beta = 21.0°$. Dashed lines indicate flap static pressures.

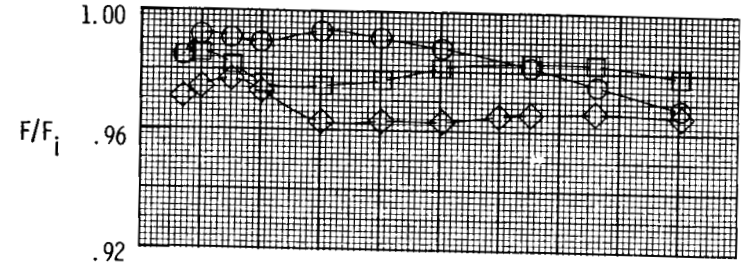

Configuration		$l_r/h_{t,n}$	$(A_e/A_t)_e$
○	HR4	6.14	1.21
□	AR1	3.64	1.60
◇	GR3	11.14	1.99

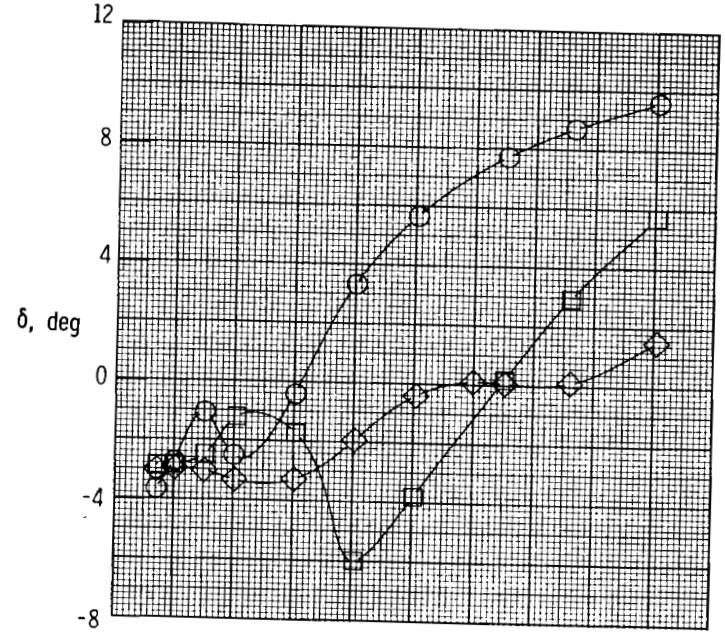

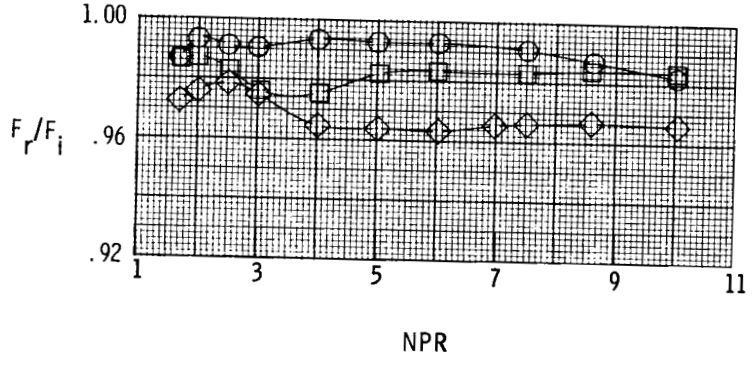

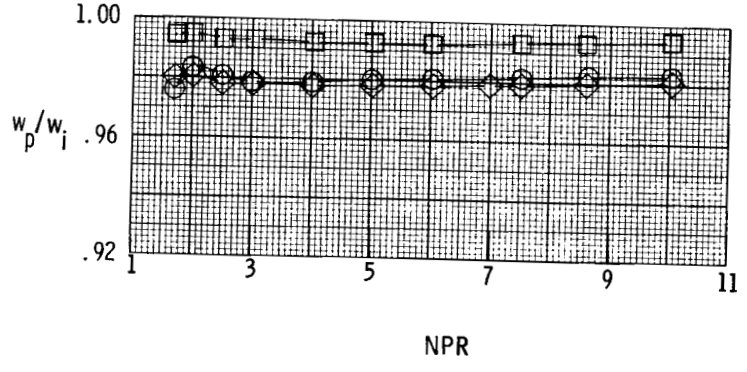

Figure 15. Effect of ramp length on nozzle performance parameters for $\theta = 8.9°$, $\rho - \theta = 5.0°$, $l_f/h_{t,n} = 4.74$, and $\beta = 18.0°$.

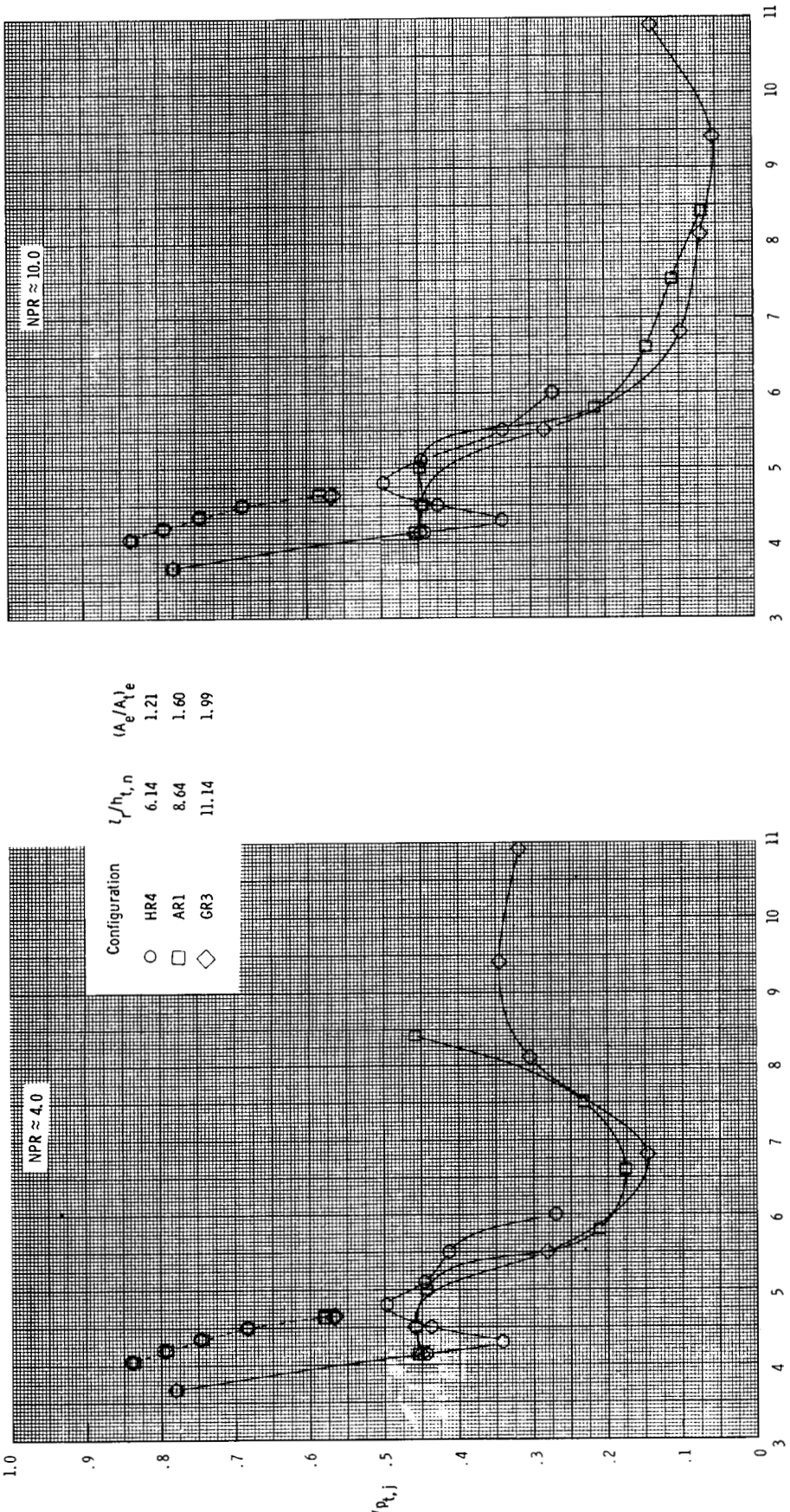

Figure 16. Effect of ramp length on nozzle internal static pressure distributions at two nozzle pressure ratios for $\theta = 8.9°$, $\rho - \theta = 5.0°$, $l_f/h_{t,n} = 4.74$, and $\beta = 18.0°$. Dashed lines indicate flap static pressures.

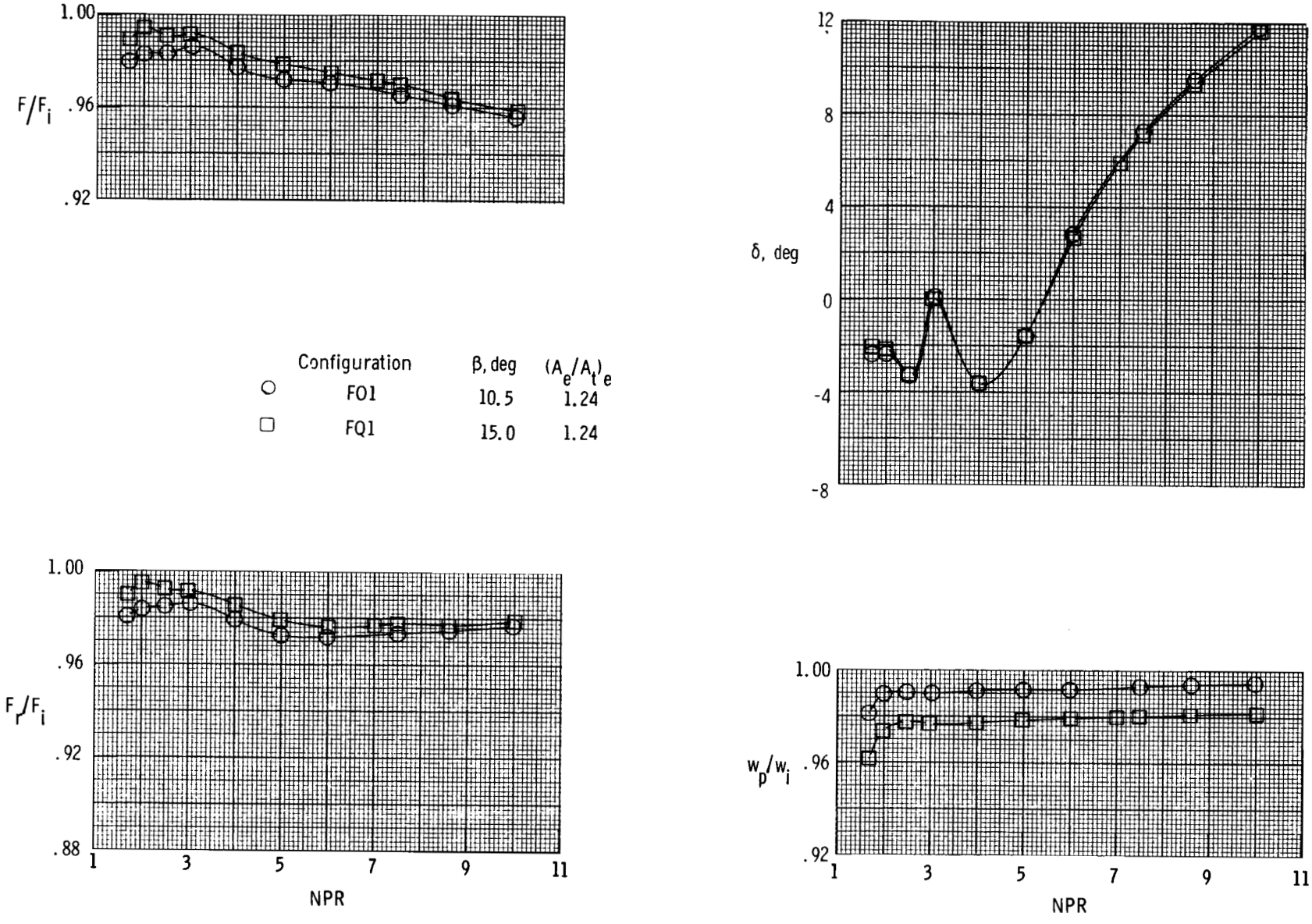

(a) $\rho - \theta = 2.0°$.

Figure 17. Effect of flap angle on nozzle performance parameters for $\theta = 4.4°$ and $l_f/h_{t,n} = 4.74$.

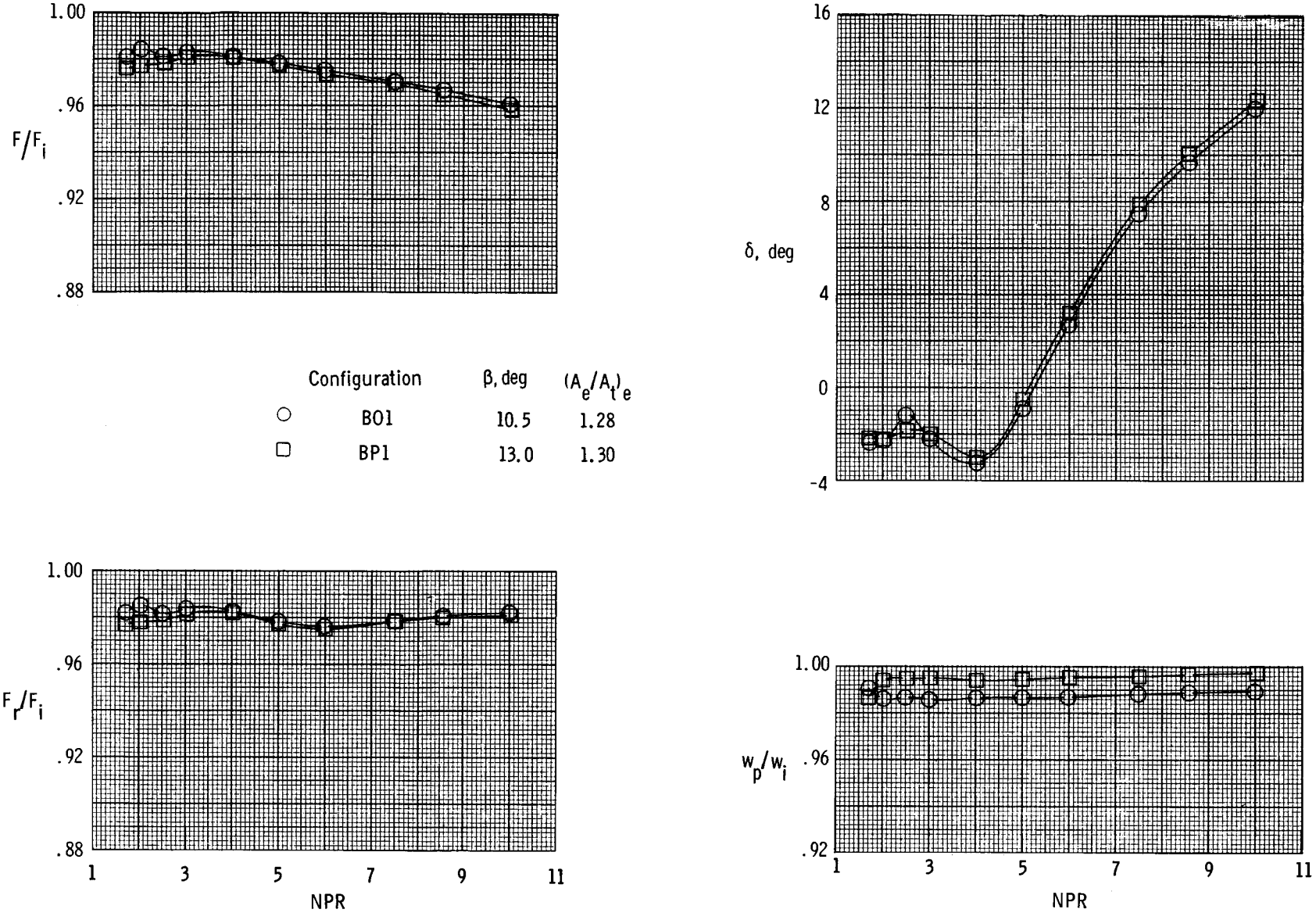

(b) $\rho - \theta = 5.0°$.

Figure 17. Concluded.

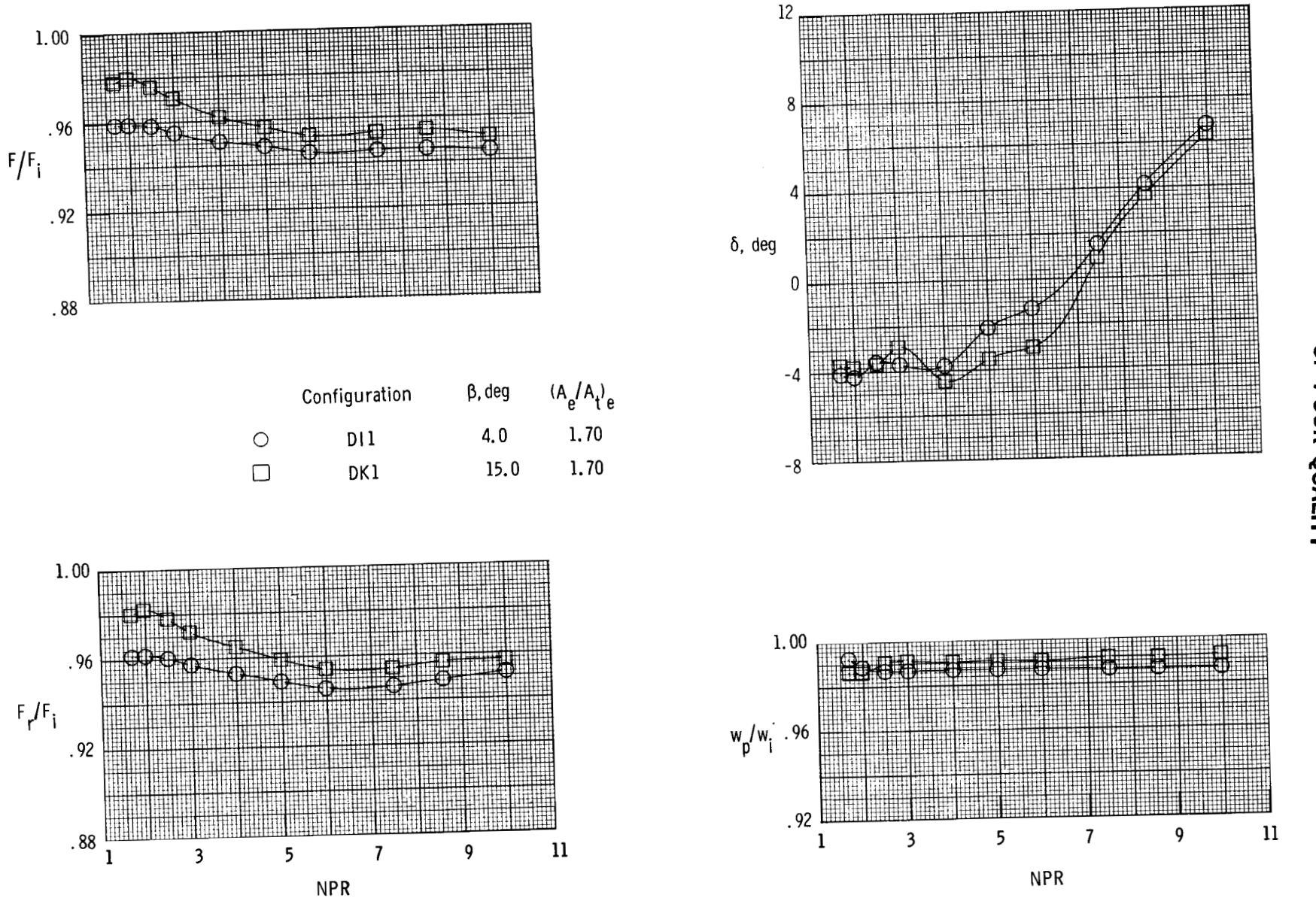

(a) $\rho - \theta = 2.0°$.

Figure 18. Effect of flap angle on nozzle performance parameters for $\theta = 8.9°$ and $l_f/h_{t,n} = 4.14$.

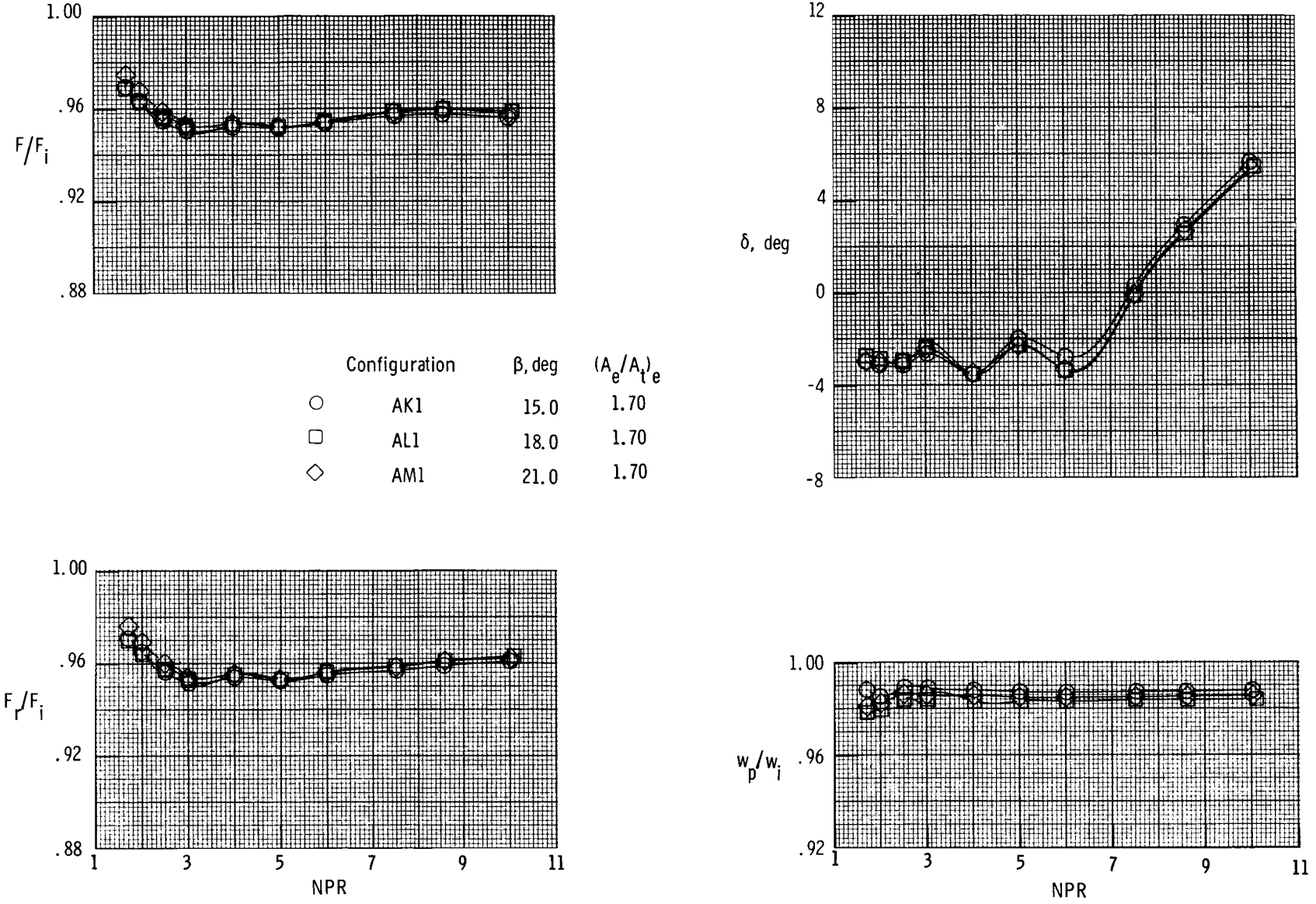

(b) $\rho - \theta = 5.0°$.

Figure 18. Continued.

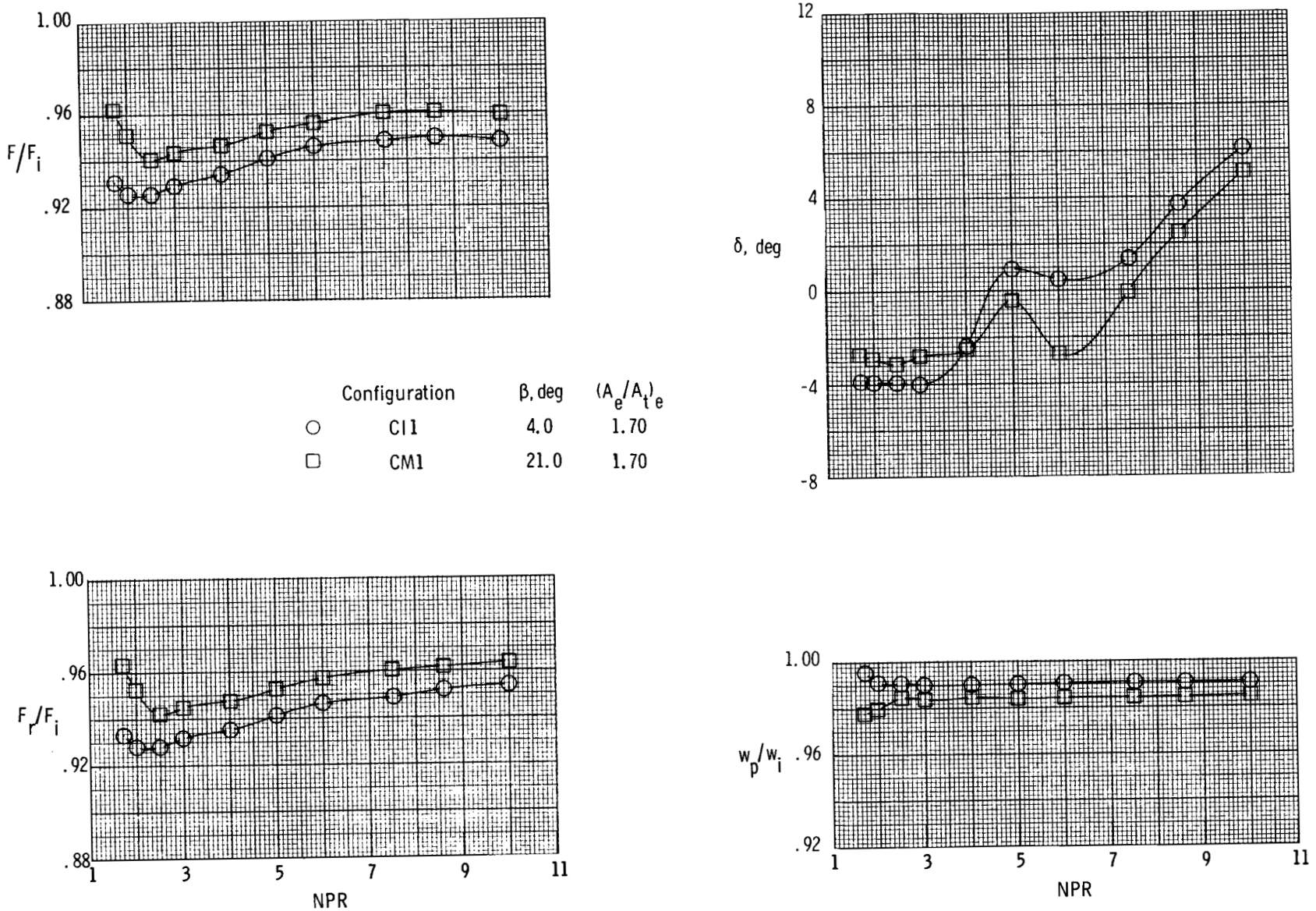

(c) $\rho - \theta = 8.0°$.

Figure 18. Concluded.

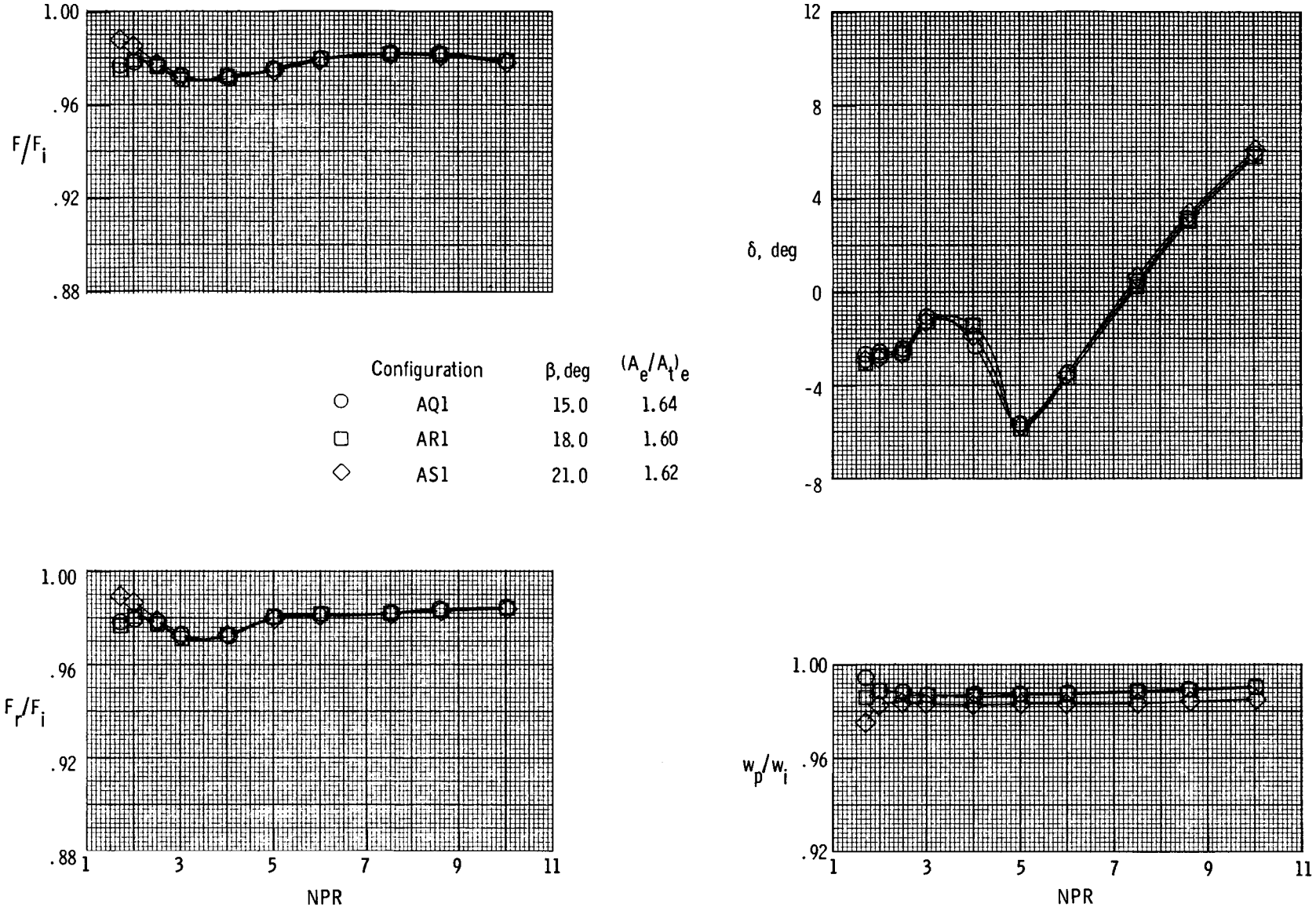

(a) $l_f/h_{t,n} = 4.74$.

Figure 19. Effect of flap angle on nozzle performance parameters for $\theta = 8.9°$ and $\rho - \theta = 5.0°$.

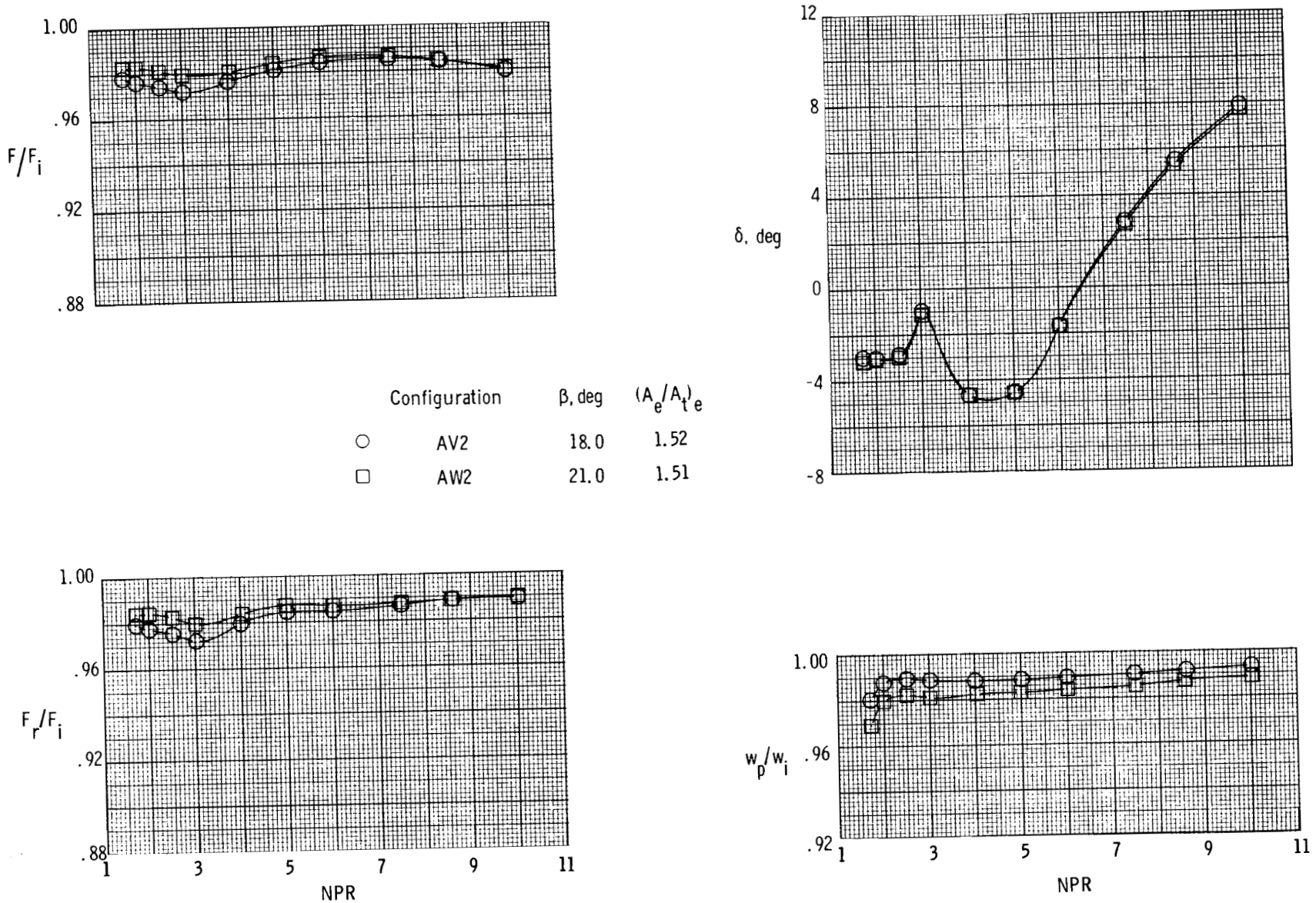

(b) $l_f/h_{t,n} = 5.14$.

Figure 19. Concluded.

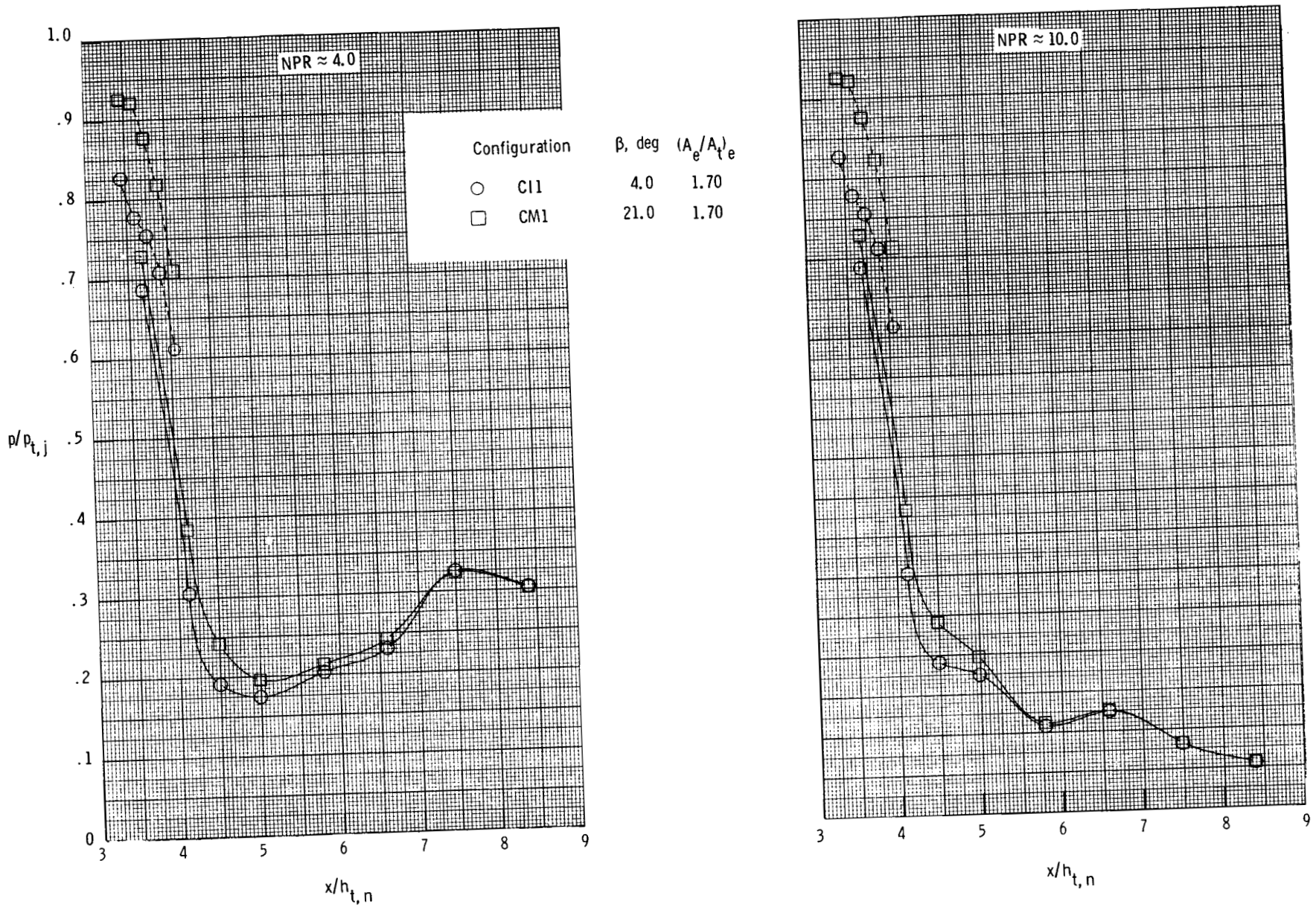

Figure 20. Effect of flap angle on nozzle internal static pressure distributions at two nozzle pressure ratios for $\theta = 8.9°$, $\rho - \theta = 8.0°$, and $l_f/h_{t,n} = 4.14$. Dashed lines indicate flap static pressures.

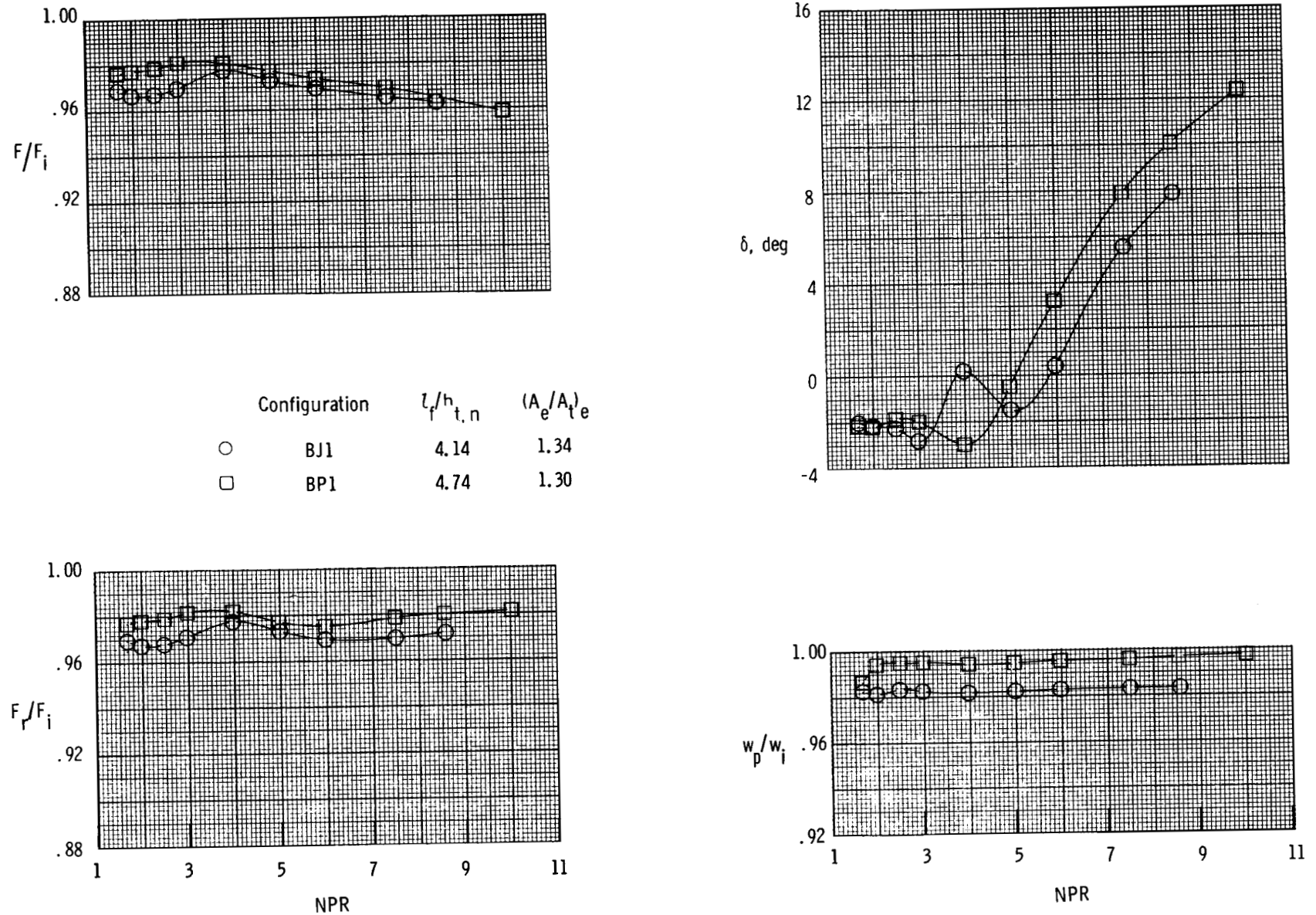

Figure 21. Effect of flap length on nozzle performance parameters for $\theta = 4.4°$, $\rho - \theta = 5.0°$, and $\beta = 13.5°$.

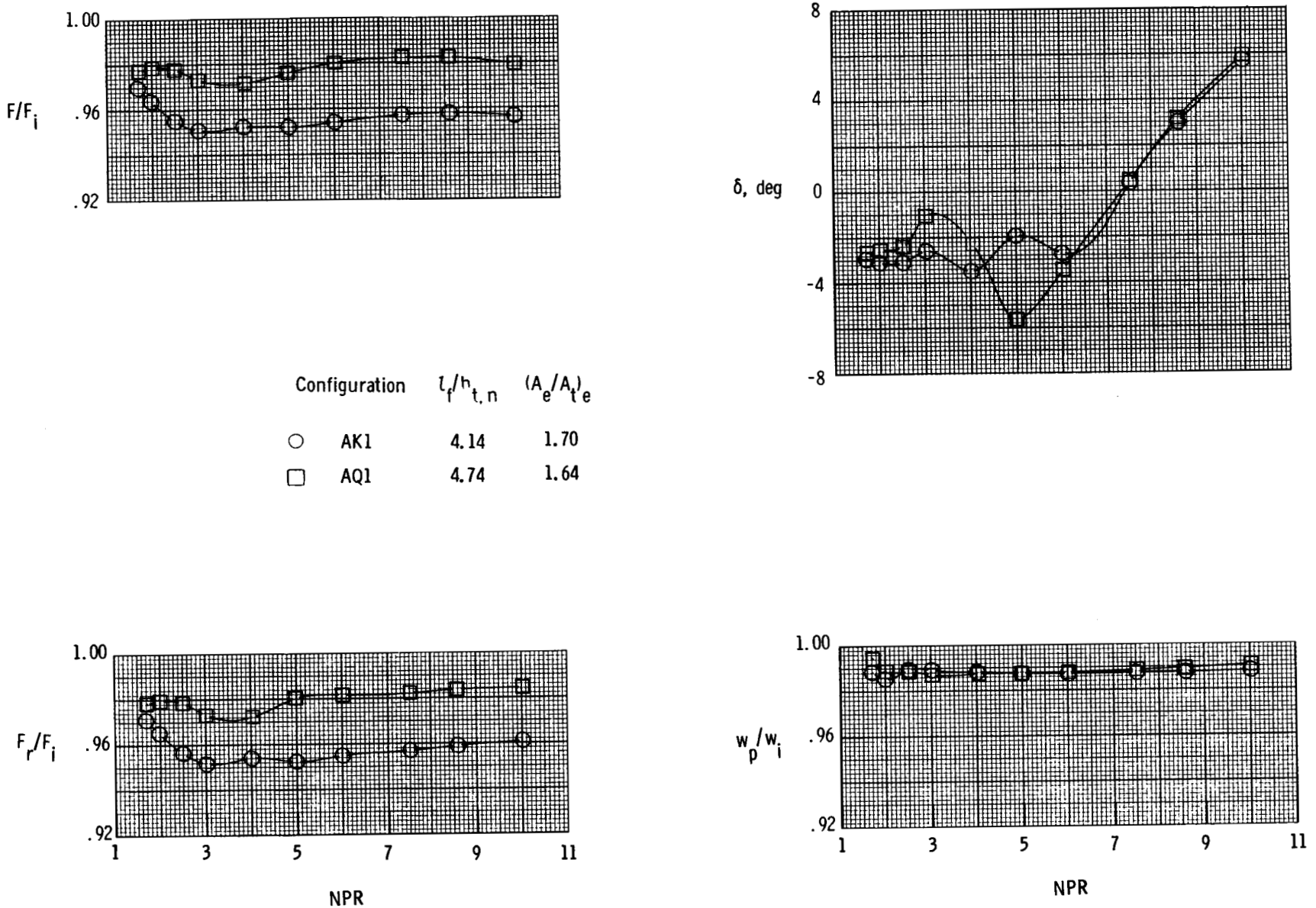

(a) $\beta = 15.0°$.

Figure 22. Effect of flap length on nozzle performance parameters for $\theta = 8.9°$ and $\rho - \theta = 5.0°$.

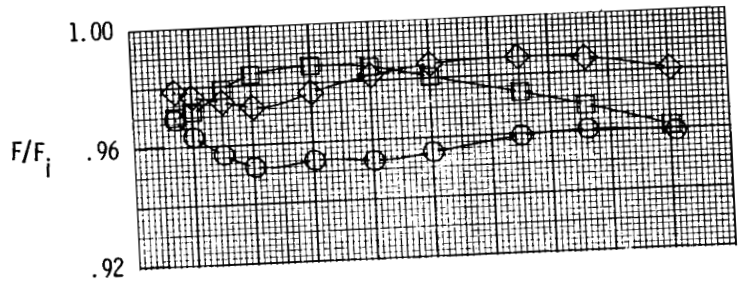

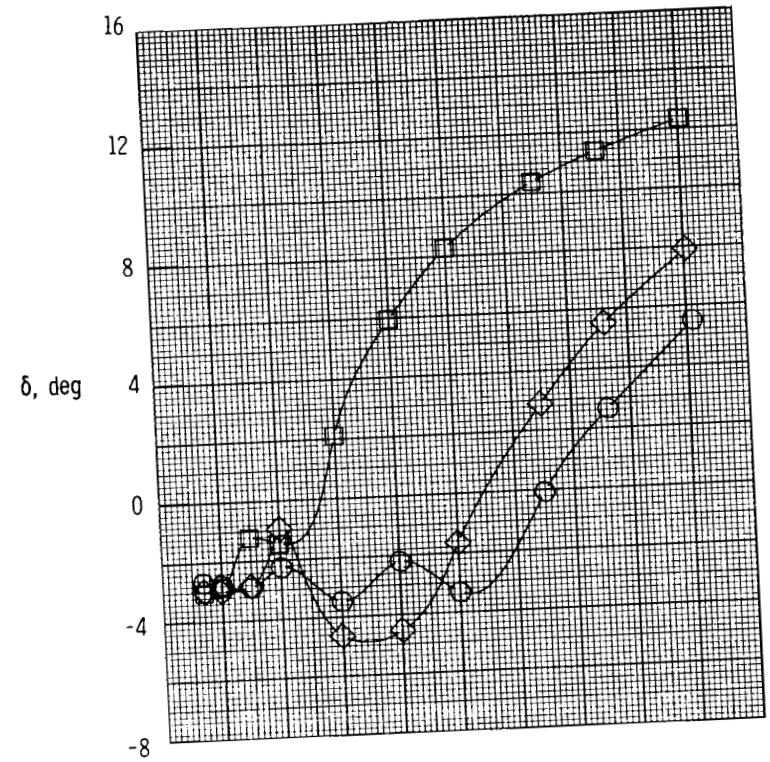

Configuration		$l_f/h_{t,n}$	$(A_e/A_t)_e$
○	AL1	4.14	1.70
□	AR1	4.74	1.60
◇	AV2	5.14	1.52

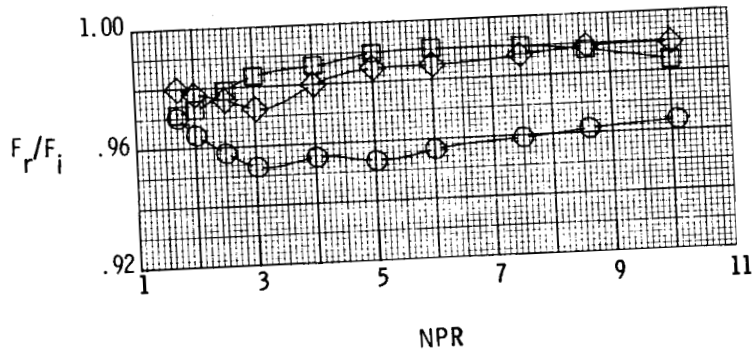

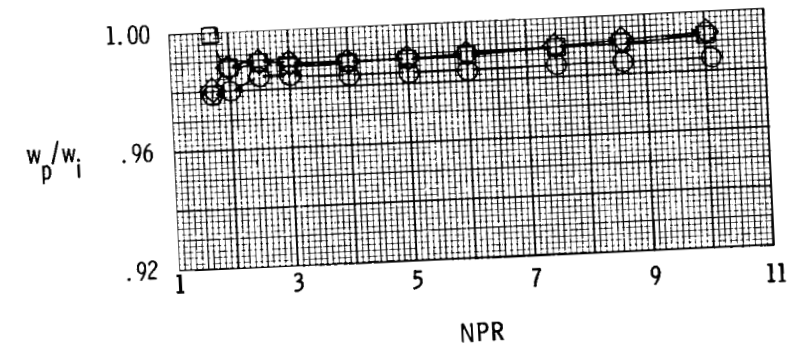

(b) $\beta = 18.0°$.

Figure 22. Continued.

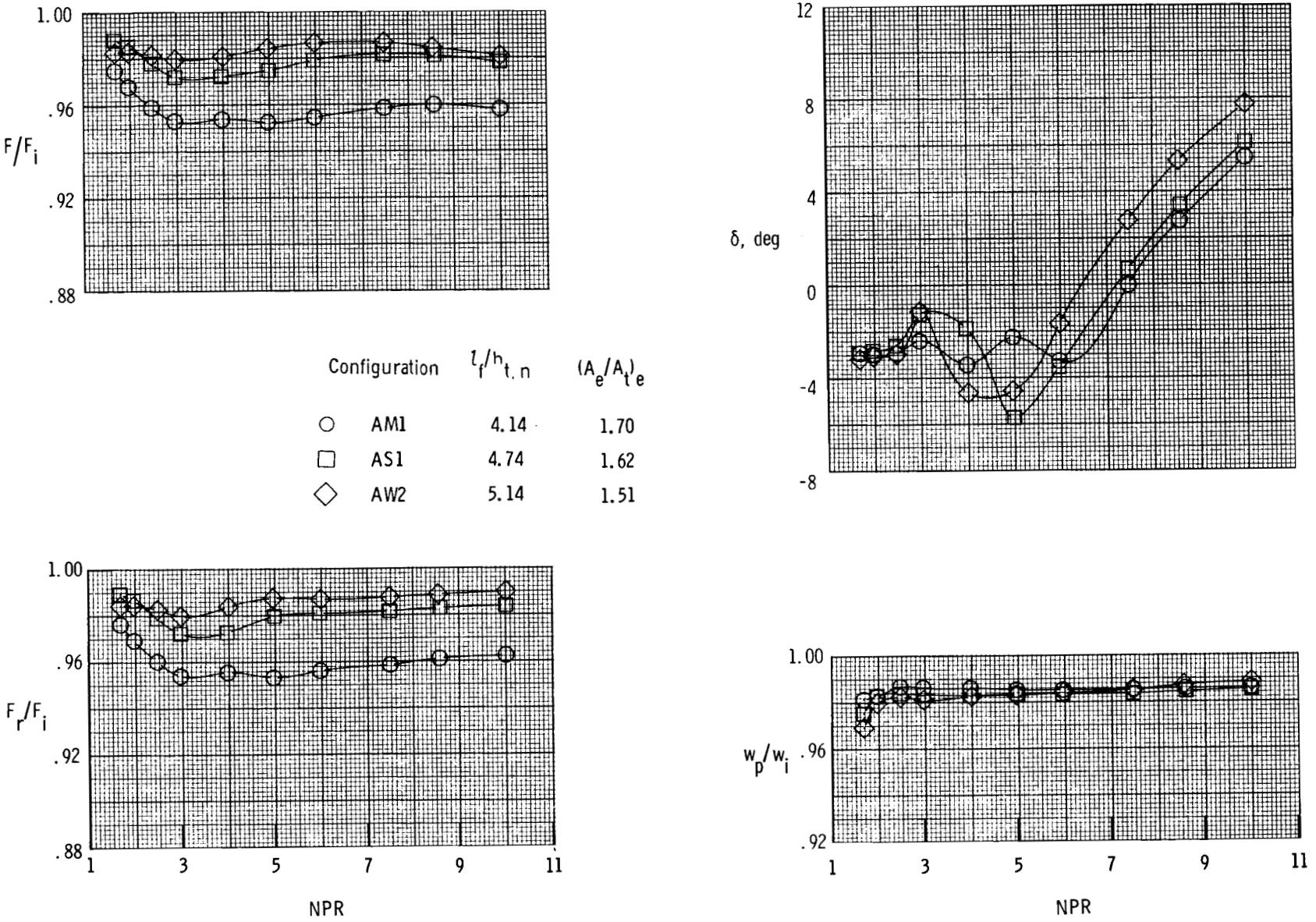

(c) $\beta = 21.0°$.

Figure 22. Concluded.

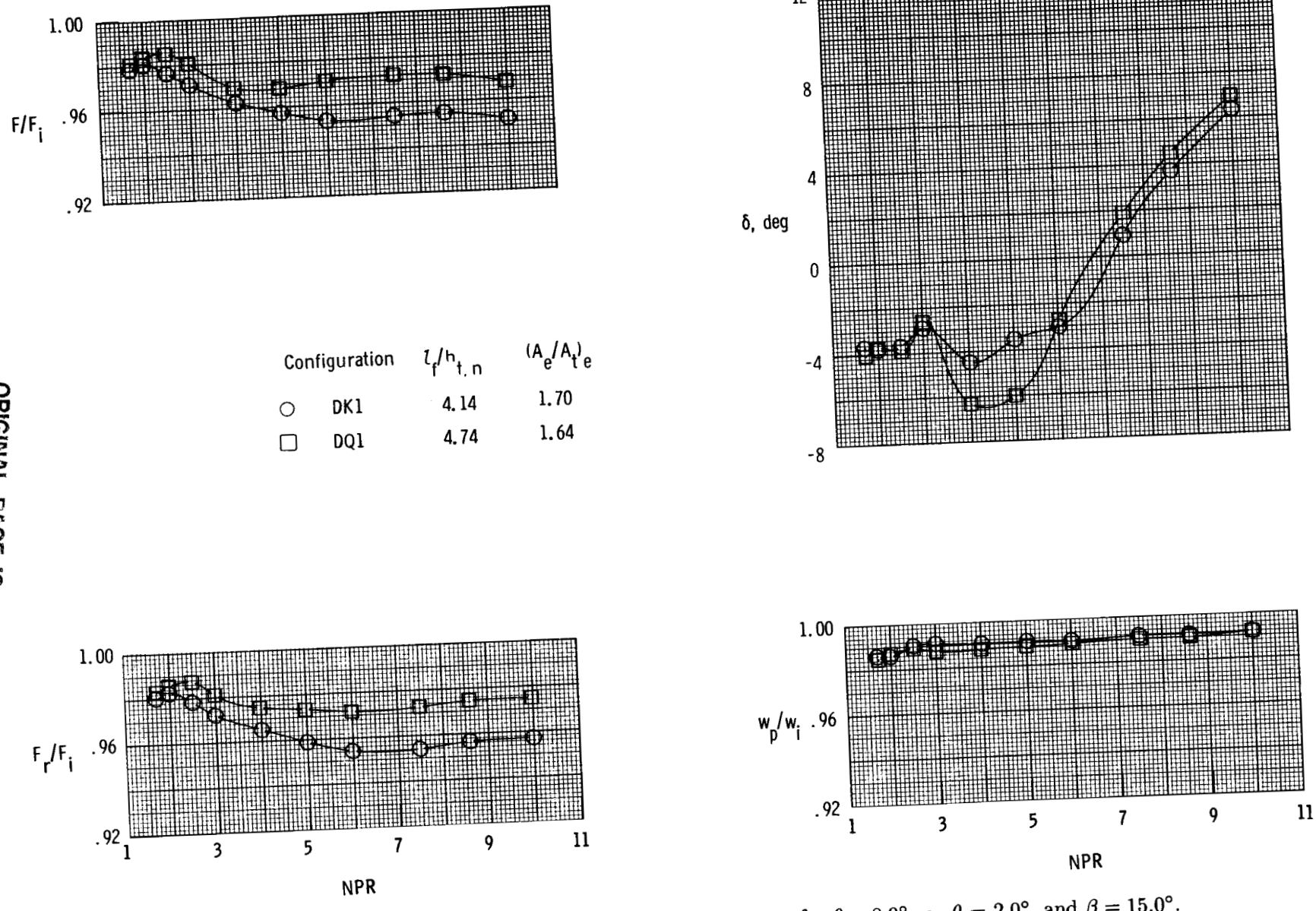

Figure 23. Effect of flap length on nozzle performance parameters for $\theta = 8.9°$, $\rho - \theta = 2.0°$, and $\beta = 15.0°$.

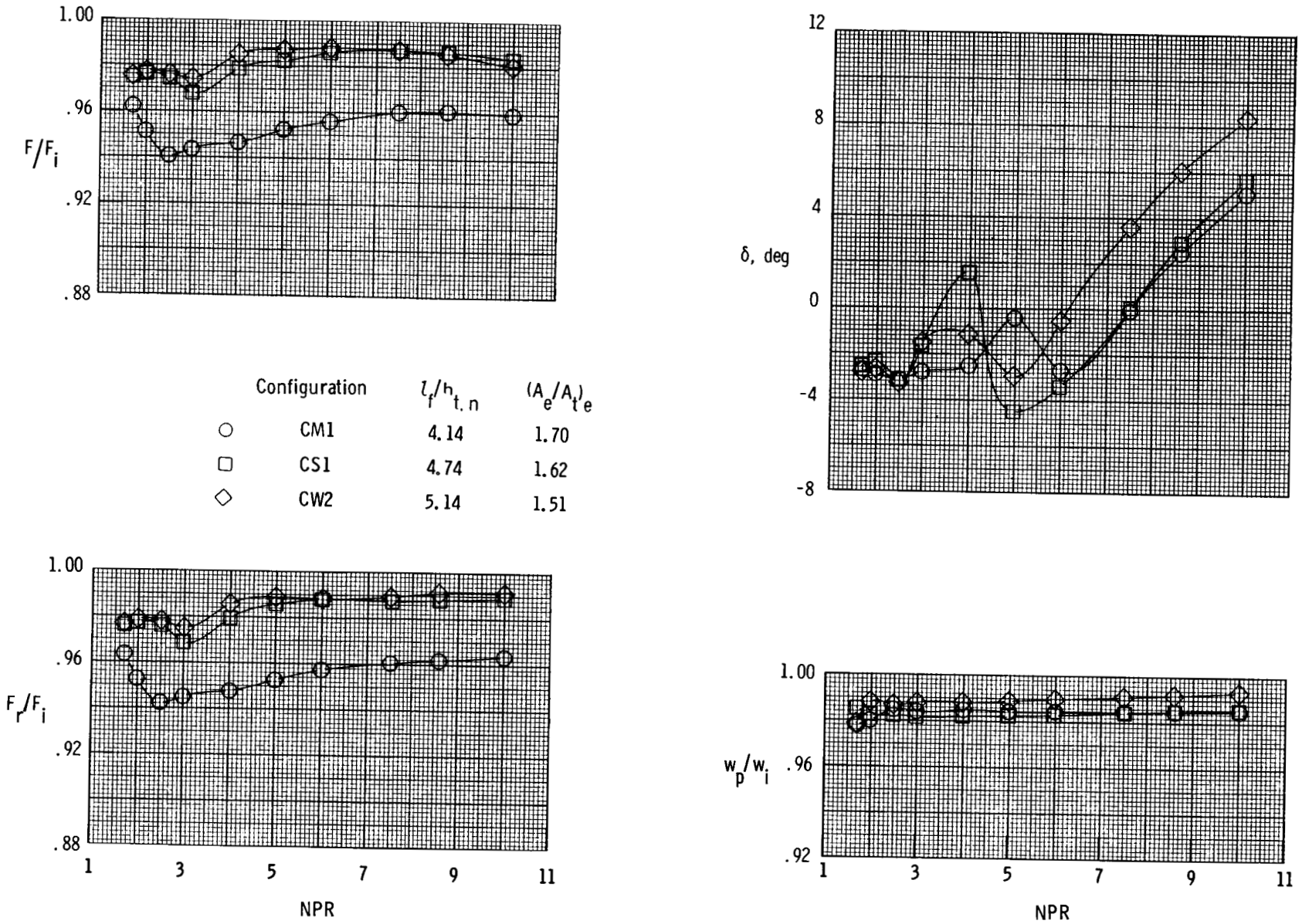

Figure 24. Effect of flap length on nozzle performance parameters for $\theta = 8.9°$, $\rho - \theta = 8.0°$, and $\beta = 21.0°$.

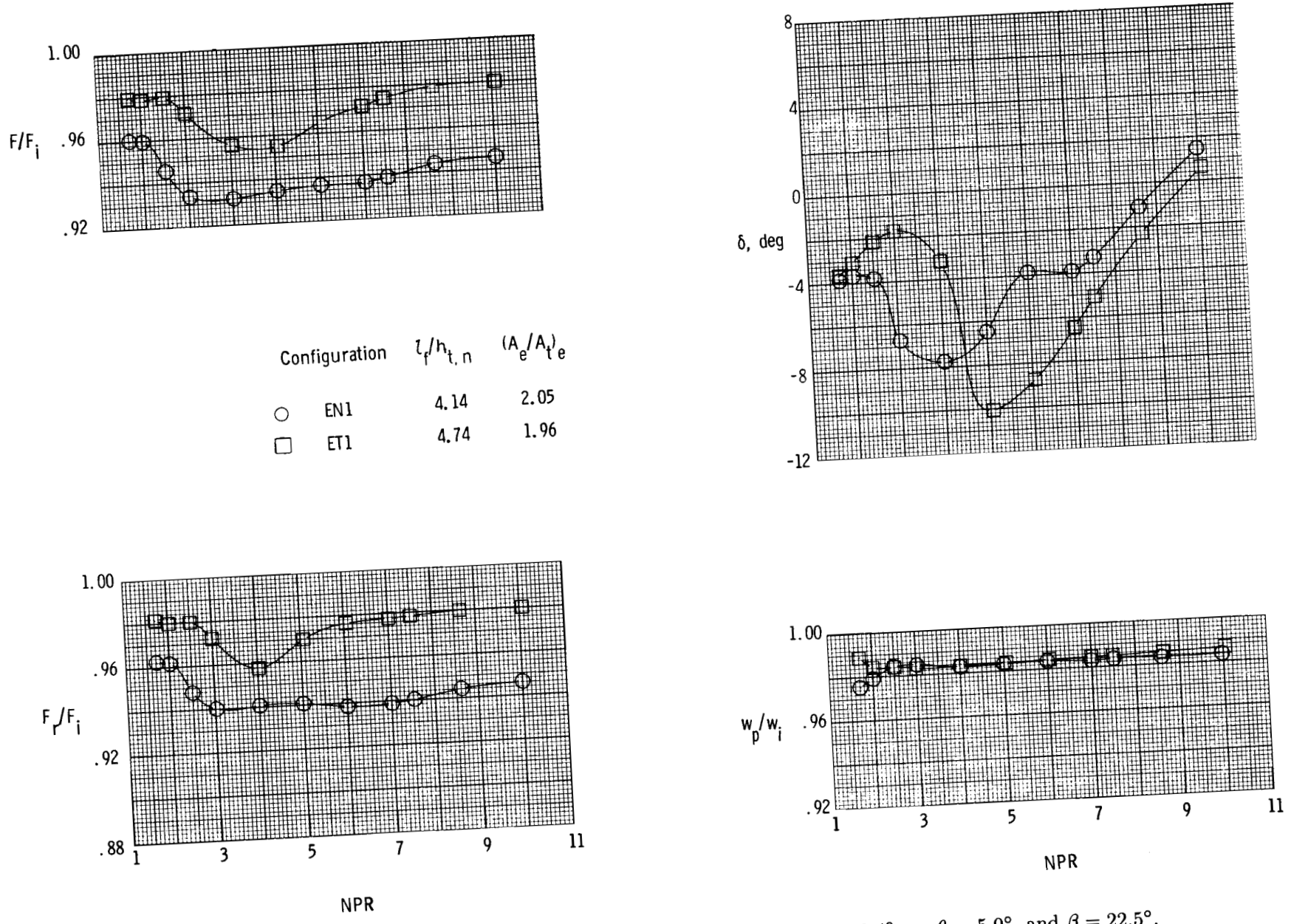

Figure 25. Effect of flap length on nozzle performance parameters for $\theta = 13.4°$, $\rho - \theta = 5.0°$, and $\beta = 22.5°$.

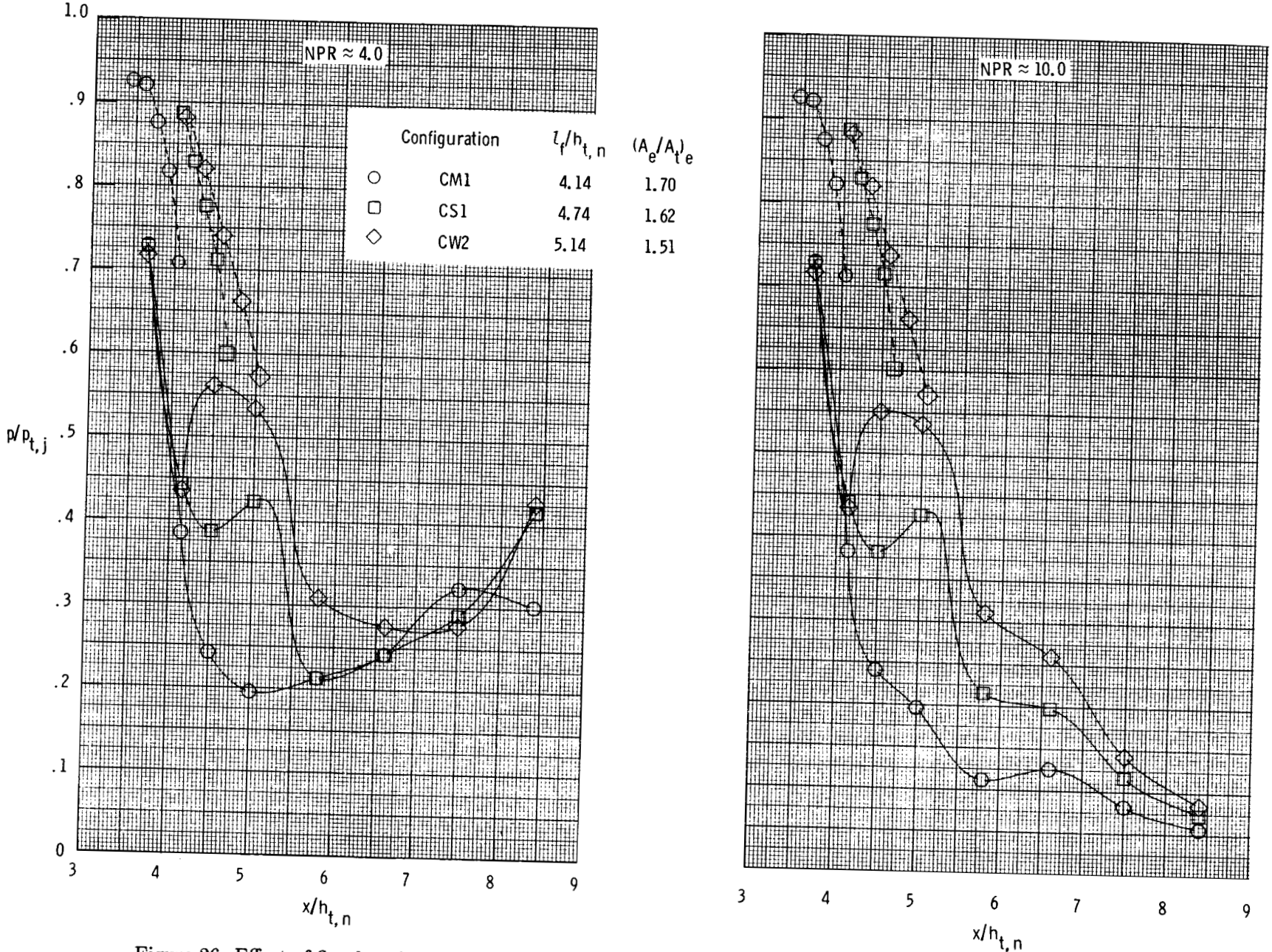

Figure 26. Effect of flap length on nozzle internal static pressure distributions at two nozzle pressure ratios for $\theta = 8.9°$, $\rho - \theta = 8.0°$, and $\beta = 21.0°$. Dashed lines indicate flap static pressures.

Appendix A

Internal Geometry of Ramps and Flaps

The internal geometry of all ramps tested is given in table A1, and the geometry of all flaps tested is given in table A2. The geometry is presented in terms of nondimensionalized x and y locations.

Table A1. Ramp Geometry

All ramps		Ramp A		Ramp B		Ramp C		Ramp D	
$x/h_{t,n}$	$y/h_{t,n}$	$x/h_{t,n}$	$y/h_{t,n}$	$x/h_{t,n}$	$y/h_{t,n}$	$x/h_{t,n}$	$y/h_{t,n}$	$x/h_{t,n}$	$y/h_{t,n}$
0.000	1.389	4.296	0.019	4.231	0.006	4.251	0.010	4.251	0.010
2.350	1.299	6.095	.464	4.246	.009	4.275	.014	4.263	.012
2.405	1.294	6.126	.472	5.080	.147	4.329	.028	6.613	.464
2.449	1.286	6.157	.479	5.099	.150	5.765	.464	6.714	.483
2.504	1.272	6.219	.493	5.118	.153	5.824	.481	6.816	.502
2.559	1.252	6.281	.507	5.157	.159	5.882	.497	6.917	.519
2.603	1.232	6.342	.519	5.195	.165	5.941	.512	7.018	.536
2.658	1.202	6.404	.531	5.233	.170	6.000	.525	7.120	.551
2.702	1.173	6.466	.542	5.272	.165	6.059	.537	7.221	.566
2.757	1.133	6.528	.552	5.310	.179	6.117	.548	7.322	.580
2.801	1.096	6.590	.562	5.349	.184	6.176	.558	7.424	.594
2.856	1.044	6.651	.571	5.387	.188	6.235	.566	7.525	.606
2.900	.999	6.713	.579	5.425	.192	6.294	.574	7.627	.618
3.600	.239	6.775	.587	5.464	.195	6.352	.581	7.728	.629
3.654	.184	6.837	.594	5.502	.199	6.411	.588	7.829	.639
3.708	.139	6.899	.601	5.541	.202	6.470	.593	7.931	.649
3.751	.108	6.960	.608	5.579	.205	6.529	.599	8.032	.658
3.805	.076	7.022	.613	5.618	.208	6.587	.603	8.133	.666
3.859	.050	7.084	.619	5.656	.211	6.646	.607	8.235	.673
3.902	.034	7.146	.624	5.694	.213	6.705	.611	8.336	.680
3.956	.019	7.208	.628	5.733	.215	6.764	.614	8.437	.686
4.010	.009	7.269	.633	5.771	.218	6.823	.617	8.539	.692
4.054	.004	7.331	.637	5.810	.220	6.881	.620	8.640	.696
4.108	.001	7.393	.640	5.848	.222	6.940	.622		
4.140	.000	7.455	.644	5.886	.224	8.640	.696		
4.152	.000	7.516	.647	5.925	.226				
4.202	.003	7.578	.650	5.963	.227				
		7.609	.651	6.002	.229				
		7.640	.653	6.021	.230				
		8.640	.696	6.040	.231				
				8.640	.344				

Table A1. Concluded

All ramps		Ramp E		Ramp F		Ramp G		Ramp H	
$x/h_{t,n}$	$y/h_{t,n}$	$x/h_{t,n}$	$y/h_{t,n}$	$x/h_{t,n}$	$y/h_{t,n}$	$x/h_{t,n}$	$y/h_{t,n}$	$x/h_{t,n}$	$y/h_{t,n}$
0.000	1.389	4.251	0.010	4.213	0.004	4.296	0.019	4.251	0.010
2.350	1.299	4.275	.014	5.500	.149	7.174	.731	4.296	.019
2.405	1.294	4.307	.022	5.600	.160	7.224	.743	5.032	.203
2.449	1.286	4.327	.028	5.700	.170	7.273	.755	5.046	.207
2.504	1.272	4.345	.033	5.800	.180	7.372	.777	5.061	.210
2.559	1.252	6.357	.703	5.900	.190	7.470	.798	5.089	.217
2.603	1.232	6.471	.759	6.000	.199	7.569	.818	5.131	.225
2.658	1.202	6.585	.773	6.100	.208	7.667	.836	5.174	.234
2.702	1.173	6.700	.804	6.200	.216	7.766	.854	5.216	.241
2.757	1.133	6.814	.833	6.300	.225	7.865	.870	5.259	.247
2.801	1.096	6.928	.860	6.400	.232	7.963	.884	5.301	.253
2.856	1.044	7.042	.884	6.500	.240	8.062	.898	5.344	.259
2.900	.999	7.156	.906	6.600	.247	8.161	.911	5.386	.263
3.600	.239	7.270	.926	6.700	.253	8.259	.923	5.429	.268
3.654	.184	7.384	.944	6.800	.260	8.358	.934	5.471	.271
3.708	.139	7.499	.961	6.900	.266	8.457	.945	5.514	.275
3.751	.108	7.613	.976	7.000	.272	8.555	.954	5.556	.278
3.805	.076	7.727	.989	7.100	.277	8.654	.963	5.598	.280
3.859	.050	7.841	1.001	7.200	.282	8.752	.971	5.641	.283
3.902	.034	7.955	1.011	7.300	.287	8.851	.978	5.683	.285
3.956	.019	8.069	1.021	7.400	.292	8.950	.985	5.712	.286
4.010	.009	8.183	1.029	7.500	.297	9.048	.992	5.726	.287
4.054	.004	8.298	1.036	8.640	.246	9.147	.998	5.740	.287
4.108	.001	8.412	1.093			9.246	1.003	6.140	.305
4.140	.000	8.526	1.049			9.344	1.008		
4.152	.000	8.640	1.054			9.443	1.013		
4.202	.003					9.541	1.018		
						9.591	1.020		
						9.640	1.022		
						11.140	1.088		

Table A2. Flap Geometry

Flap I		Flap J		Flap K		Flap L		Flap M	
$x/h_{t,n}$	$y/h_{t,n}$	$x/h_{t,n}$	$y/h_{t,n}$	$x/h_{t,n}$	$y/h_{t,n}$	$x/h_{t,n}$	$y/h_{t,n}$	$x/h_{t,n}$	$y/h_{t,n}$
0.000	−1.390	0.000	−1.390	0.000	−1.390	0.000	−1.390	0.000	−1.390
2.228	−1.390	2.455	−1.390	3.152	−1.252	3.328	−1.245	3.444	−1.240
2.478	−1.323	2.572	−1.376	3.260	−1.236	3.461	−1.221	3.601	−1.207
2.785	−1.146	4.140	−1.000	4.140	−1.000	4.140	−1.000	4.140	−1.000
3.000	−1.080								
4.140	−1.000								

Flap N		Flap O		Flap P		Flap Q		Flap R	
$x/h_{t,n}$	$y/h_{t,n}$	$x/h_{t,n}$	$y/h_{t,n}$	$x/h_{t,n}$	$y/h_{t,n}$	$x/h_{t,n}$	$y/h_{t,n}$	$x/h_{t,n}$	$y/h_{t,n}$
0.000	−1.390	0.000	−1.390	0.000	−1.390	0.000	−1.390	0.000	−1.390
3.487	−1.238	2.260	−1.390	3.536	−1.236	3.598	−1.233	3.683	−1.229
3.657	−1.200	2.351	−1.382	3.631	−1.222	3.705	−1.216	3.816	−1.205
4.140	−1.000	4.740	−.939	4.740	−.956	4.740	−.939	4.740	−.905

Flap S		Flap T		Flap U		Flap V		Flap W	
$x/h_{t,n}$	$y/h_{t,n}$	$x/h_{t,n}$	$y/h_{t,n}$	$x/h_{t,n}$	$y/h_{t,n}$	$x/h_{t,n}$	$y/h_{t,n}$	$x/h_{t,n}$	$y/h_{t,n}$
0.000	−1.390	0.000	−1.390	0.000	−1.390	0.000	−1.390	0.000	−1.390
3.884	−1.220	3.892	−1.220	3.989	−1.216	3.862	−1.222	4.031	−1.214
4.042	−1.188	4.059	−1.184	4.096	−1.199	3.994	−1.197	4.189	−1.181
4.740	−.920	4.740	−.902	5.140	−.920	5.140	−.825	5.140	−.816

Appendix B

Internal Nozzle Static Pressures

Table B1 presents internal nozzle static pressure data for the ramp and the flap as a function of axial location and nozzle pressure ratio for each configuration tested.

Table B1. Ratio of Static Pressure to Jet Total Pressure for Ramp and Flap

(a) Configuration DQ1

ramp pressures, $p/p_{t,j}$

NPR	$x/h_{t,n}$ 3.675	4.140	4.500	5.000	5.800	6.600	7.500	8.400
1.705	.764	.486	.601	.598	.594	.614	.633	.610
1.997	.755	.452	.565	.514	.512	.533	.557	.538
2.504	.755	.449	.558	.457	.345	.434	.475	.438
3.000	.753	.450	.554	.457	.257	.241	.483	.402
3.993	.753	.456	.552	.457	.231	.139	.160	.354
4.993	.753	.456	.550	.458	.232	.121	.101	.129
6.008	.752	.457	.551	.458	.232	.121	.083	.085
7.508	.752	.463	.551	.459	.232	.121	.083	.069
8.607	.752	.463	.551	.460	.232	.121	.084	.069
9.988	.752	.438	.549	.461	.233	.121	.084	.069

flap pressures, $p/p_{t,j}$

NPR	$x/h_{t,n}$ 4.050	4.200	4.350	4.500	4.650
1.705	.813	.780	.741	.696	.627
1.997	.809	.765	.722	.669	.588
2.504	.809	.765	.722	.667	.584
3.000	.810	.766	.721	.666	.582
3.993	.810	.765	.721	.666	.581
4.993	.809	.765	.721	.665	.581
6.008	.809	.764	.721	.666	.581
7.508	.809	.764	.720	.666	.581
8.607	.809	.763	.720	.666	.582
9.988	.808	.763	.720	.666	.582

Table B1. Continued

(b) Configuration AR1

ramp pressures, $p/p_{t,j}$

NPR	$x/h_{t,n}$							
	3.675	4.140	4.500	5.000	5.800	6.600	7.500	8.400
1.717	.783	.468	.592	.594	.609	.666	.625	.571
2.002	.784	.458	.469	.524	.527	.605	.548	.485
2.509	.782	.457	.445	.448	.358	.578	.476	.363
3.036	.781	.457	.455	.445	.244	.403	.520	.303
4.016	.780	.455	.458	.445	.212	.177	.233	.459
5.016	.781	.455	.456	.445	.212	.143	.175	.147
5.995	.781	.455	.454	.446	.212	.143	.110	.113
7.492	.781	.455	.451	.447	.213	.143	.108	.070
8.520	.781	.455	.446	.448	.213	.144	.108	.069
10.006	.761	.455	.445	.449	.213	.144	.109	.069

flap pressures, $p/p_{t,j}$

NPR	$x/h_{t,n}$				
	4.050	4.200	4.350	4.500	4.650
1.717	.842	.800	.757	.708	.630
2.002	.837	.792	.745	.689	.589
2.509	.838	.792	.746	.686	.583
3.036	.837	.792	.744	.685	.581
4.016	.836	.792	.744	.684	.580
5.016	.836	.792	.744	.684	.580
5.995	.836	.792	.744	.685	.581
7.492	.836	.792	.744	.686	.582
8.520	.836	.793	.744	.686	.583
10.006	.836	.792	.743	.687	.584

Table B1. Continued

(c) Configuration CS1

ramp pressures, $p/p_{t,j}$

NPR	$x/h_{t,n}$							
	3.675	4.140	4.500	5.000	5.800	6.600	7.500	8.400
1.702	.734	.455	.556	.607	.686	.680	.603	.583
1.992	.730	.448	.391	.553	.629	.621	.506	.503
2.501	.729	.446	.387	.425	.534	.582	.404	.354
2.998	.727	.445	.387	.425	.243	.575	.393	.267
4.005	.728	.444	.387	.424	.214	.242	.291	.417
4.999	.728	.443	.387	.424	.214	.197	.227	.193
5.996	.728	.443	.386	.425	.214	.197	.120	.159
7.520	.728	.442	.385	.426	.215	.198	.115	.075
8.553	.728	.442	.384	.427	.215	.198	.116	.073
9.610	.728	.442	.384	.427	.215	.198	.116	.073
10.010	.728	.442	.382	.428	.215	.198	.116	.073

flap pressures, $p/p_{t,j}$

NPR	$x/h_{t,n}$				
	4.050	4.200	4.350	4.500	4.650
1.702	.889	.834	.784	.727	.632
1.992	.887	.831	.779	.716	.606
2.501	.889	.830	.777	.714	.602
2.998	.889	.830	.777	.714	.601
4.005	.888	.831	.777	.713	.600
4.999	.888	.830	.777	.713	.600
5.996	.888	.830	.776	.714	.600
7.520	.888	.831	.776	.715	.601
8.553	.888	.831	.776	.716	.602
8.610	.888	.830	.776	.715	.602
10.010	.888	.830	.776	.716	.603

Table B1. Continued

(d) Configuration DU2

ramp pressures, $p/p_{t,j}$

NPR	$x/h_{t,n}$ 3.675	4.140	4.500	5.000	5.800	6.600	7.500	8.400
1.698	.747	.475	.638	.626	.599	.617	.636	.613
2.001	.738	.425	.611	.570	.498	.532	.557	.539
2.502	.737	.422	.607	.562	.373	.346	.540	.425
2.995	.735	.422	.603	.561	.343	.247	.442	.480
4.003	.734	.422	.601	.561	.344	.174	.161	.205
4.977	.733	.422	.601	.561	.345	.174	.113	.127
4.980	.733	.423	.601	.561	.345	.174	.113	.127
4.994	.733	.423	.602	.562	.345	.174	.113	.126
6.000	.733	.423	.602	.562	.345	.175	.112	.091
7.491	.733	.422	.602	.562	.346	.175	.113	.086
8.626	.732	.421	.602	.562	.346	.174	.113	.087
8.605	.732	.421	.602	.562	.346	.174	.113	.087
10.058	.732	.420	.603	.562	.347	.174	.114	.087

flap pressures, $p/p_{t,j}$

NPR	$x/h_{t,n}$ 4.090	4.330	4.570	4.810	5.050
1.598	.861	.788	.730	.689	.619
2.001	.853	.773	.708	.660	.574
2.502	.855	.774	.707	.658	.569
2.995	.854	.773	.705	.656	.566
4.003	.854	.772	.704	.655	.564
4.977	.854	.771	.703	.655	.563
4.980	.854	.771	.703	.655	.563
4.994	.854	.771	.703	.655	.563
6.000	.855	.771	.703	.655	.563
7.491	.854	.770	.701	.655	.564
8.626	.854	.769	.701	.655	.564
8.605	.853	.769	.700	.655	.563
10.058	.853	.768	.700	.655	.564

Table B1. Continued

(e) Configuration AV2

ramp pressures, $p/p_{t,j}$

NPR	$x/h_{t,n}$ 3.675	4.140	4.500	5.000	5.800	6.600	7.500	8.400
1.706	.788	.492	.636	.625	.617	.671	.628	.581
1.996	.781	.468	.611	.569	.523	.608	.550	.494
2.503	.778	.465	.606	.557	.362	.574	.475	.372
3.011	.777	.464	.602	.556	.314	.307	.553	.324
3.995	.776	.462	.599	.556	.313	.200	.231	.379
5.005	.776	.462	.599	.556	.313	.196	.155	.147
6.003	.775	.461	.599	.556	.313	.196	.135	.103
7.481	.775	.461	.599	.556	.313	.196	.135	.081
8.607	.775	.460	.599	.557	.314	.196	.136	.081
10.030	.776	.460	.599	.557	.314	.197	.136	.081

flap pressures, $p/p_{t,j}$

NPR	$x/h_{t,n}$ 4.090	4.330	4.570	4.810	5.050
1.706	.861	.799	.746	.694	.635
1.996	.853	.787	.725	.666	.588
2.503	.854	.785	.722	.661	.575
3.011	.853	.784	.722	.660	.571
3.995	.852	.783	.721	.658	.569
5.005	.852	.783	.720	.658	.568
6.003	.851	.782	.719	.658	.568
7.481	.851	.781	.719	.658	.568
8.607	.850	.781	.719	.658	.568
10.030	.850	.780	.718	.658	.569

Table B1. Continued

(f) Configuration CW2

ramp pressures, $p/p_{t,j}$

NPR	$x/h_{t,n}$ 3.675	4.140	4.500	5.000	5.800	6.600	7.500	8.400
1.697	.732	.468	.624	.628	.690	.683	.605	.586
1.996	.720	.442	.582	.552	.630	.621	.505	.500
2.498	.719	.438	.581	.535	.385	.589	.411	.349
3.007	.719	.438	.570	.535	.309	.543	.432	.260
3.999	.718	.436	.562	.535	.309	.276	.278	.427
4.997	.717	.435	.559	.535	.310	.258	.183	.189
6.009	.717	.434	.557	.536	.310	.259	.141	.124
7.496	.717	.435	.554	.536	.310	.259	.141	.086
8.591	.717	.436	.553	.536	.311	.259	.141	.084
10.007	.717	.435	.551	.537	.311	.260	.142	.084

flap pressures, $p/p_{t,j}$

NPR	$x/h_{t,n}$ 4.090	4.330	4.570	4.810	5.050
1.697	.890	.835	.766	.702	.628
1.996	.884	.823	.745	.670	.581
2.498	.883	.822	.743	.666	.576
3.007	.884	.822	.742	.665	.573
3.999	.883	.822	.742	.664	.572
4.997	.883	.822	.741	.663	.570
6.009	.883	.822	.741	.663	.570
7.496	.883	.822	.740	.663	.570
8.591	.883	.822	.739	.663	.571
10.007	.883	.821	.739	.662	.571

Table B1. Continued

(g) Configuration DI1

ramp pressures, $p/p_{t,j}$

NPR	$x/h_{t,n}$ 3.675	4.140	4.500	5.000	5.800	6.600	7.500	8.400
1.689	.724	.326	.304	.608	.605	.619	.635	.613
1.990	.722	.319	.257	.419	.561	.535	.555	.532
2.492	.720	.317	.255	.223	.358	.483	.457	.456
3.006	.719	.318	.255	.223	.288	.310	.395	.409
4.007	.719	.317	.255	.223	.124	.222	.242	.289
5.001	.718	.318	.255	.222	.125	.161	.190	.232
5.992	.718	.318	.255	.222	.125	.073	.124	.207
7.499	.718	.319	.255	.222	.125	.073	.057	.107
8.624	.718	.319	.255	.222	.125	.074	.057	.053
8.625	.718	.319	.256	.222	.125	.074	.058	.053
8.590	.718	.319	.255	.222	.125	.073	.057	.053
10.000	.718	.319	.255	.222	.125	.073	.058	.052

flap pressures, $p/p_{t,j}$

NPR	$x/h_{t,n}$ 3.450	3.600	3.750	3.900	4.050
1.689	.825	.799	.765	.719	.631
1.990	.825	.798	.763	.712	.614
2.492	.827	.798	.762	.710	.610
3.006	.828	.798	.761	.710	.609
4.007	.828	.798	.762	.710	.609
5.001	.828	.798	.761	.710	.609
5.992	.828	.797	.762	.711	.609
7.499	.828	.797	.761	.712	.610
8.624	.828	.797	.761	.712	.610
8.625	.828	.797	.761	.712	.610
8.590	.828	.797	.761	.712	.610
10.000	.827	.796	.760	.713	.611

Table B1. Continued

(h) Configuration CI1

ramp pressures, $p/p_{t,j}$

NPR	$x/h_{t,n}$ 3.675	4.140	4.500	5.000	5.800	6.600	7.500	8.400
1.719	.691	.316	.386	.508	.614	.661	.620	.586
1.999	.689	.311	.361	.404	.482	.571	.558	.509
2.495	.688	.309	.194	.343	.352	.418	.480	.429
2.993	.687	.308	.192	.195	.310	.326	.395	.366
4.007	.687	.306	.191	.175	.204	.231	.325	.304
5.003	.688	.305	.191	.174	.107	.130	.285	.309
6.002	.688	.305	.191	.174	.107	.124	.178	.250
7.524	.688	.304	.191	.174	.108	.124	.081	.097
8.608	.688	.303	.190	.174	.108	.124	.081	.056
10.004	.689	.303	.190	.174	.108	.124	.081	.056

flap pressures, $p/p_{t,j}$

NPR	$x/h_{t,n}$ 3.450	3.600	3.750	3.900	4.050
1.719	.828	.781	.761	.719	.634
1.999	.823	.779	.757	.712	.617
2.495	.829	.778	.756	.710	.614
2.993	.829	.779	.756	.709	.612
4.007	.828	.778	.755	.709	.611
5.003	.829	.778	.756	.709	.611
6.002	.828	.778	.756	.710	.612
7.524	.828	.780	.756	.711	.612
8.608	.823	.780	.756	.711	.612
10.004	.828	.779	.756	.712	.613

Table B1. Continued

(i) Configuration DK1

ramp pressures, $p/p_{t,j}$

NPR	$x/h_{t,n}$ 3.675	4.140	4.500	5.000	5.800	6.600	7.500	8.400
1.692	.758	.414	.371	.612	.600	.617	.635	.614
1.978	.754	.399	.321	.465	.534	.535	.559	.538
1.986	.753	.398	.321	.454	.534	.534	.557	.536
2.501	.751	.392	.307	.259	.379	.462	.472	.433
2.996	.751	.392	.307	.241	.290	.331	.407	.422
4.010	.751	.394	.307	.240	.127	.220	.236	.287
5.009	.750	.394	.307	.240	.127	.143	.182	.232
5.999	.750	.393	.307	.240	.127	.074	.061	.174
7.487	.750	.395	.307	.240	.127	.074	.057	.108
8.596	.750	.393	.308	.240	.127	.074	.057	.053
9.997	.750	.393	.308	.240	.127	.074	.058	.052

flap pressures, $p/p_{t,j}$

NPR	$x/h_{t,n}$ 3.450	3.600	3.750	3.900	4.050
1.692	.900	.874	.840	.789	.699
1.978	.897	.872	.834	.780	.678
1.986	.898	.871	.834	.779	.678
2.501	.899	.871	.833	.775	.671
2.996	.900	.871	.833	.775	.670
4.010	.900	.871	.833	.775	.669
5.009	.900	.871	.832	.773	.669
5.999	.899	.870	.832	.773	.669
7.487	.898	.870	.831	.774	.669
8.596	.898	.870	.831	.775	.670
9.997	.898	.870	.831	.778	.671

Table B1. Continued

(j) Configuration AL1

ramp pressures, $p/p_{t,j}$

NPR	$x/h_{t,n}$ 3.675	4.140	4.500	5.000	5.890	6.600	7.500	8.400
1.697	.786	.425	.331	.623	.619	.668	.630	.586
2.014	.781	.411	.292	.364	.566	.597	.544	.491
2.005	.780	.410	.292	.383	.564	.598	.546	.493
2.497	.777	.405	.280	.244	.387	.536	.494	.370
2.491	.776	.405	.280	.244	.389	.539	.495	.371
2.996	.775	.404	.277	.229	.315	.348	.450	.367
3.013	.776	.404	.277	.229	.313	.343	.444	.371
4.010	.776	.403	.276	.225	.180	.227	.262	.304
5.012	.775	.402	.275	.224	.116	.169	.229	.266
6.004	.775	.402	.275	.224	.116	.091	.080	.208
7.493	.775	.402	.274	.225	.116	.091	.078	.098
8.609	.776	.402	.275	.225	.117	.091	.078	.055
10.098	.776	.402	.274	.225	.117	.091	.079	.054

flap pressures, $p/p_{t,j}$

NPR	$x/h_{t,n}$ 3.450	3.600	3.750	3.900	4.050
1.697	.932	.899	.869	.821	.744
2.014	.929	.896	.863	.811	.724
2.005	.927	.895	.862	.810	.724
2.497	.929	.895	.860	.806	.716
2.491	.929	.894	.860	.805	.715
2.996	.928	.893	.859	.804	.713
3.013	.929	.895	.860	.805	.714
4.010	.928	.894	.859	.804	.713
5.012	.927	.894	.859	.805	.712
6.004	.928	.894	.859	.805	.713
7.493	.927	.893	.858	.806	.714
8.609	.927	.894	.858	.807	.715
10.098	.927	.893	.858	.808	.716

Table B1. Continued

(k) Configuration CM1

ramp pressures, $p/p_{t,j}$

NPR	$x/h_{t,n}$							
	3.675	4.140	4.500	5.000	5.800	6.600	7.500	8.400
1.707	.740	.415	.330	.588	.680	.675	.603	.583
1.990	.734	.400	.260	.440	.576	.624	.527	.499
2.502	.730	.391	.246	.352	.386	.491	.483	.401
3.002	.730	.387	.243	.199	.324	.355	.434	.352
4.011	.730	.386	.242	.196	.214	.243	.323	.303
5.002	.729	.384	.242	.196	.111	.127	.276	.322
6.006	.729	.384	.241	.196	.111	.125	.084	.226
7.504	.729	.383	.241	.196	.111	.125	.081	.093
8.607	.730	.383	.241	.196	.111	.125	.082	.056
10.016	.730	.383	.241	.196	.112	.126	.082	.056

flap pressures, $p/p_{t,j}$

NPR	$x/h_{t,n}$				
	3.450	3.600	3.750	3.900	4.050
1.707	.930	.926	.886	.833	.738
1.990	.925	.923	.881	.823	.720
2.502	.927	.922	.879	.819	.712
3.002	.926	.922	.878	.819	.710
4.011	.927	.922	.877	.819	.709
5.002	.926	.922	.876	.819	.709
6.006	.927	.922	.877	.820	.710
7.504	.926	.922	.876	.821	.711
8.607	.926	.922	.876	.822	.712
10.016	.926	.922	.876	.823	.713

Table B1. Continued

(l) Configuration AQ1

ramp pressures, $p/p_{t,j}$

NPR	$x/h_{t,n}$							
	3.675	4.140	4.500	5.000	5.800	6.600	7.500	8.400
1.706	.775	.439	.531	.599	.616	.671	.629	.585
2.013	.772	.436	.381	.557	.516	.606	.547	.492
2.506	.771	.435	.379	.450	.440	.579	.479	.371
3.016	.771	.434	.379	.449	.230	.354	.522	.307
4.042	.772	.432	.378	.449	.223	.159	.240	.465
4.990	.771	.432	.377	.449	.223	.150	.147	.156
6.019	.771	.431	.377	.450	.223	.150	.112	.144
7.513	.771	.431	.376	.451	.224	.151	.113	.072
8.583	.771	.432	.376	.452	.224	.151	.113	.072
10.018	.772	.432	.375	.453	.224	.151	.114	.072

flap pressures, $p/p_{t,j}$

NPR	$x/h_{t,n}$				
	4.050	4.200	4.350	4.500	4.650
1.706	.809	.766	.723	.667	.593
2.013	.807	.763	.719	.661	.577
2.506	.807	.763	.718	.659	.575
3.016	.808	.763	.718	.659	.573
4.042	.809	.763	.718	.658	.572
4.990	.809	.763	.718	.658	.572
6.019	.808	.763	.718	.658	.572
7.513	.808	.763	.718	.659	.573
8.583	.808	.763	.718	.660	.573
10.018	.809	.763	.718	.661	.574

Table B1. Continued

(m) Configuration AS1

ramp pressures, $p/p_{t,j}$

NPR	$x/h_{t,n}$ 3.675	4.140	4.500	5.000	5.800	6.600	7.500	8.400
1.708	.787	.482	.606	.602	.614	.670	.628	.583
1.991	.781	.465	.571	.518	.529	.608	.552	.498
2.489	.778	.462	.558	.450	.347	.582	.484	.369
2.998	.777	.461	.554	.449	.260	.421	.522	.314
3.996	.777	.460	.551	.449	.217	.183	.238	.465
5.016	.776	.459	.550	.449	.217	.146	.151	.152
5.984	.776	.459	.550	.449	.217	.146	.115	.105
7.500	.777	.459	.549	.450	.217	.146	.111	.073
8.622	.777	.459	.549	.451	.217	.146	.111	.071
10.029	.777	.459	.549	.452	.217	.147	.111	.071

flap pressures, $p/p_{t,j}$

NPR	$x/h_{t,n}$ 4.050	4.200	4.350	4.500	4.650
1.708	.894	.843	.797	.740	.647
1.991	.890	.834	.784	.720	.612
2.489	.889	.833	.782	.715	.605
2.998	.890	.833	.782	.715	.605
3.996	.890	.833	.782	.715	.603
5.016	.889	.832	.780	.715	.603
5.984	.889	.832	.780	.715	.603
7.500	.888	.832	.780	.716	.604
8.622	.888	.832	.779	.716	.605
10.029	.889	.832	.779	.717	.606

Table B1. Continued

(n) Configuration AK1

ramp pressures, $p/p_{t,j}$

NPR	$x/h_{t,n}$ 3.675	4.140	4.500	5.000	5.800	6.600	7.500	8.400
1.692	.774	.406	.310	.626	.623	.670	.632	.591
1.985	.773	.392	.277	.422	.577	.604	.552	.500
2.460	.770	.386	.266	.236	.386	.529	.502	.391
2.502	.771	.386	.266	.235	.376	.512	.501	.377
3.016	.770	.385	.265	.221	.310	.333	.430	.383
4.004	.770	.384	.264	.220	.179	.222	.260	.312
4.995	.770	.383	.264	.220	.116	.177	.227	.261
6.004	.770	.382	.264	.220	.116	.091	.078	.217
7.508	.770	.382	.264	.220	.117	.091	.078	.100
8.587	.770	.382	.263	.221	.117	.091	.079	.055
10.009	.771	.383	.263	.221	.117	.091	.079	.055

flap pressures, $p/p_{t,j}$

NPR	$x/h_{t,n}$ 3.450	3.600	3.750	3.900	4.050
1.692	.903	.875	.846	.795	.700
1.985	.900	.871	.838	.784	.680
2.460	.900	.870	.836	.780	.672
2.502	.900	.871	.837	.780	.673
3.016	.901	.870	.836	.780	.671
4.004	.899	.870	.835	.779	.669
4.995	.899	.869	.835	.779	.669
6.004	.899	.869	.835	.779	.669
7.508	.898	.870	.835	.780	.670
8.587	.899	.870	.835	.781	.671
10.009	.898	.870	.834	.782	.672

Table B1. Continued

(o) Configuration AM1

ramp pressures, $p/p_{t,j}$

NPR	$x/h_{t,n}$							
	3.675	4.140	4.500	5.000	5.800	6.600	7.500	8.400
1.708	.786	.425	.326	.623	.617	.666	.627	.585
1.999	.780	.413	.294	.389	.568	.602	.549	.498
2.491	.777	.406	.280	.246	.386	.531	.497	.374
2.987	.776	.405	.277	.230	.317	.348	.450	.375
4.003	.775	.403	.276	.226	.178	.227	.263	.311
4.990	.775	.402	.275	.226	.117	.168	.229	.268
5.995	.775	.402	.275	.225	.117	.091	.081	.206
7.497	.776	.402	.275	.226	.117	.091	.079	.097
8.605	.776	.403	.275	.226	.117	.091	.079	.055
10.038	.776	.403	.275	.226	.117	.091	.079	.055

flap pressures, $p/p_{t,j}$

NPR	$x/h_{t,n}$				
	3.450	3.600	3.750	3.900	4.050
1.708	.931	.927	.885	.832	.737
1.999	.928	.923	.880	.824	.719
2.491	.926	.922	.877	.819	.712
2.987	.927	.922	.877	.818	.710
4.003	.927	.921	.877	.818	.709
4.990	.926	.921	.876	.818	.709
5.995	.926	.921	.876	.819	.709
7.497	.927	.921	.876	.821	.711
8.605	.927	.921	.876	.821	.711
10.038	.927	.921	.876	.822	.713

Table B1. Continued

(p) Configuration BP1

ramp pressures, $p/p_{t,j}$

NPR	$x/h_{t,n}$							
	3.675	4.140	4.500	5.000	5.800	6.600	7.500	8.400
1.699	.756	.442	.615	.640	.644	.600	.592	.578
2.008	.745	.416	.571	.559	.569	.500	.497	.484
2.517	.744	.414	.565	.461	.474	.451	.328	.493
3.016	.743	.413	.563	.460	.349	.340	.354	.331
4.008	.742	.412	.561	.460	.314	.202	.191	.191
4.999	.741	.411	.561	.460	.313	.164	.121	.118
6.006	.740	.410	.561	.460	.313	.163	.088	.115
7.508	.740	.410	.561	.461	.313	.163	.087	.113
8.576	.740	.409	.562	.461	.314	.164	.088	.054
10.035	.740	.409	.562	.462	.314	.162	.088	.053

flap pressures, $p/p_{t,j}$

NPR	$x/h_{t,n}$				
	4.050	4.200	4.350	4.500	4.650
1.699	.811	.774	.739	.700	.636
2.008	.795	.754	.712	.665	.588
2.517	.796	.754	.710	.661	.579
3.016	.796	.754	.710	.660	.578
4.008	.796	.754	.709	.659	.577
4.999	.795	.754	.709	.659	.576
6.006	.795	.754	.709	.659	.575
7.508	.794	.753	.708	.658	.574
8.576	.794	.753	.707	.659	.575
10.035	.793	.752	.707	.659	.575

Table B1. Continued

(q) Configuration FO1

ramp pressures, $p/p_{t,j}$

NPR	$x/h_{t,n}$ 3.675	4.140	4.500	5.000	5.800	6.600	7.500	8.400
1.687	.811	.463	.638	.616	.618	.616	.503	.597
2.003	.803	.392	.600	.524	.531	.514	.501	.510
2.494	.801	.384	.596	.489	.370	.510	.394	.371
3.035	.799	.385	.594	.489	.276	.261	.481	.364
3.992	.798	.385	.593	.488	.262	.158	.155	.314
4.997	.797	.383	.593	.489	.263	.138	.097	.148
5.992	.797	.380	.593	.489	.262	.138	.079	.149
7.505	.797	.378	.593	.490	.263	.138	.079	.114
8.611	.797	.376	.593	.490	.263	.138	.079	.052
9.983	.797	.373	.593	.491	.264	.138	.079	.052

flap pressures, $p/p_{t,j}$

NPR	$x/h_{t,n}$ 4.050	4.200	4.350	4.500	4.650
1.687	.784	.753	.722	.684	.629
2.003	.770	.734	.698	.654	.585
2.494	.770	.733	.697	.650	.578
3.035	.770	.733	.695	.649	.577
3.992	.769	.732	.695	.649	.576
4.997	.769	.732	.695	.649	.576
5.992	.768	.731	.693	.649	.574
7.505	.767	.730	.693	.649	.574
8.611	.766	.730	.692	.648	.574
9.983	.766	.729	.691	.649	.574

Table B1. Continued

(r) Configuration FQ1

ramp pressures, $p/p_{t,j}$

NPR	$x/h_{t,n}$ 3.675	4.140	4.500	5.000	5.800	6.600	7.500	8.400
1.702	.817	.568	.666	.624	.615	.610	.598	.591
2.000	.808	.530	.632	.544	.528	.512	.500	.511
2.491	.806	.526	.621	.499	.377	.460	.414	.368
2.990	.805	.529	.619	.498	.299	.269	.481	.366
4.001	.805	.527	.619	.498	.262	.167	.155	.302
4.984	.805	.526	.618	.499	.262	.137	.103	.140
5.030	.804	.526	.618	.499	.262	.137	.102	.146
4.976	.805	.526	.619	.499	.262	.137	.104	.139
6.015	.805	.526	.619	.500	.263	.138	.080	.146
7.009	.805	.525	.619	.500	.264	.138	.078	.125
7.500	.804	.525	.619	.500	.264	.138	.079	.114
8.501	.804	.524	.619	.501	.264	.138	.079	.054
8.624	.804	.524	.619	.501	.264	.138	.079	.052
8.601	.804	.524	.619	.501	.264	.138	.079	.052
10.019	.804	.523	.620	.502	.265	.138	.079	.052

flap pressures, $p/p_{t,j}$

NPR	$x/h_{t,n}$ 4.050	4.200	4.350	4.500	4.650
1.702	.837	.803	.771	.729	.654
2.000	.827	.789	.754	.706	.620
2.491	.827	.787	.750	.701	.614
2.990	.826	.787	.749	.701	.612
4.001	.826	.787	.749	.701	.612
4.984	.825	.787	.748	.700	.611
5.030	.826	.787	.748	.701	.612
4.976	.826	.787	.749	.701	.611
6.015	.825	.787	.748	.701	.611
7.009	.825	.786	.748	.701	.611
7.500	.825	.786	.748	.701	.612
8.501	.824	.786	.747	.701	.612
8.624	.824	.786	.747	.701	.612
8.601	.824	.786	.747	.701	.612
10.019	.824	.786	.747	.702	.613

Table B1. Continued

(s) Configuration BO1

ramp pressures, $p/p_{t,j}$

NPR	$x/h_{t,n}$							
	3.675	4.140	4.500	5.000	5.800	6.600	7.500	8.400
1.708	.755	.408	.600	.631	.632	.598	.589	.576
2.018	.750	.399	.462	.567	.561	.502	.496	.482
2.488	.747	.397	.436	.464	.492	.417	.348	.469
2.999	.746	.396	.437	.463	.360	.343	.366	.322
4.006	.745	.395	.435	.463	.311	.237	.190	.187
4.994	.744	.394	.433	.463	.311	.161	.138	.115
5.978	.744	.394	.431	.463	.311	.161	.085	.084
7.488	.744	.393	.428	.464	.311	.161	.085	.117
8.578	.744	.392	.426	.465	.311	.161	.085	.064
9.998	.744	.392	.424	.465	.312	.160	.086	.052

flap pressures, $p/p_{t,j}$

NPR	$x/h_{t,n}$				
	4.050	4.200	4.350	4.500	4.650
1.708	.767	.726	.689	.648	.599
2.018	.760	.718	.671	.615	.540
2.488	.760	.717	.671	.614	.537
2.999	.760	.716	.670	.613	.535
4.006	.760	.716	.669	.612	.533
4.994	.760	.716	.669	.612	.533
5.978	.760	.716	.669	.613	.533
7.488	.759	.715	.668	.613	.533
8.578	.759	.715	.668	.614	.533
9.998	.759	.715	.668	.614	.534

Table B1. Continued

(t) Configuration ET1

ramp pressures, $p/p_{t,j}$

NPR	$x/h_{t,n}$ 3.675	4.140	4.500	5.000	5.800	6.600	7.500	8.400
1.699	.779	.471	.532	.598	.605	.668	.668	.608
2.005	.776	.467	.379	.557	.502	.601	.596	.527
2.502	.774	.469	.377	.409	.447	.561	.519	.444
2.990	.773	.469	.379	.408	.227	.425	.537	.404
4.010	.773	.469	.380	.408	.197	.132	.391	.480
5.058	.773	.470	.380	.408	.197	.114	.124	.199
6.038	.773	.471	.380	.409	.198	.114	.104	.121
7.001	.773	.472	.379	.410	.199	.114	.104	.087
7.494	.773	.472	.379	.410	.199	.114	.104	.085
8.634	.773	.473	.378	.410	.199	.114	.104	.085
9.982	.773	.473	.377	.411	.199	.114	.105	.085

flap pressures, $p/p_{t,j}$

NPR	$x/h_{t,n}$ 4.050	4.200	4.350	4.500	4.650
1.699	.897	.846	.798	.736	.636
2.005	.895	.843	.793	.727	.612
2.502	.897	.844	.794	.725	.610
2.990	.897	.845	.794	.726	.610
4.010	.897	.845	.793	.725	.608
5.058	.897	.844	.792	.725	.607
6.038	.897	.845	.793	.726	.608
7.001	.897	.844	.793	.726	.608
7.494	.897	.844	.792	.727	.608
8.634	.897	.844	.792	.727	.608
9.982	.897	.844	.791	.728	.609

Table B1. Continued

(u) Configuration BJ1

ramp pressures, $p/p_{t,j}$

NPR	$x/h_{t,n}$ 3.675	4.140	4.500	5.000	5.800	6.600	7.500	8.400
1.700	.758	.396	.509	.639	.642	.598	.590	.578
2.006	.752	.381	.342	.538	.588	.503	.501	.485
2.501	.750	.376	.328	.275	.523	.442	.360	.436
2.996	.748	.375	.327	.257	.248	.478	.327	.263
3.996	.746	.374	.326	.256	.179	.229	.295	.329
5.014	.746	.373	.325	.255	.178	.108	.162	.216
6.000	.746	.371	.324	.256	.178	.105	.068	.147
6.004	.746	.371	.324	.256	.178	.105	.068	.147
7.514	.746	.371	.324	.256	.178	.105	.062	.119
8.602	.746	.371	.323	.256	.178	.105	.063	.103
10.073	.746	.371	.324	.256	.178	.106	.063	.069

flap pressures, $p/p_{t,j}$

NPR	$x/h_{t,n}$ 3.450	3.600	3.750	3.900	4.050
1.700	.890	.863	.835	.788	.723
2.006	.885	.858	.829	.778	.703
2.501	.894	.859	.828	.775	.698
2.996	.884	.859	.827	.773	.695
3.996	.883	.858	.826	.773	.694
5.014	.883	.859	.826	.773	.694
6.000	.883	.859	.826	.774	.694
6.004	.883	.859	.826	.774	.694
7.514	.883	.858	.826	.775	.696
8.602	.882	.858	.825	.776	.697
10.073	.882	.858	.825	.776	.698

Table B1. Continued

(v) Configuration EN1

ramp pressures, $p/p_{t,j}$

NPR	$x/h_{t,n}$ 3.675	4.140	4.500	5.000	5.800	6.600	7.500	8.400
1.696	.786	.423	.290	.602	.610	.662	.663	.608
1.998	.775	.408	.249	.385	.571	.593	.590	.523
2.489	.774	.403	.237	.202	.346	.486	.533	.454
3.013	.772	.403	.233	.189	.298	.310	.396	.404
2.991	.771	.403	.233	.190	.301	.314	.401	.406
3.998	.771	.402	.233	.185	.219	.229	.246	.294
4.991	.770	.403	.232	.184	.101	.151	.172	.288
5.991	.769	.404	.232	.184	.100	.104	.159	.224
6.997	.769	.405	.232	.184	.101	.067	.070	.195
7.525	.769	.405	.232	.185	.102	.067	.070	.065
7.508	.769	.405	.232	.184	.102	.067	.070	.066
8.596	.769	.406	.231	.185	.102	.067	.070	.064
9.983	.769	.406	.231	.185	.101	.067	.070	.064

flap pressures, $p/p_{t,j}$

NPR	$x/h_{t,n}$ 3.450	3.600	3.750	3.900	4.050
1.696	.926	.931	.900	.846	.765
1.998	.923	.928	.896	.838	.746
2.489	.925	.928	.895	.834	.738
3.013	.925	.928	.894	.832	.735
2.991	.925	.929	.895	.833	.736
3.998	.925	.929	.894	.833	.735
4.991	.925	.929	.894	.833	.735
5.991	.925	.929	.894	.834	.736
6.997	.925	.929	.893	.834	.736
7.525	.925	.929	.893	.835	.736
7.508	.925	.928	.893	.835	.736
8.596	.925	.928	.893	.836	.737
9.983	.925	.928	.892	.836	.738

Table B1. Continued

(w) Configuration AU2

ramp pressures, $p/p_{t,j}$

NPR	$x/h_{t,n}$							
	3.675	4.140	4.500	5.000	5.800	6.600	7.500	8.400
1.702	.752	.401	.553	.607	.622	.674	.633	.588
2.015	.747	.390	.356	.560	.520	.611	.550	.493
2.504	.746	.390	.355	.536	.407	.565	.486	.374
2.998	.746	.389	.356	.534	.331	.307	.560	.349
4.003	.745	.387	.355	.532	.331	.216	.228	.257
5.001	.745	.386	.355	.533	.331	.216	.198	.145
6.010	.744	.385	.354	.533	.332	.216	.150	.120
7.482	.745	.384	.352	.534	.332	.216	.150	.091
8.586	.745	.383	.352	.534	.332	.216	.150	.091
9.999	.745	.383	.351	.534	.333	.216	.151	.091

flap pressures, $p/p_{t,j}$

NPR	$x/h_{t,n}$				
	4.090	4.330	4.570	4.810	5.050
1.702	.845	.755	.681	.638	.588
2.015	.841	.744	.654	.575	.478
2.504	.841	.744	.653	.574	.476
2.998	.842	.744	.652	.573	.474
4.003	.841	.743	.651	.572	.471
5.001	.841	.743	.651	.572	.471
6.010	.841	.743	.650	.572	.471
7.482	.841	.742	.650	.573	.471
8.586	.840	.742	.649	.573	.471
9.999	.840	.741	.649	.573	.472

Table B1. Continued

(x) Configuration AW2

ramp pressures, $p/p_{t,j}$

NPR	$x/h_{t,n}$ 3.675	4.140	4.500	5.000	5.800	6.600	7.500	8.400
1.712	.794	.535	.661	.641	.616	.670	.626	.585
2.000	.785	.503	.635	.589	.510	.608	.549	.500
2.500	.783	.497	.627	.572	.376	.570	.474	.377
3.006	.781	.495	.625	.571	.313	.312	.553	.324
4.029	.782	.493	.624	.571	.314	.206	.229	.351
4.987	.781	.492	.624	.571	.314	.195	.163	.151
6.009	.781	.492	.624	.571	.314	.196	.133	.108
7.500	.781	.491	.624	.572	.314	.196	.134	.081
8.583	.781	.490	.624	.572	.315	.196	.134	.081
10.033	.781	.489	.624	.572	.315	.196	.135	.081

flap pressures, $p/p_{t,j}$

NPR	$x/h_{t,n}$ 4.090	4.330	4.570	4.810	5.050
1.712	.901	.852	.790	.729	.644
2.000	.894	.843	.776	.706	.607
2.500	.894	.841	.772	.700	.599
3.006	.894	.841	.771	.699	.597
4.029	.894	.840	.772	.698	.596
4.987	.893	.840	.770	.698	.594
6.009	.893	.840	.770	.698	.598
7.500	.893	.840	.770	.698	.598
8.583	.893	.839	.769	.699	.598
10.033	.893	.839	.769	.699	.599

Table B1. Continued

(y) Configuration HR4

ramp pressures, $p/p_{t,j}$

NPR	$x/h_{t,n}$ 3.675	4.140	4.300	4.500	4.800	5.100	5.500	6.000
1.696	.800	.467	.442	.621	.652	.708	.695	.611
1.994	.791	.453	.348	.497	.598	.660	.646	.538
2.494	.786	.449	.345	.429	.501	.528	.619	.479
2.986	.782	.448	.345	.437	.501	.450	.426	.453
3.995	.781	.445	.342	.438	.497	.447	.414	.270
4.986	.780	.444	.341	.435	.497	.446	.415	.269
6.005	.780	.443	.340	.433	.497	.445	.415	.268
7.493	.779	.442	.339	.428	.496	.445	.415	.269
8.516	.779	.442	.339	.427	.496	.445	.397	.269
8.610	.779	.442	.339	.427	.497	.446	.392	.269
10.012	.779	.442	.338	.425	.497	.446	.337	.270

flap pressures, $p/p_{t,j}$

NPR	$x/h_{t,n}$ 4.050	4.200	4.350	4.500	4.650
1.696	.848	.812	.765	.715	.618
1.994	.842	.801	.750	.690	.573
2.494	.841	.800	.749	.687	.569
2.986	.844	.802	.753	.688	.569
3.995	.842	.798	.749	.686	.567
4.986	.841	.798	.749	.686	.567
6.005	.840	.796	.747	.686	.567
7.493	.839	.794	.746	.686	.567
8.516	.838	.794	.745	.686	.567
8.610	.839	.794	.745	.686	.567
10.012	.838	.793	.745	.687	.568

Table B1. Continued

(z) Configuration GR3

ramp pressures, $p/p_{t,j}$

NPR	$x/h_{t,n}$							
	3.675	4.140	4.500	5.500	6.800	8.100	9.400	10.900
1.703	.790	.464	.594	.594	.601	.649	.609	.580
2.008	.786	.454	.463	.496	.511	.574	.522	.490
3.007	.783	.452	.458	.282	.240	.493	.376	.310
2.500	.783	.453	.454	.363	.455	.503	.421	.407
4.002	.782	.451	.460	.282	.147	.305	.345	.318
5.003	.781	.450	.458	.281	.098	.203	.270	.212
6.020	.780	.450	.456	.281	.098	.148	.246	.248
5.984	.780	.449	.455	.281	.097	.150	.246	.248
6.967	.780	.449	.453	.281	.097	.070	.177	.243
7.499	.780	.449	.451	.281	.098	.070	.144	.237
8.571	.780	.449	.449	.280	.097	.070	.053	.211
8.586	.780	.449	.449	.280	.097	.069	.053	.210
10.027	.780	.449	.447	.281	.098	.070	.053	.135

flap pressures, $p/p_{t,j}$

NPR	$x/h_{t,n}$				
	4.050	4.200	4.350	4.500	4.650
1.703	.840	.799	.757	.704	.607
2.008	.836	.792	.747	.686	.570
3.007	.837	.793	.745	.684	.566
2.500	.838	.793	.746	.684	.567
4.002	.839	.794	.747	.684	.567
5.003	.839	.794	.747	.685	.567
6.020	.839	.795	.746	.686	.568
5.984	.838	.793	.745	.685	.567
6.967	.837	.793	.745	.685	.568
7.499	.838	.793	.745	.686	.568
8.571	.837	.793	.744	.686	.568
8.586	.837	.792	.744	.686	.569
10.027	.838	.793	.744	.687	.569

Table B1. Concluded

(aa) Configuration BV2

ramp pressures, $p/p_{t,j}$

NPR	$x/h_{t,n}$ 3.675	4.140	4.500	5.000	5.800	6.600	7.500	8.400
1.691	.604	.622	.716	.697	.648	.600	.593	.580
1.992	.787	.581	.683	.645	.570	.500	.503	.487
2.500	.781	.562	.668	.607	.499	.378	.367	.434
2.990	.779	.561	.667	.604	.421	.326	.271	.378
3.992	.778	.559	.666	.604	.405	.227	.177	.144
5.041	.777	.559	.665	.604	.404	.196	.127	.101
6.014	.777	.558	.665	.604	.405	.195	.102	.095
7.515	.777	.558	.665	.604	.406	.195	.097	.084
8.594	.777	.557	.665	.604	.407	.195	.097	.055
10.013	.777	.557	.664	.604	.407	.196	.097	.055

flap pressures, $p/p_{t,j}$

NPR	$x/h_{t,n}$ 4.090	4.330	4.570	4.810	5.050
1.691	.692	.844	.798	.752	.671
1.992	.883	.828	.777	.723	.625
2.500	.879	.822	.769	.710	.606
2.990	.878	.822	.767	.709	.603
3.992	.879	.821	.767	.708	.602
5.041	.878	.820	.766	.708	.601
6.014	.878	.819	.766	.708	.601
7.515	.877	.819	.765	.709	.602
8.594	.877	.819	.765	.710	.603
10.013	.876	.818	.764	.710	.603

Appendix C

Normal-Force and Pitching-Moment Coefficients for Each Configuration

The normal-force and pitching-moment coefficients are presented as a function of nozzle pressure ratio in the following figures:

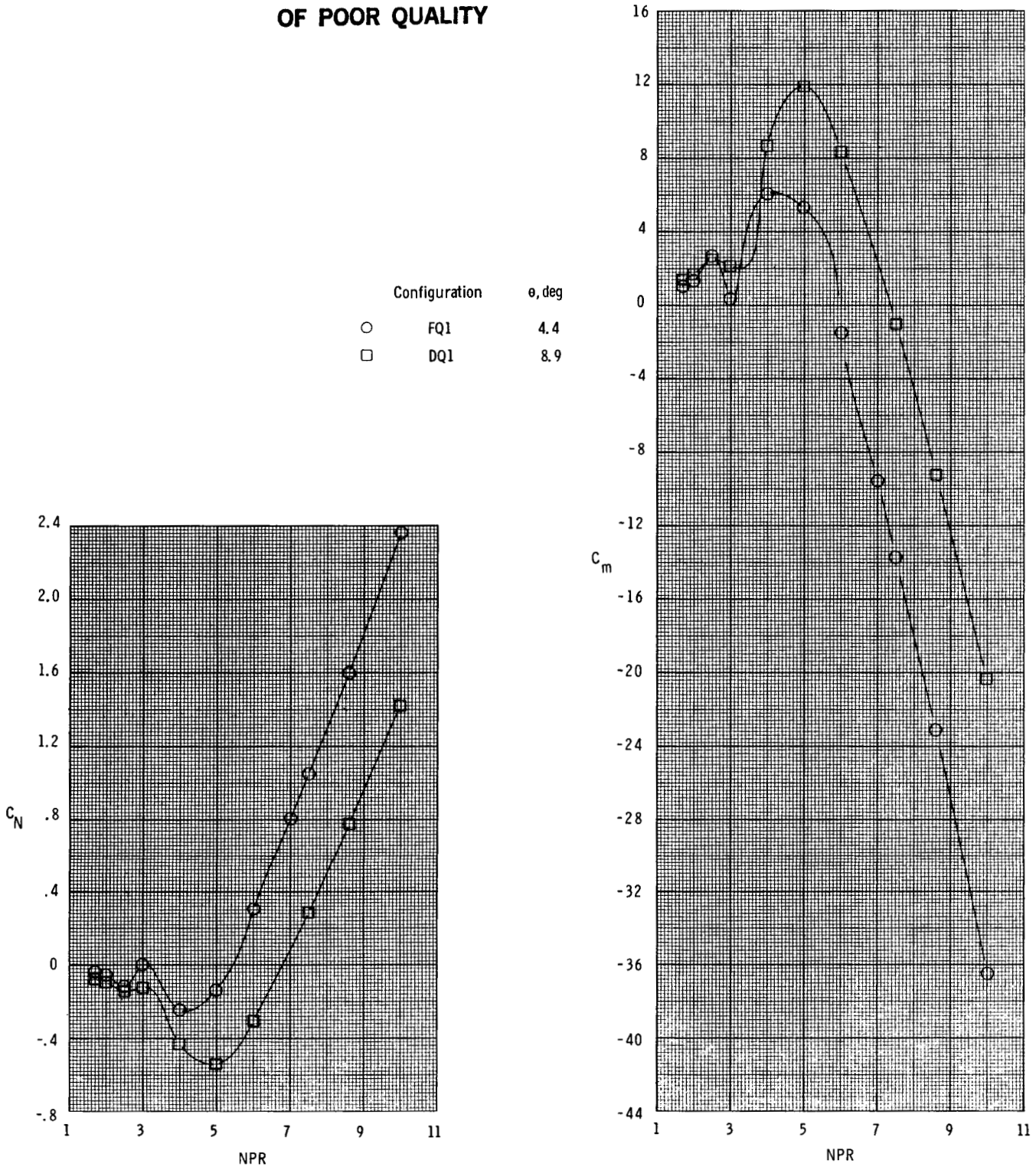

Figure C1. Effect of ramp chordal angle on normal-force and pitching-moment coefficients for $l_f/h_{t,n} = 4.74$, $\rho - \theta = 2.0°$, and $\beta = 15.0°$.

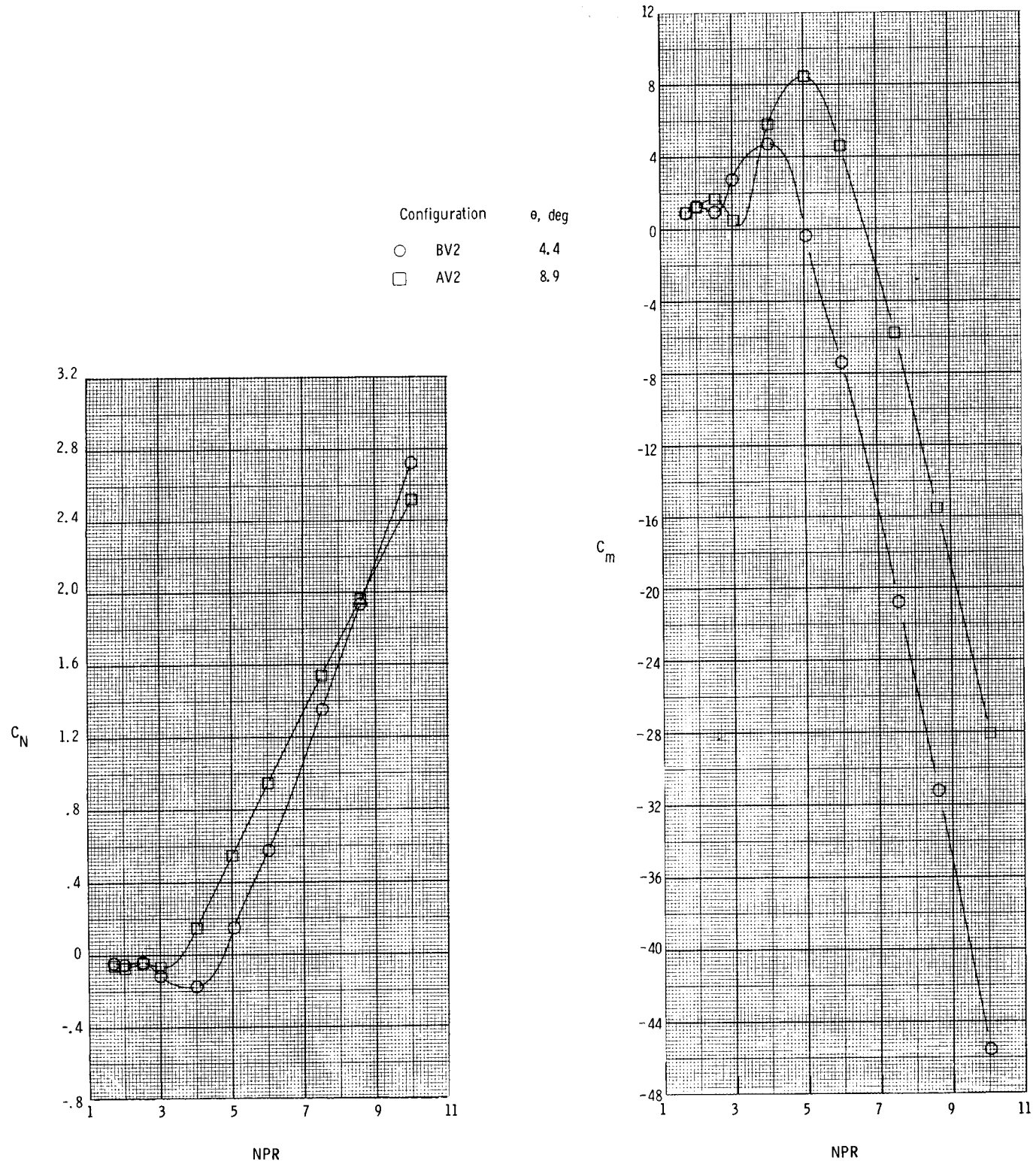

Figure C2. Effect of ramp chordal angle on normal-force and pitching-moment coefficients for $l_f/h_{t,n} = 5.14$, $\rho - \theta = 5.0°$, and $\beta = 18.0°$.

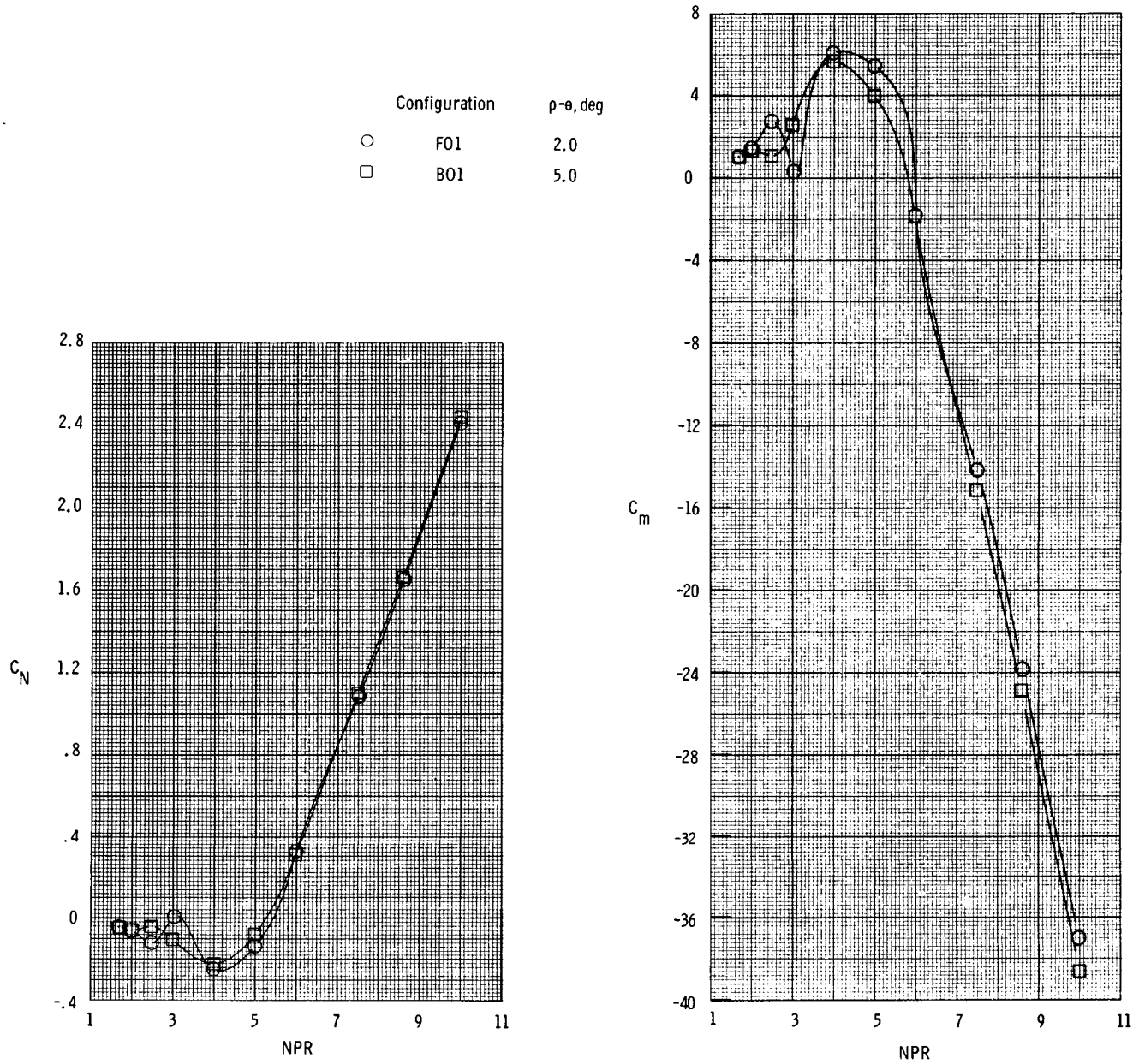

Figure C3. Effect of initial ramp angle on normal-force and pitching-moment coefficients for $\theta = 4.4°$, $l_f/h_{t,n} = 4.74$, and $\beta = 10.5°$.

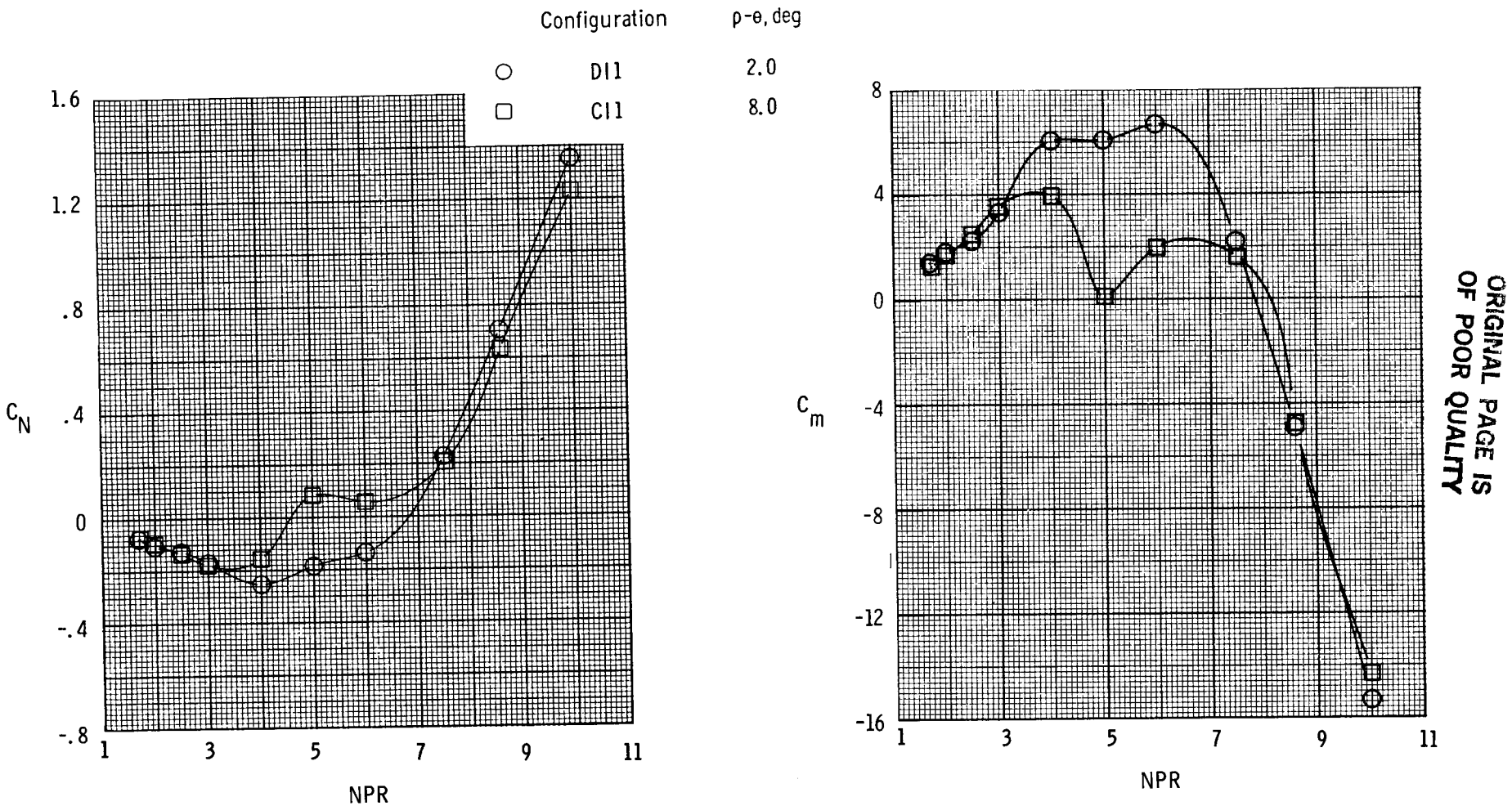

(a) $\beta = 4.0°$.

Figure C4. Effect of initial ramp angle on normal-force and pitching-moment coefficients for $\theta = 8.9°$ and $l_f/h_{t,n} = 4.14$.

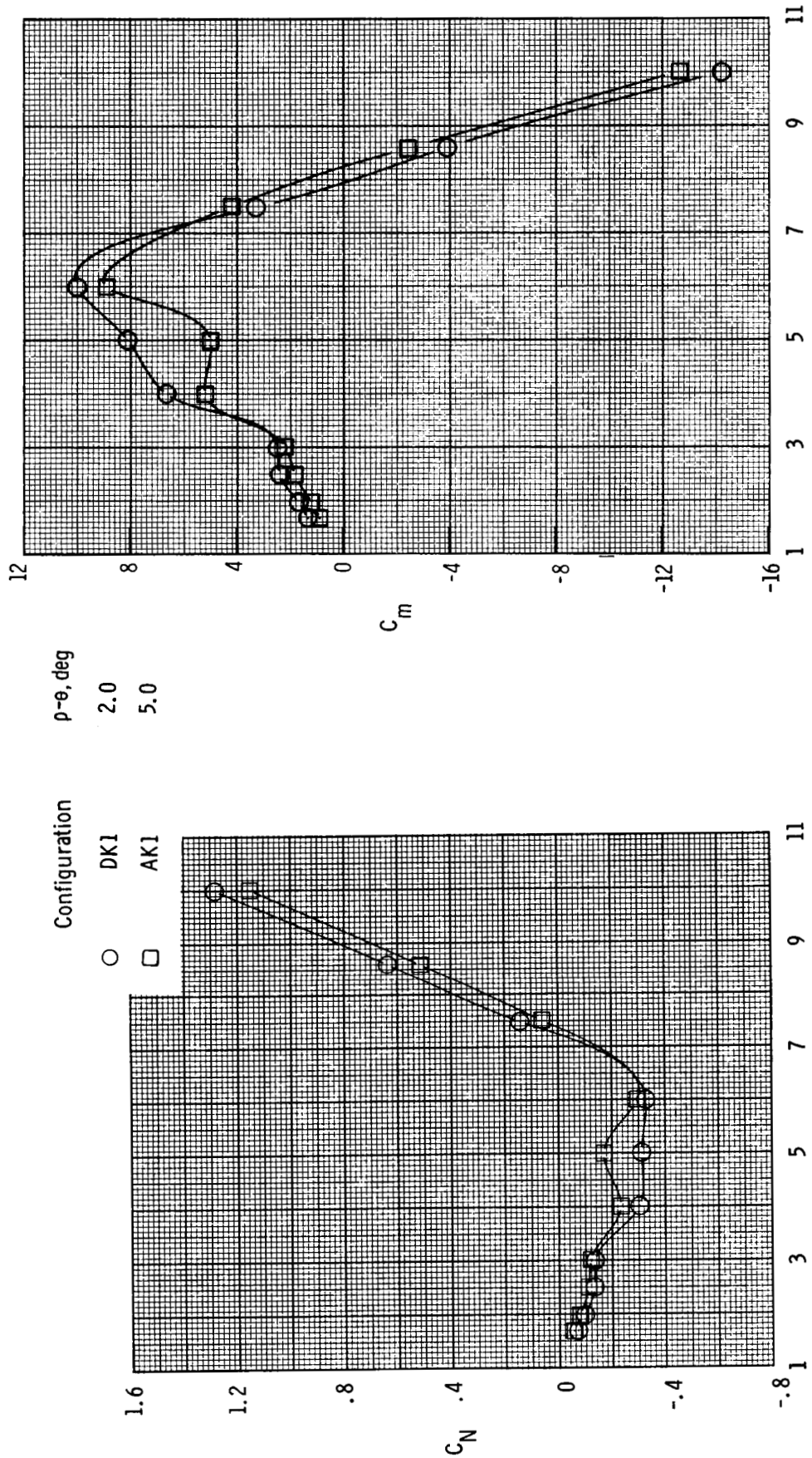

(b) $\beta = 15.0°$.

Figure C4. Continued.

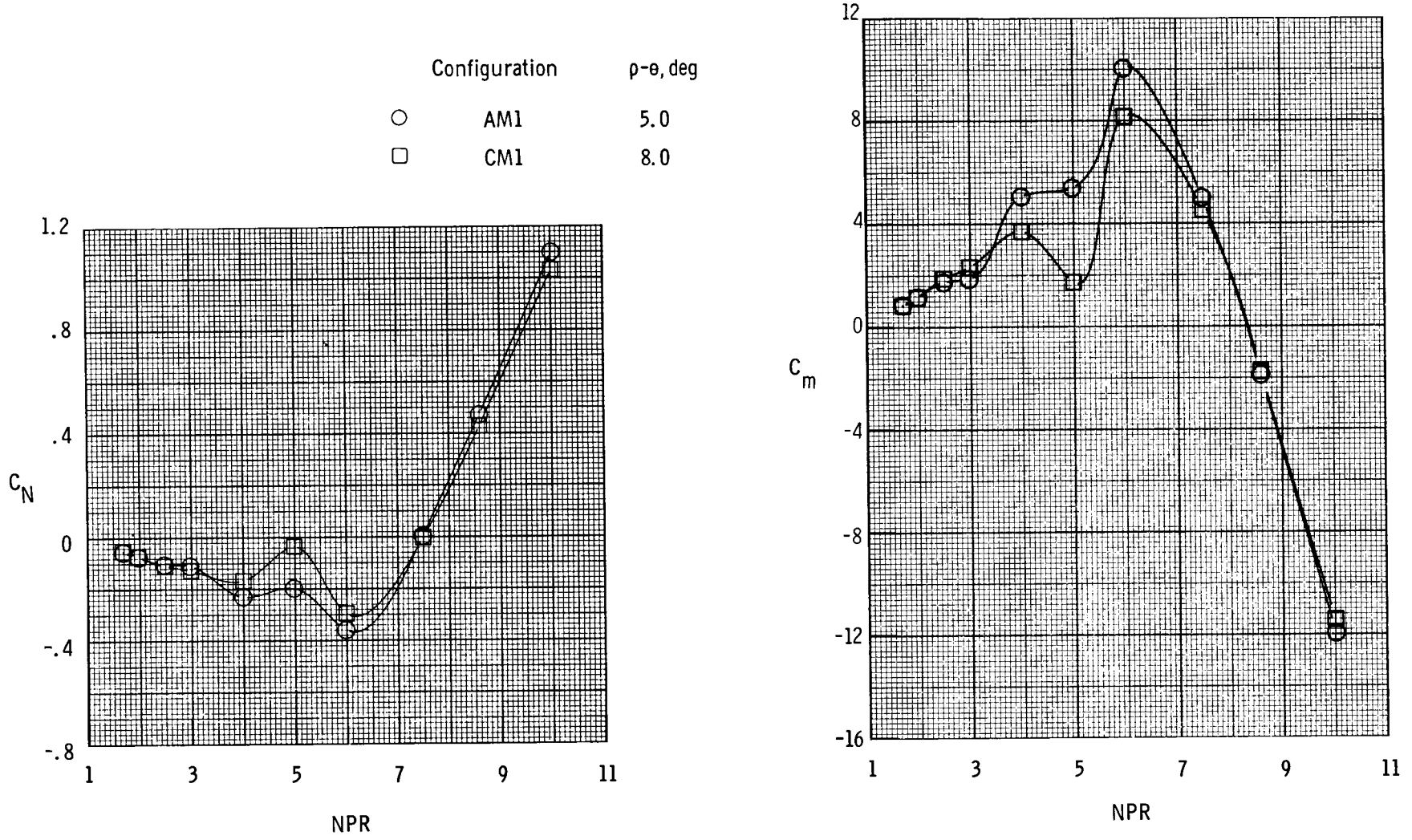

(c) $\beta = 21.0°$.

Figure C4. Concluded.

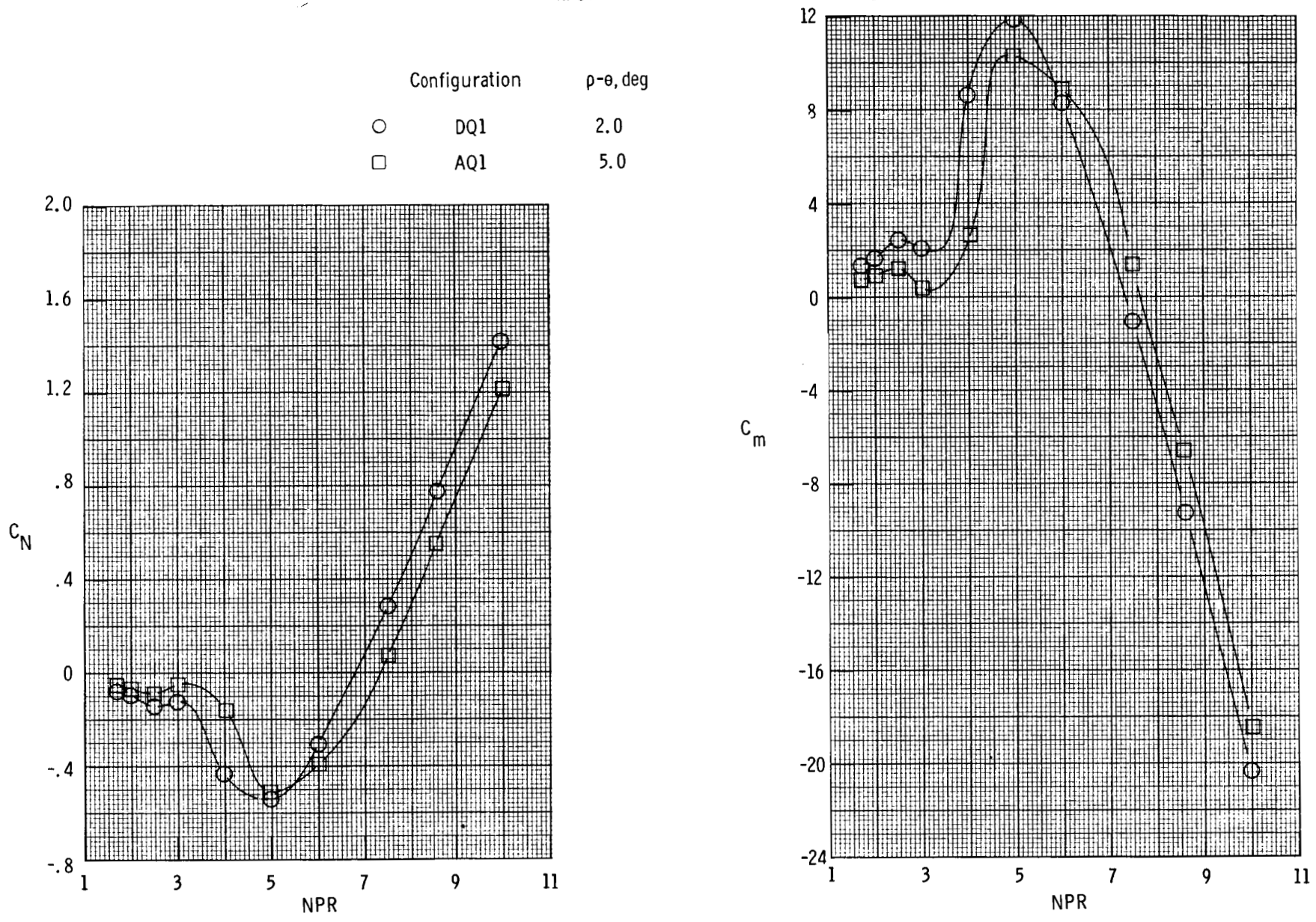

(a) $\beta = 15.0°$.

Figure C5. Effect of initial ramp angle on normal-force and pitching-moment coefficients for $\theta = 8.9°$ and $l_f/h_{t,n} = 4.74$.

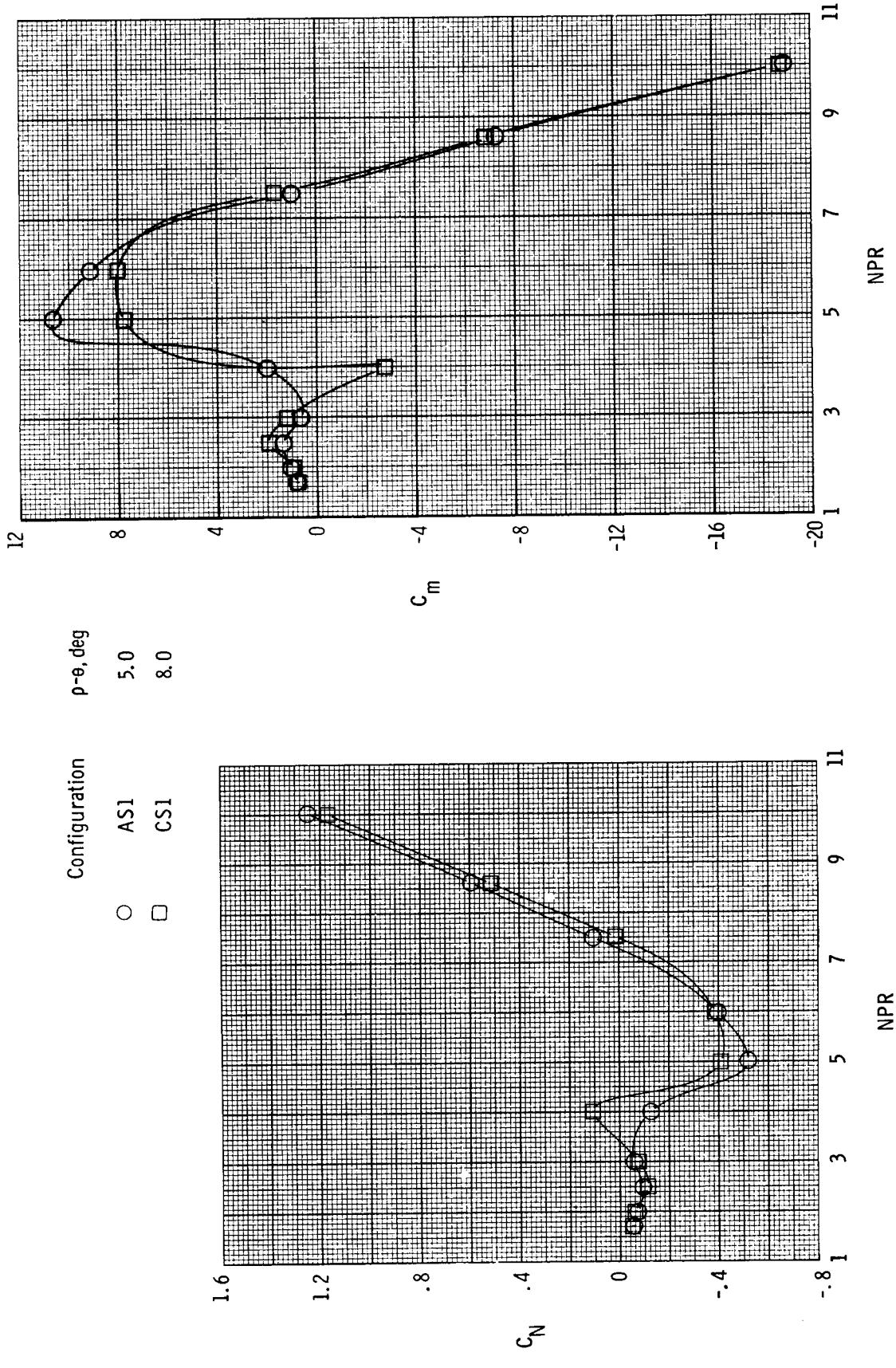

(b) $\beta = 21.0°$.

Figure C5. Concluded.

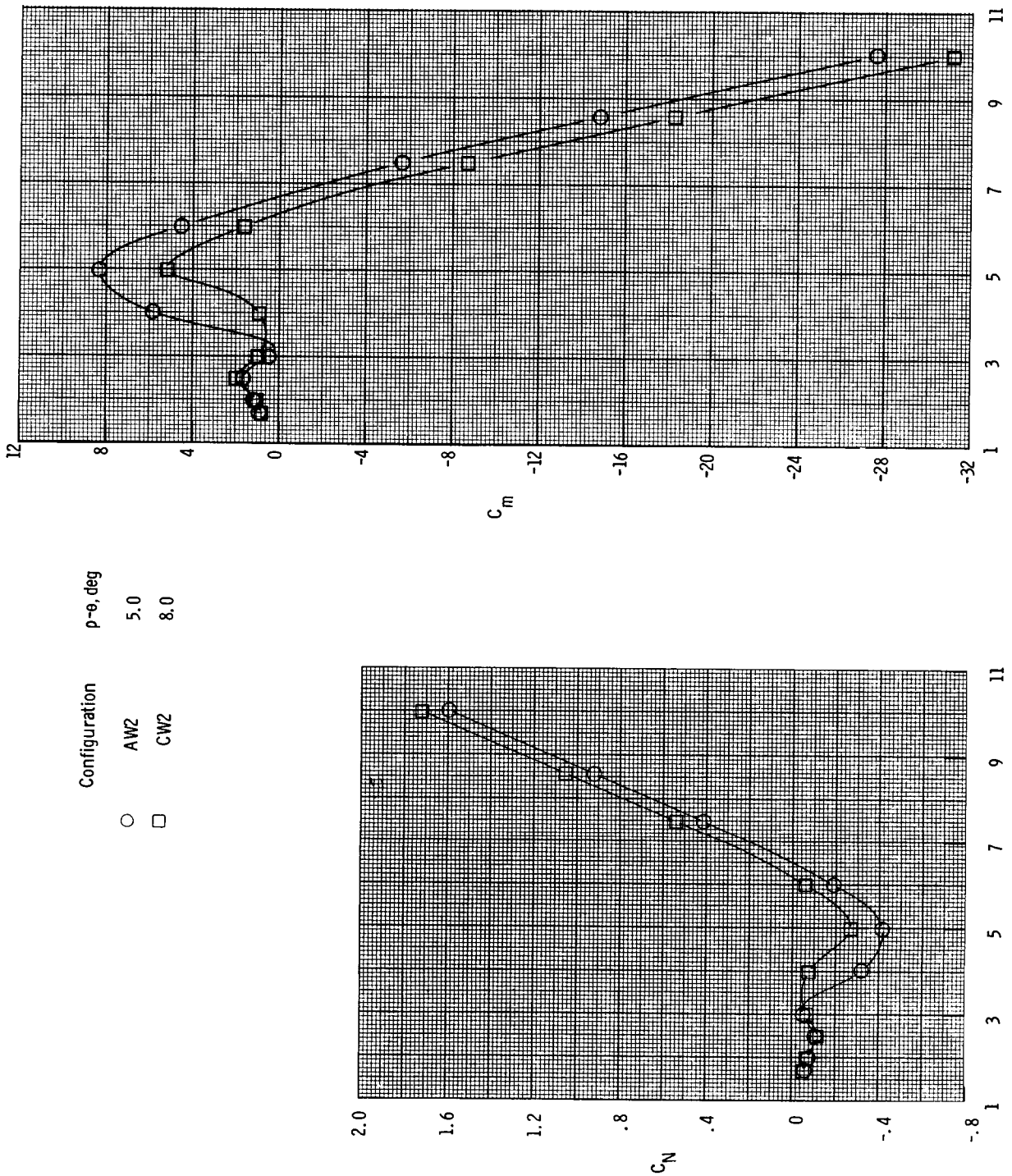

Figure C6. Effect of initial ramp angle on normal-force and pitching-moment coefficients for $\theta = 8.9°$, $l_f/h_{t,n} = 5.14$, and $\beta = 21.0°$.

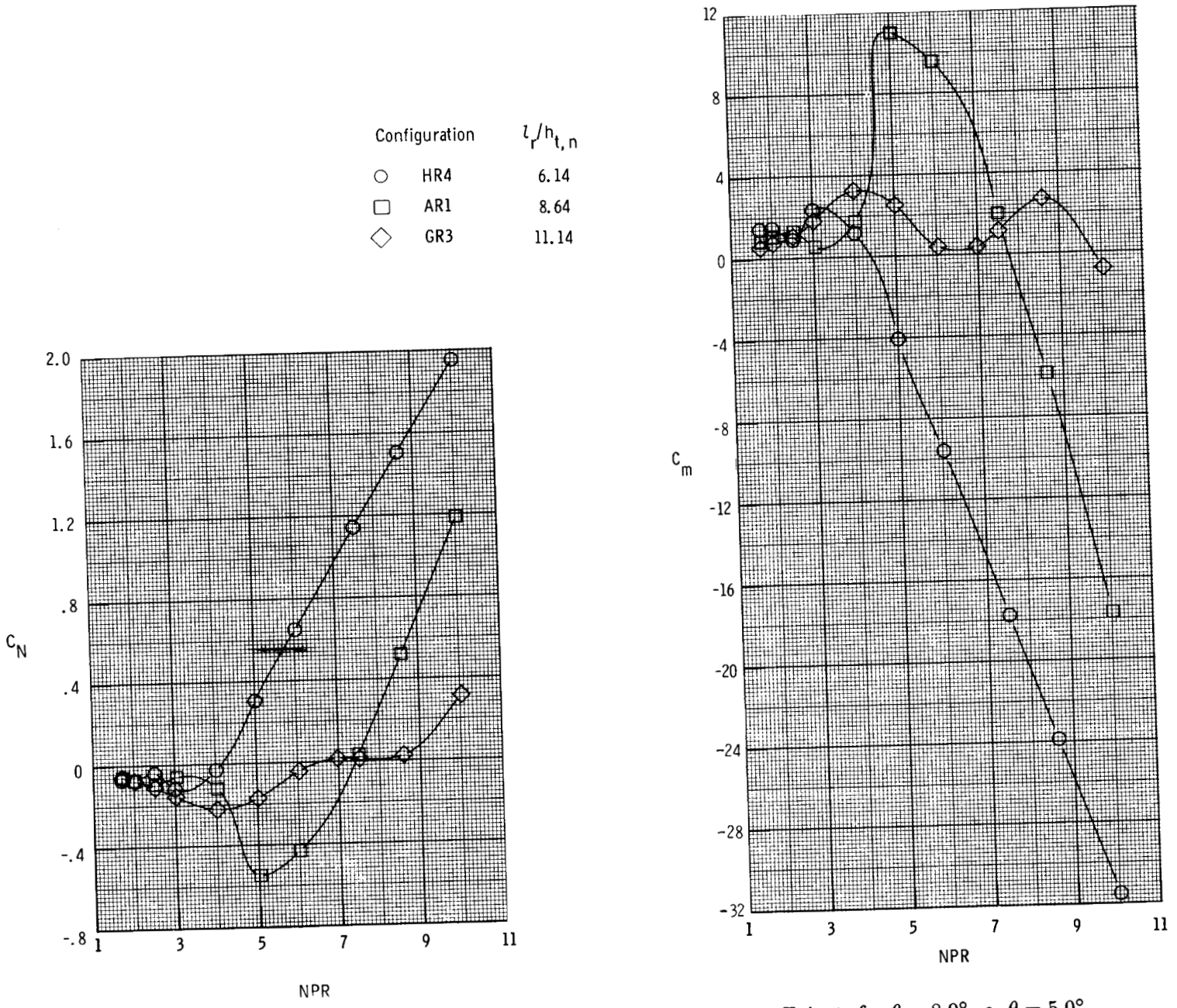

Figure C7. Effect of ramp length on normal-force and pitching-moment coefficients for $\theta = 8.9°$, $\rho - \theta = 5.0°$, $\beta = 18.0°$, and $l_f/h_{t,n} = 4.74$.

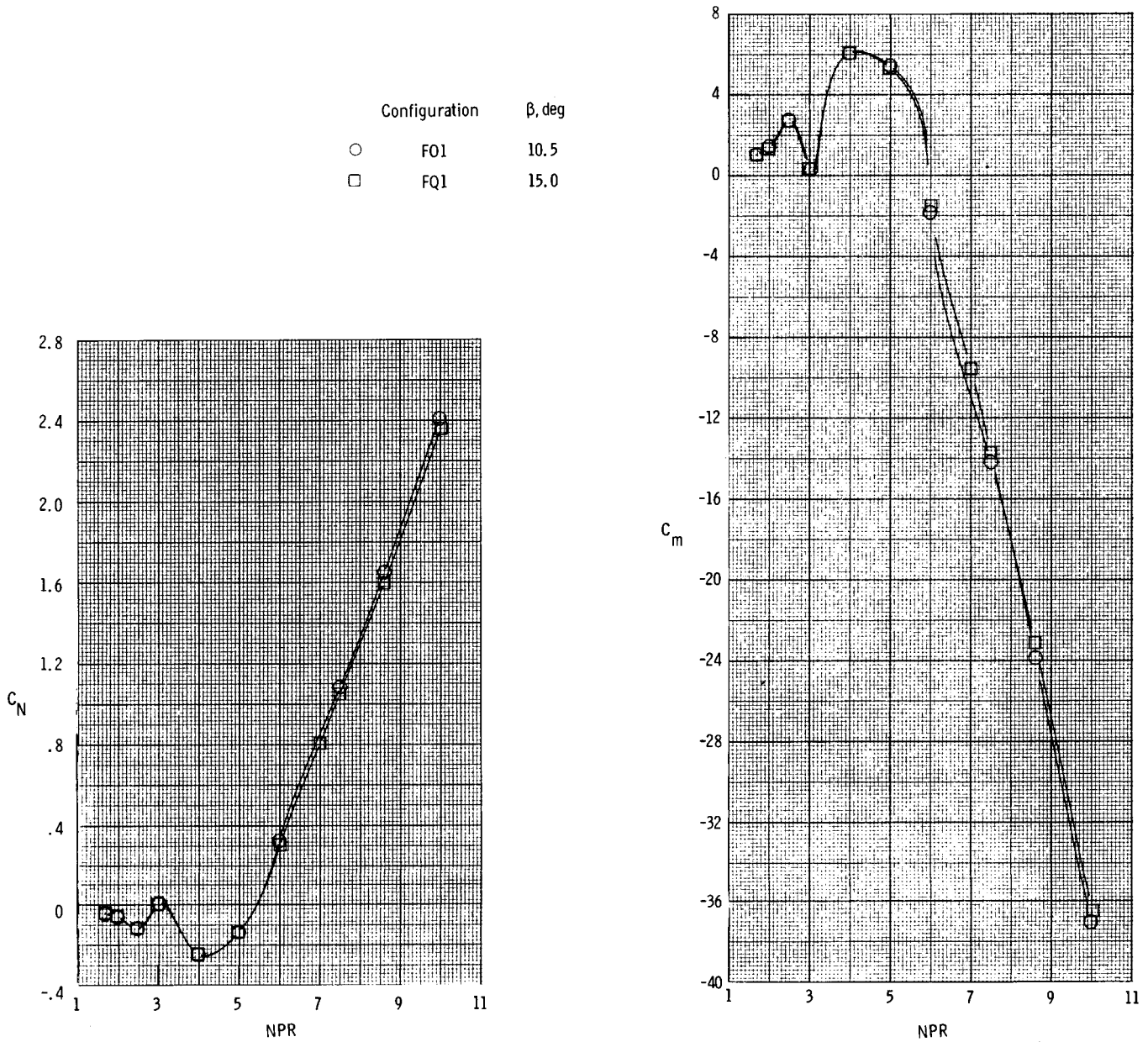

(a) $\rho - \theta = 2.0°$.

Figure C8. Effect of flap angle on normal-force and pitching-moment coefficients for $\theta = 4.4°$ and $l_f/h_{t,n} = 4.74$.

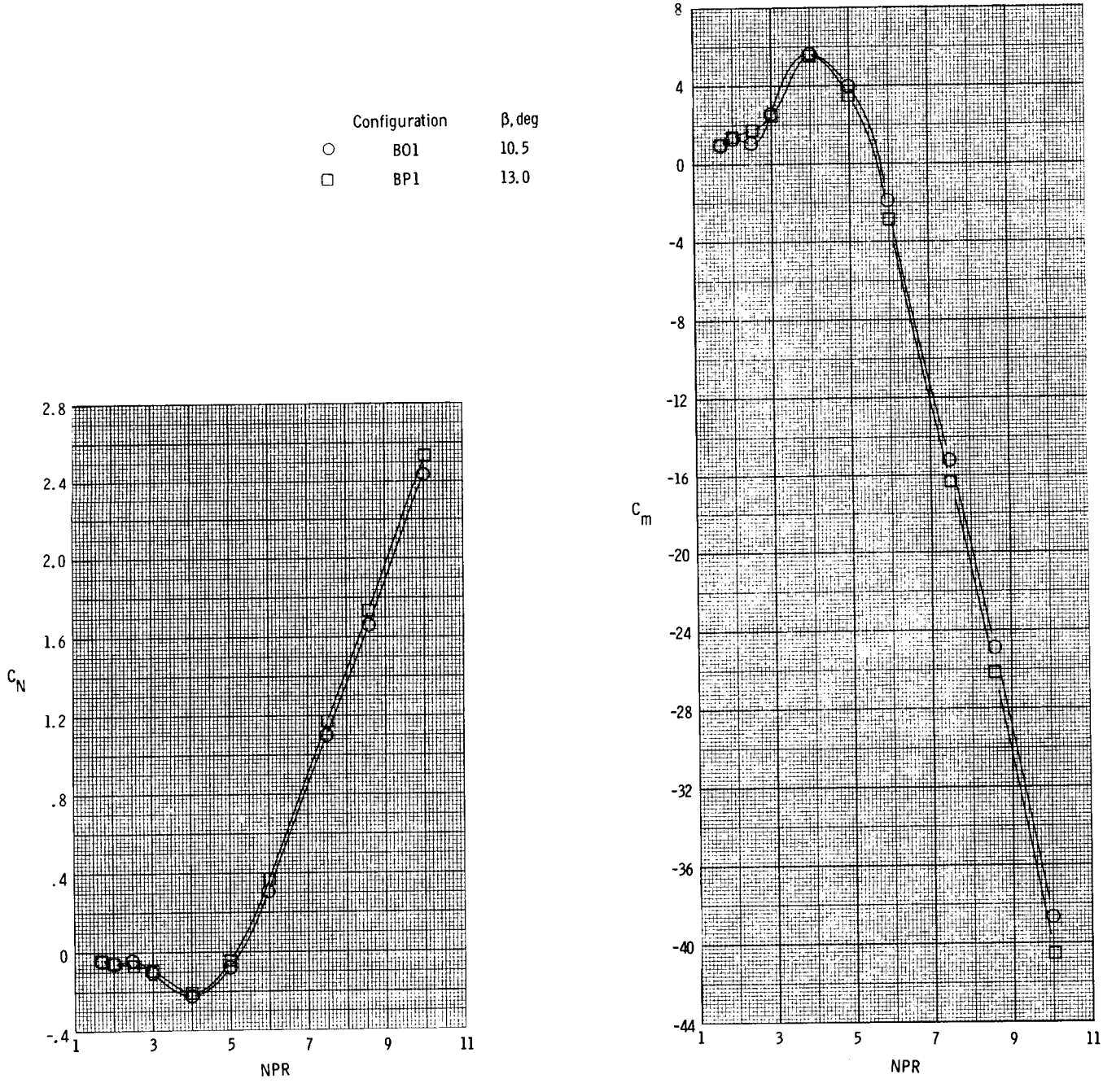

(b) $\rho - \theta = 5.0°$.

Figure C8. Concluded.

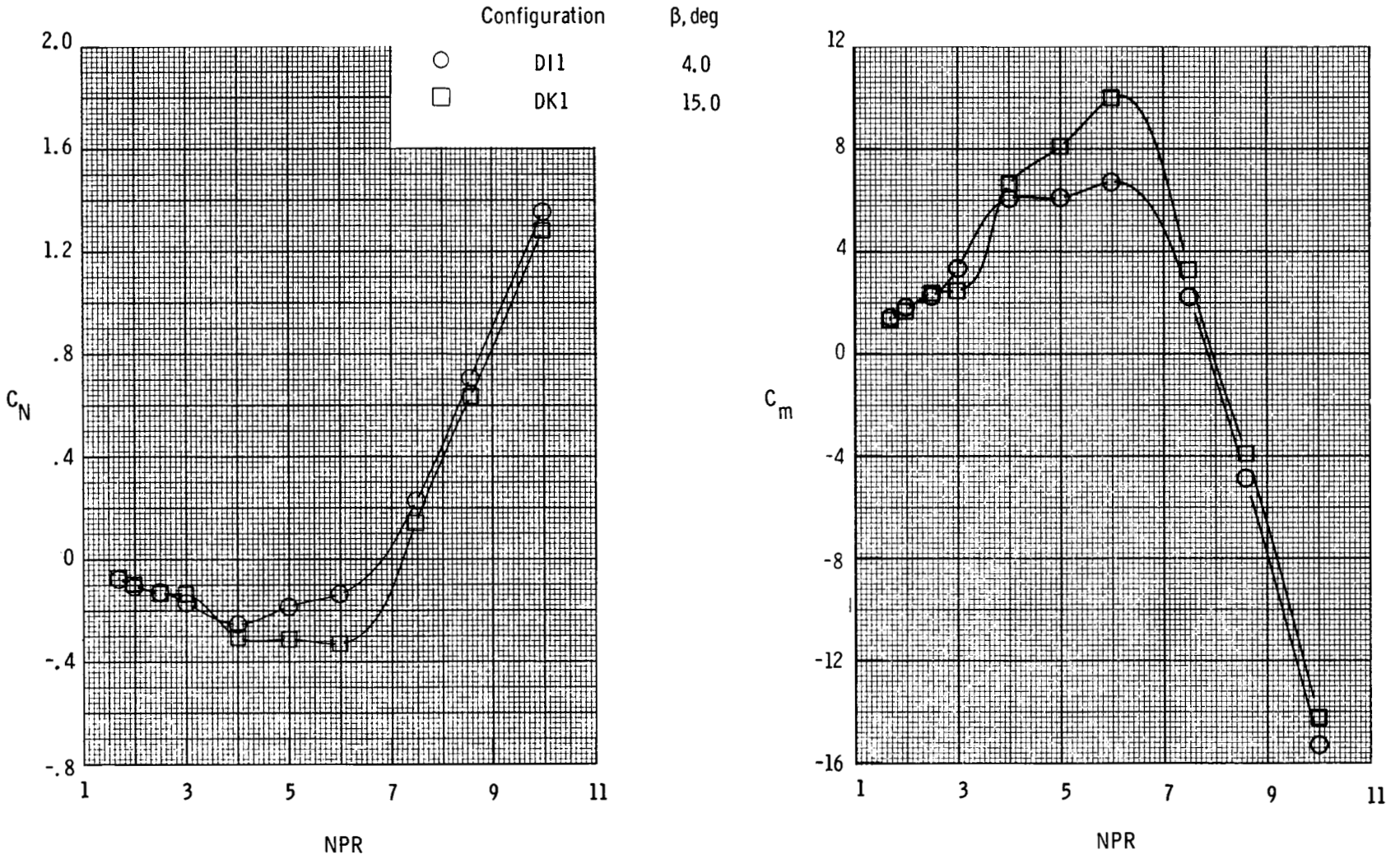

(a) $\rho - \theta = 2.0°$.

Figure C9. Effect of flap angle on normal-force and pitching-moment coefficients for $\theta = 8.9°$ and $l_f/h_{t,n} = 4.14$.

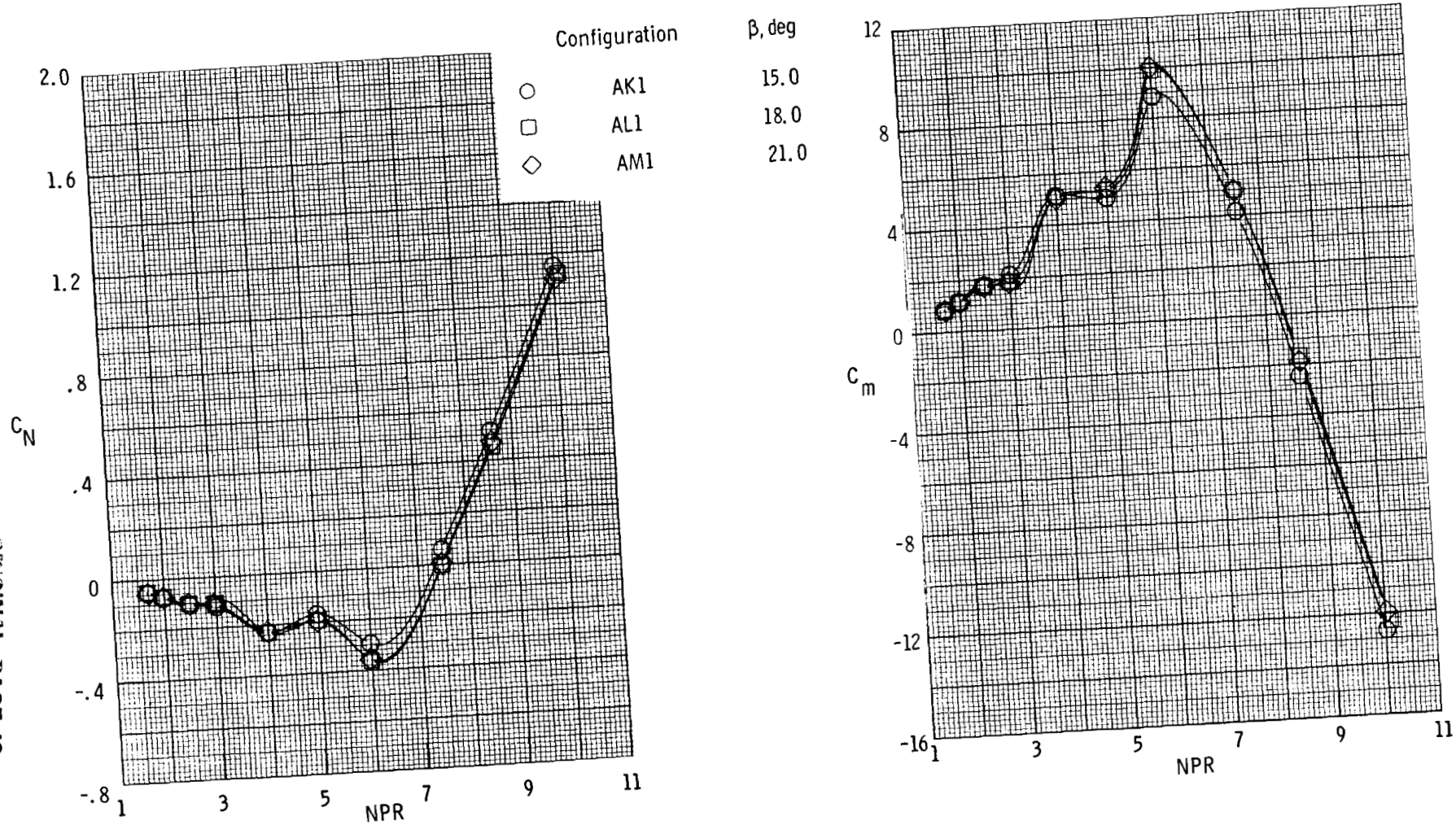

(b) $\rho-\theta = 5.0°$.

Figure C9. Continued.

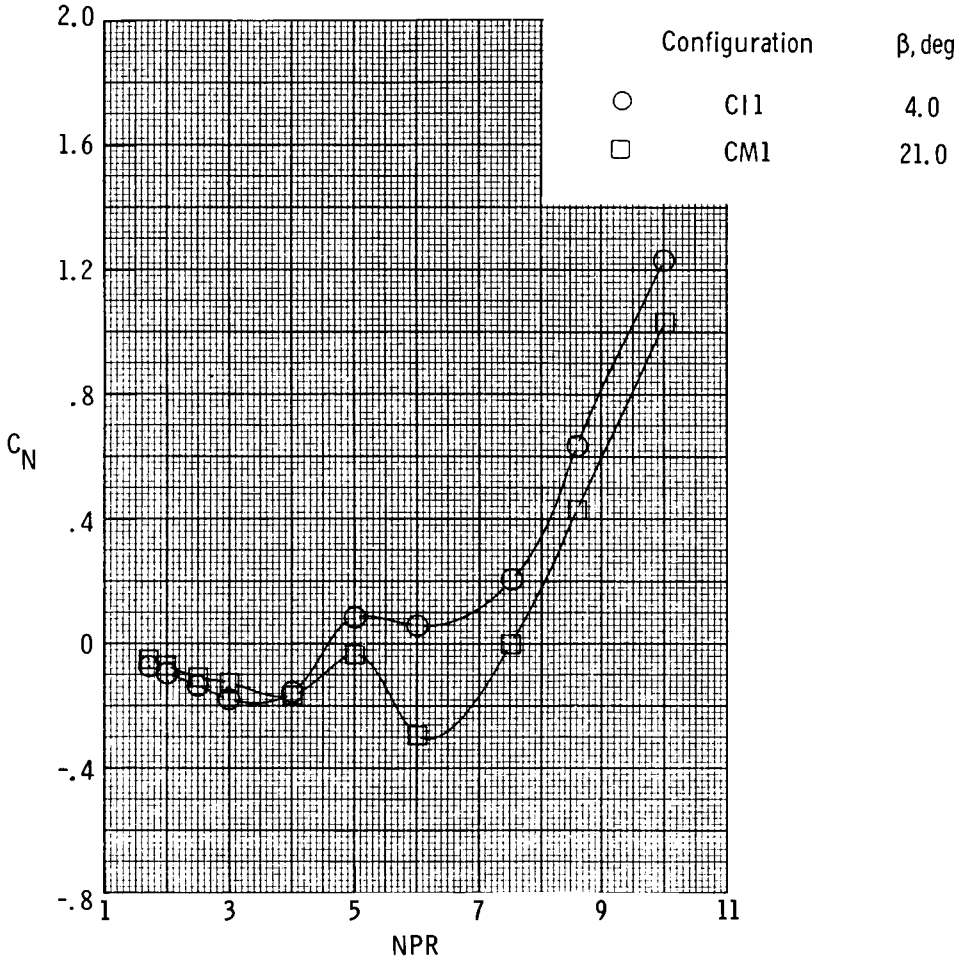

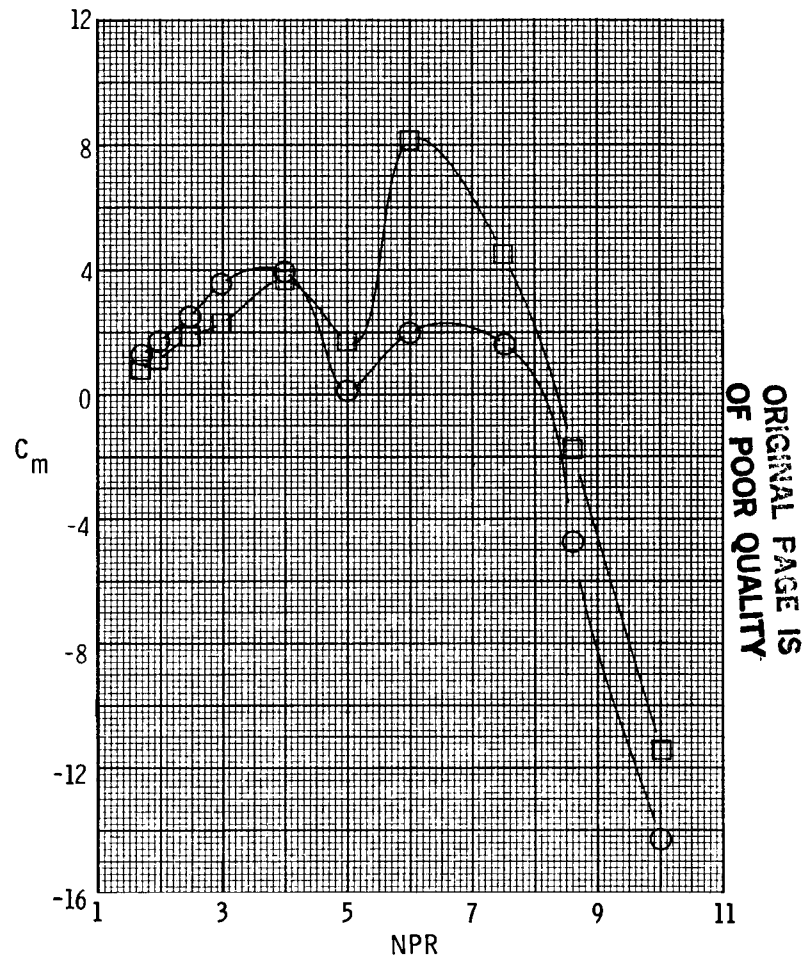

(c) $\rho-\theta = 8.0°$.

Figure C9. Concluded.

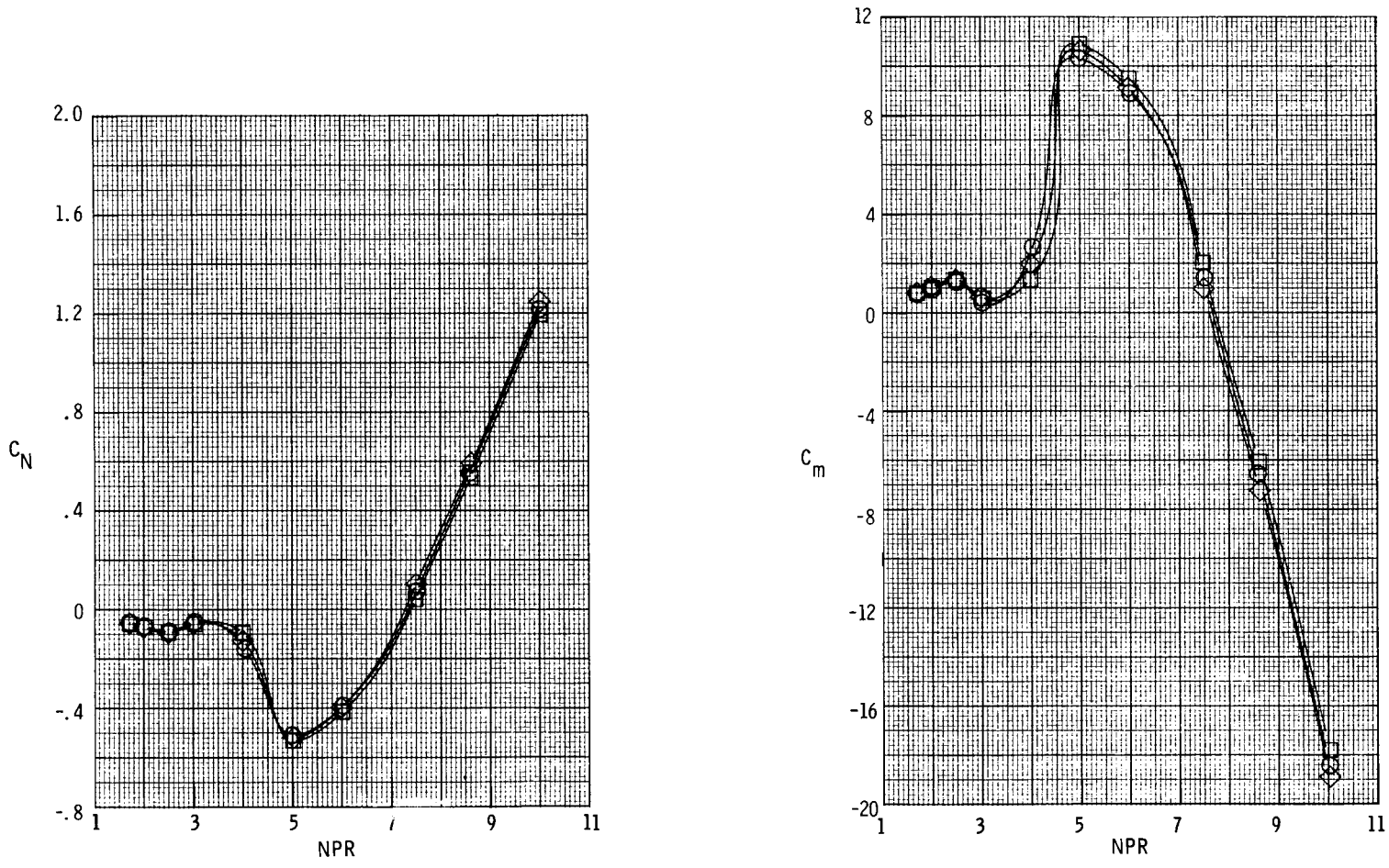

(a) $l_f/h_{t,n} = 4.74$.

Figure C10. Effect of flap angle on normal-force and pitching-moment coefficients for $\theta = 8.9°$ and $\rho - \theta = 5.0°$.

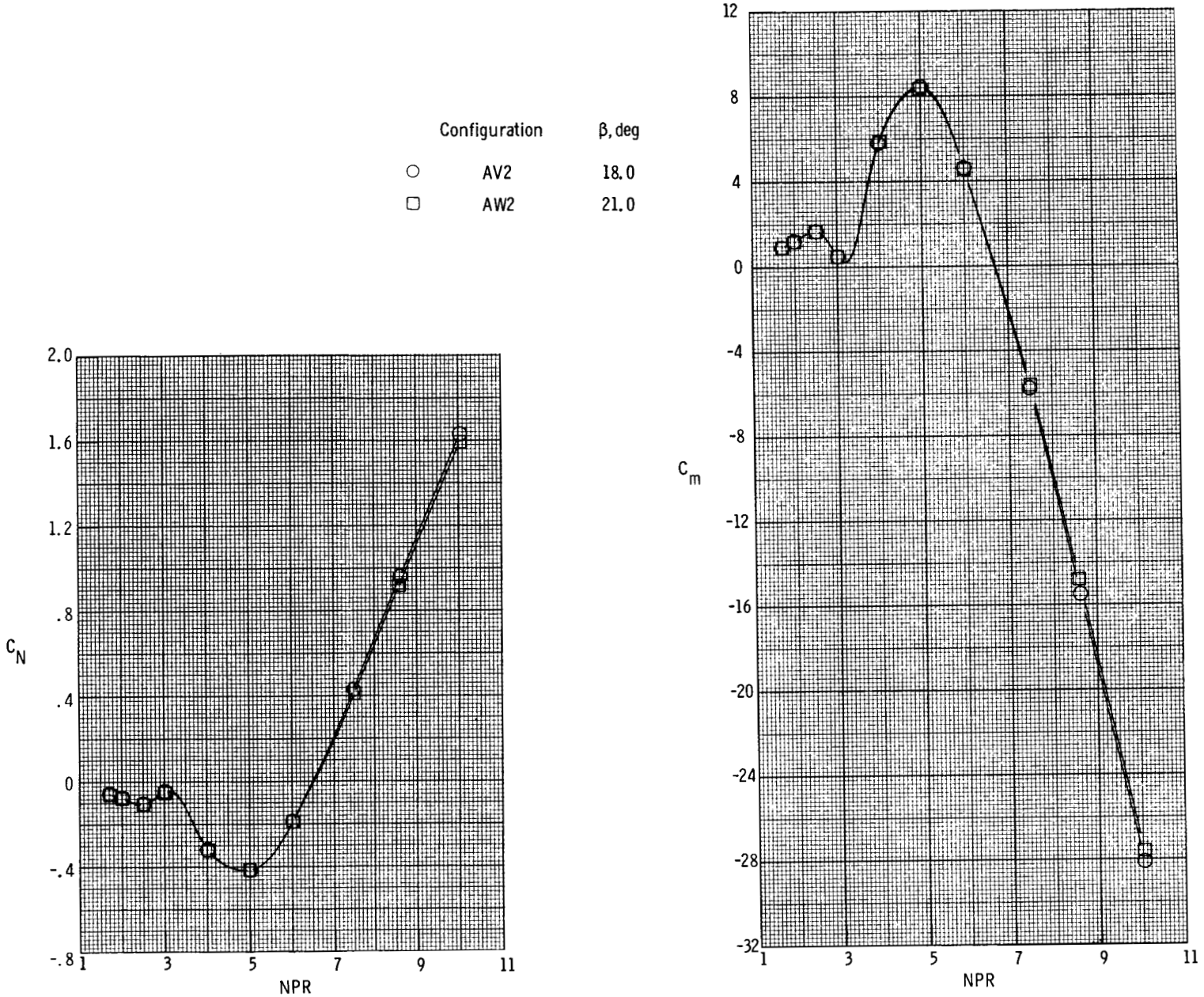

(b) $l_f/h_{t,n} = 5.14$.

Figure C10. Concluded.

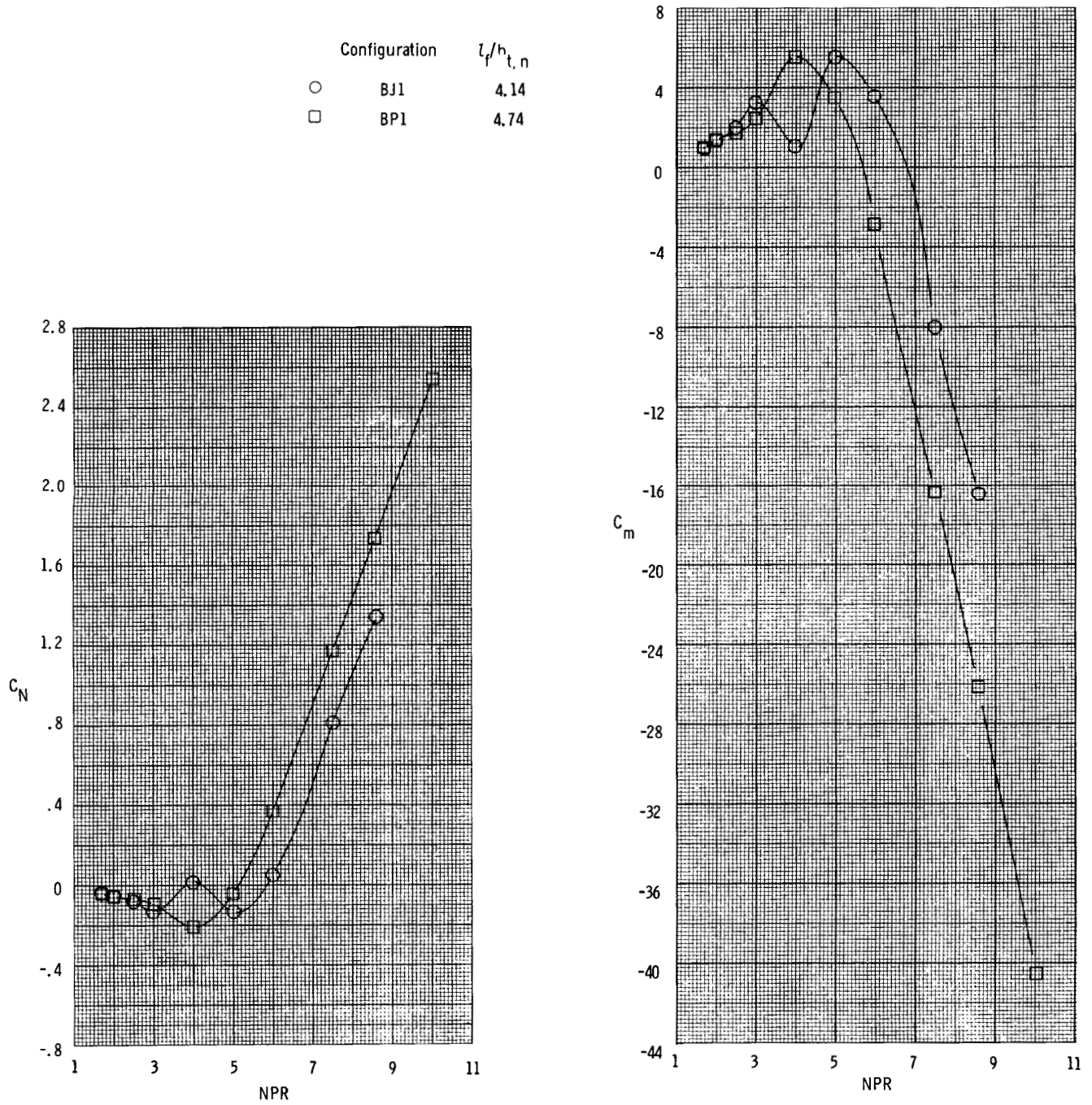

Figure C11. Effect of flap length on normal-force and pitching-moment coefficients for $\theta = 4.4°$, $\rho-\theta = 5.0°$, and $\beta = 13.5°$.

C-2

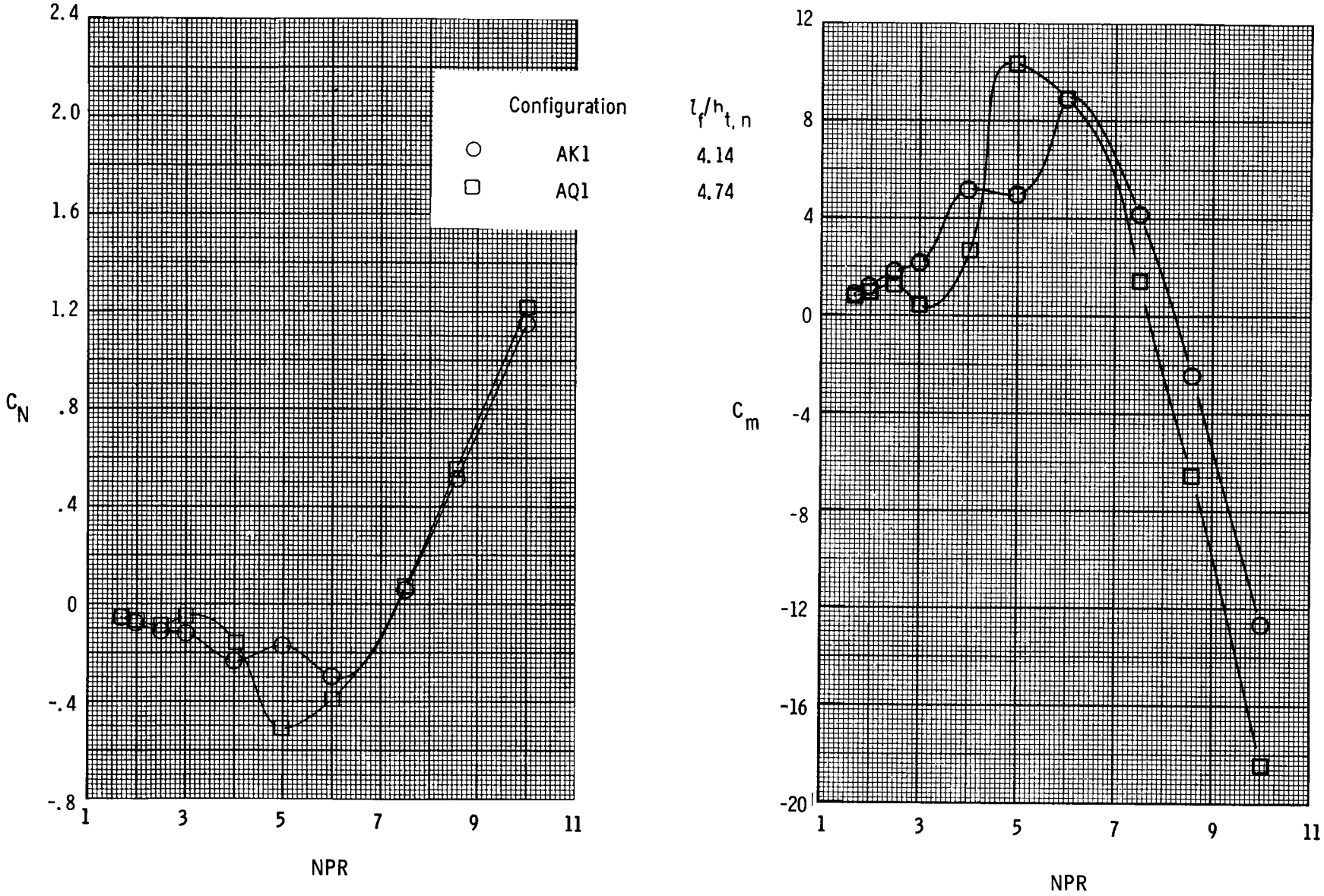

(a) $\beta = 15.0°$.

Figure C12. Effect of flap length on normal-force and pitching-moment coefficients for $\theta = 8.9°$ and $\rho - \theta = 5.0°$.

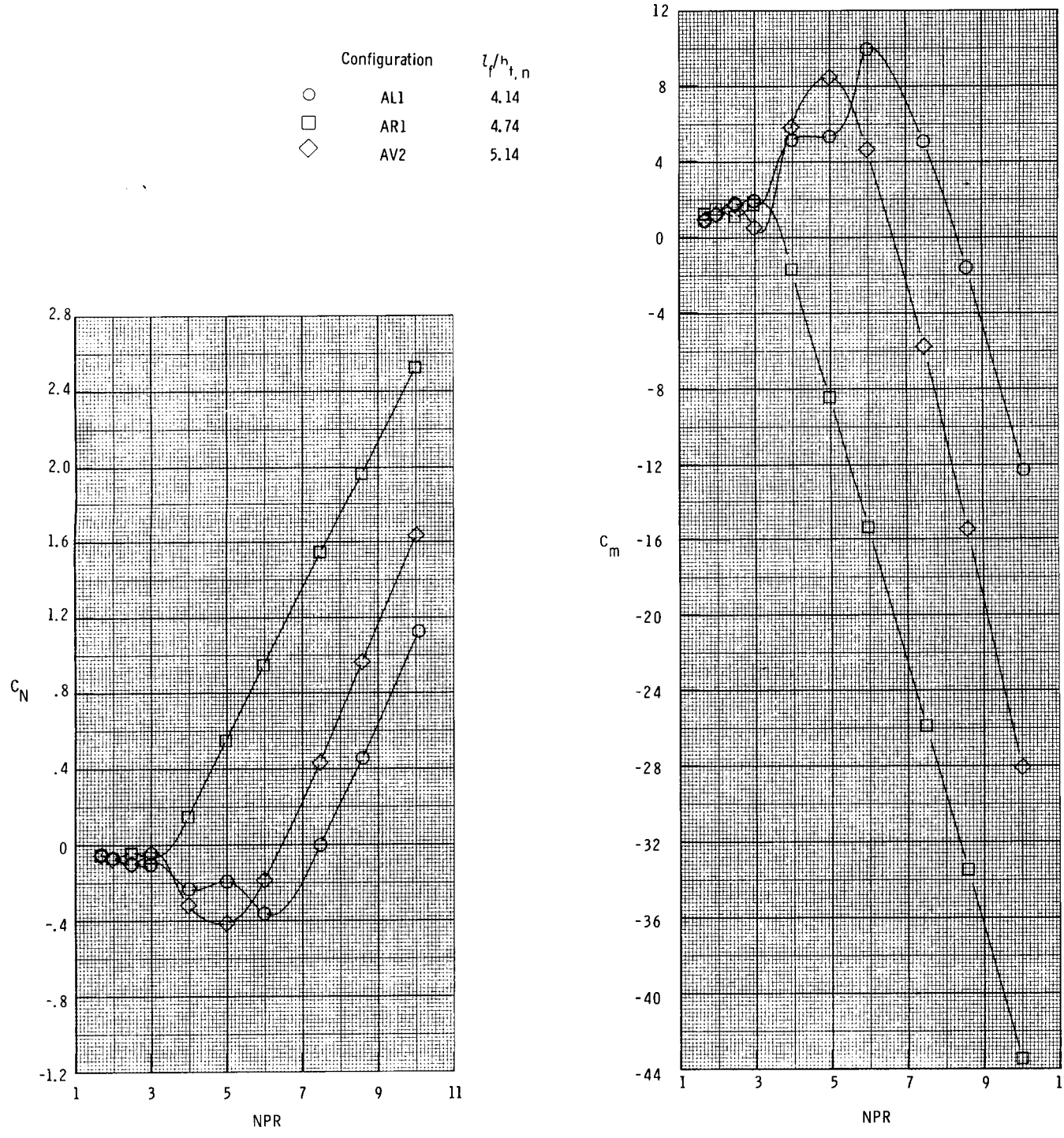

(b) $\beta = 18.0°$.

Figure C12. Continued.

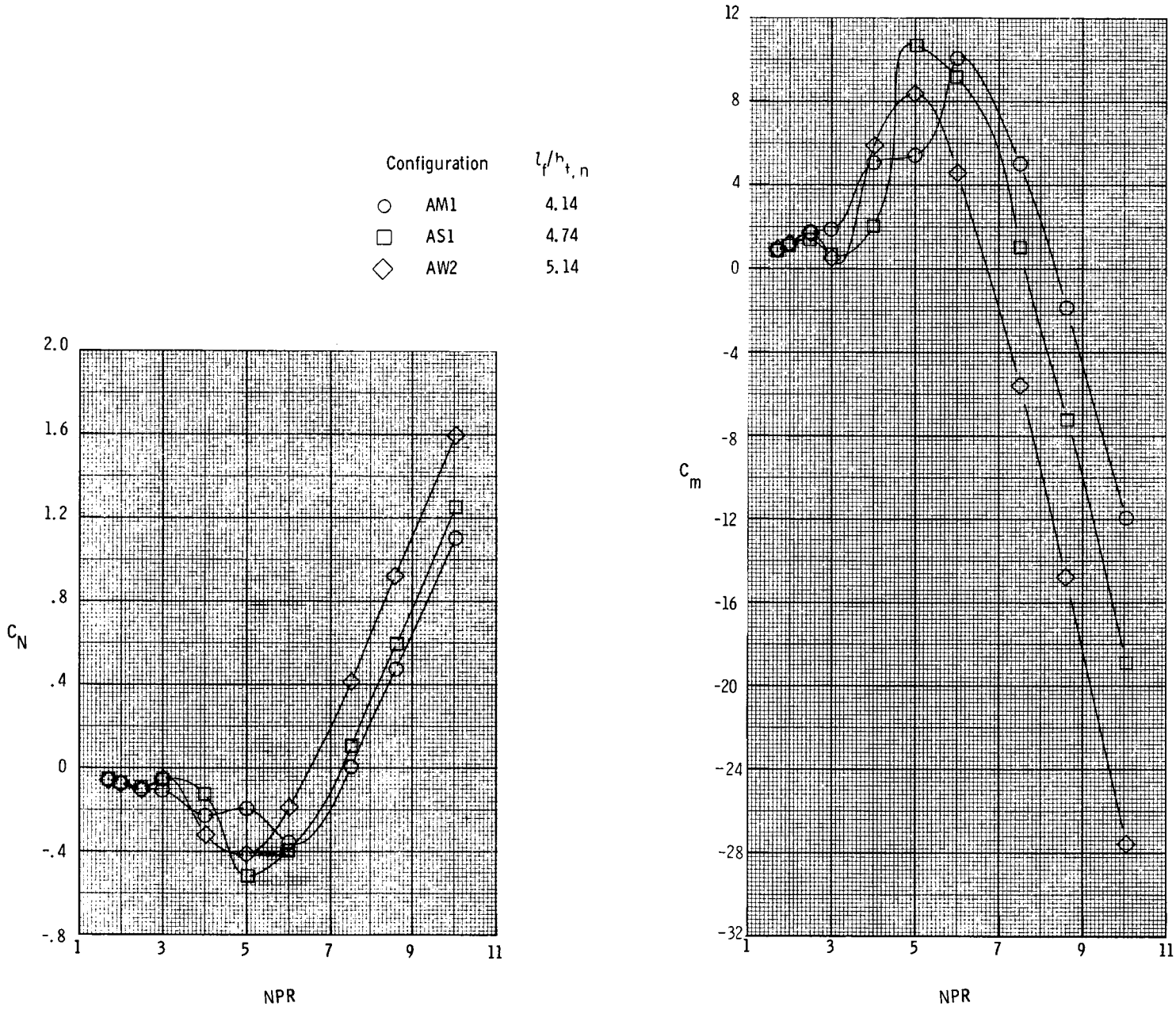

(c) $\beta = 21.0°$.

Figure C12. Concluded.

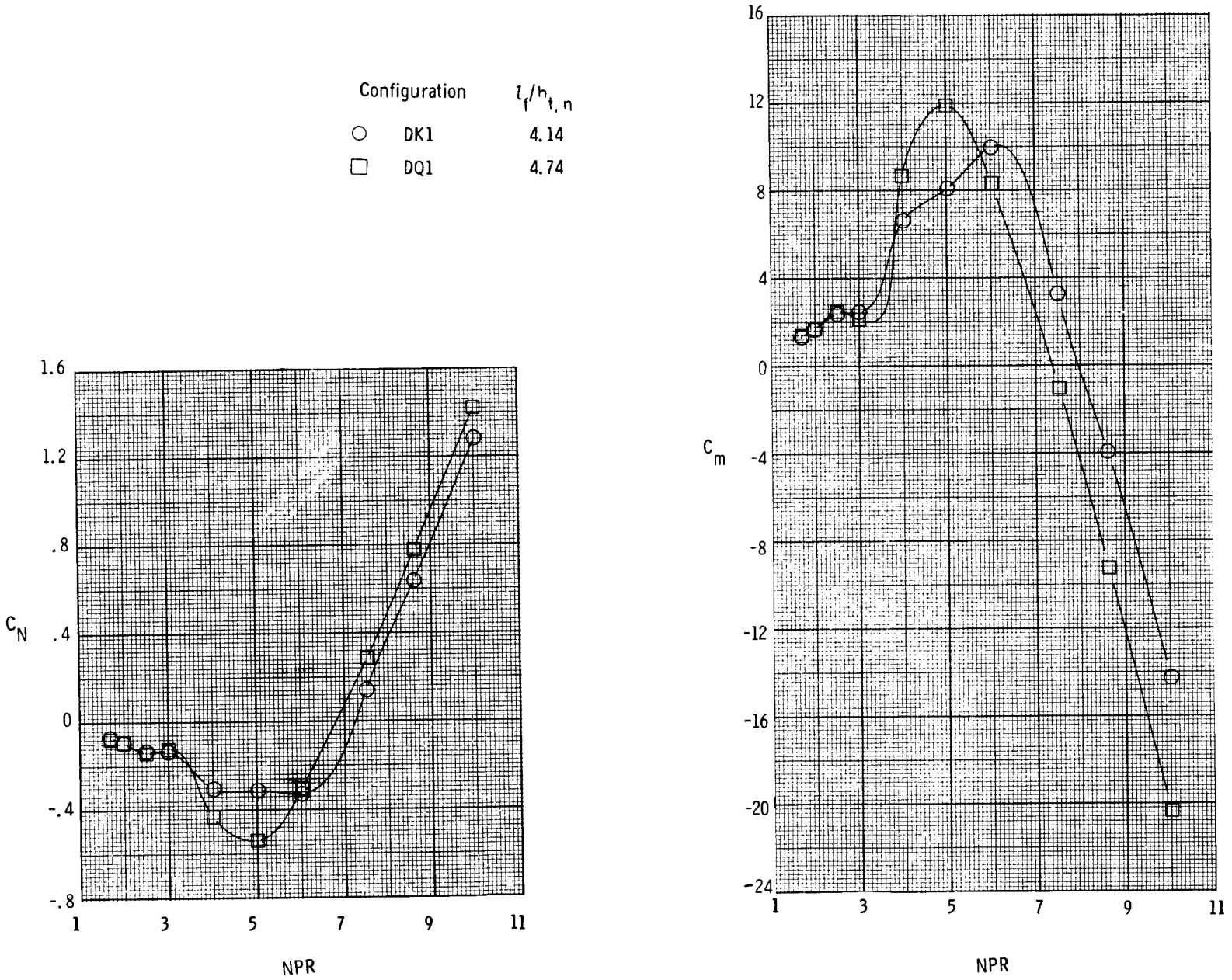

Figure C13. Effect of flap length on normal-force and pitching-moment coefficients for $\theta = 8.9°$, $\rho - \theta = 2.0°$,

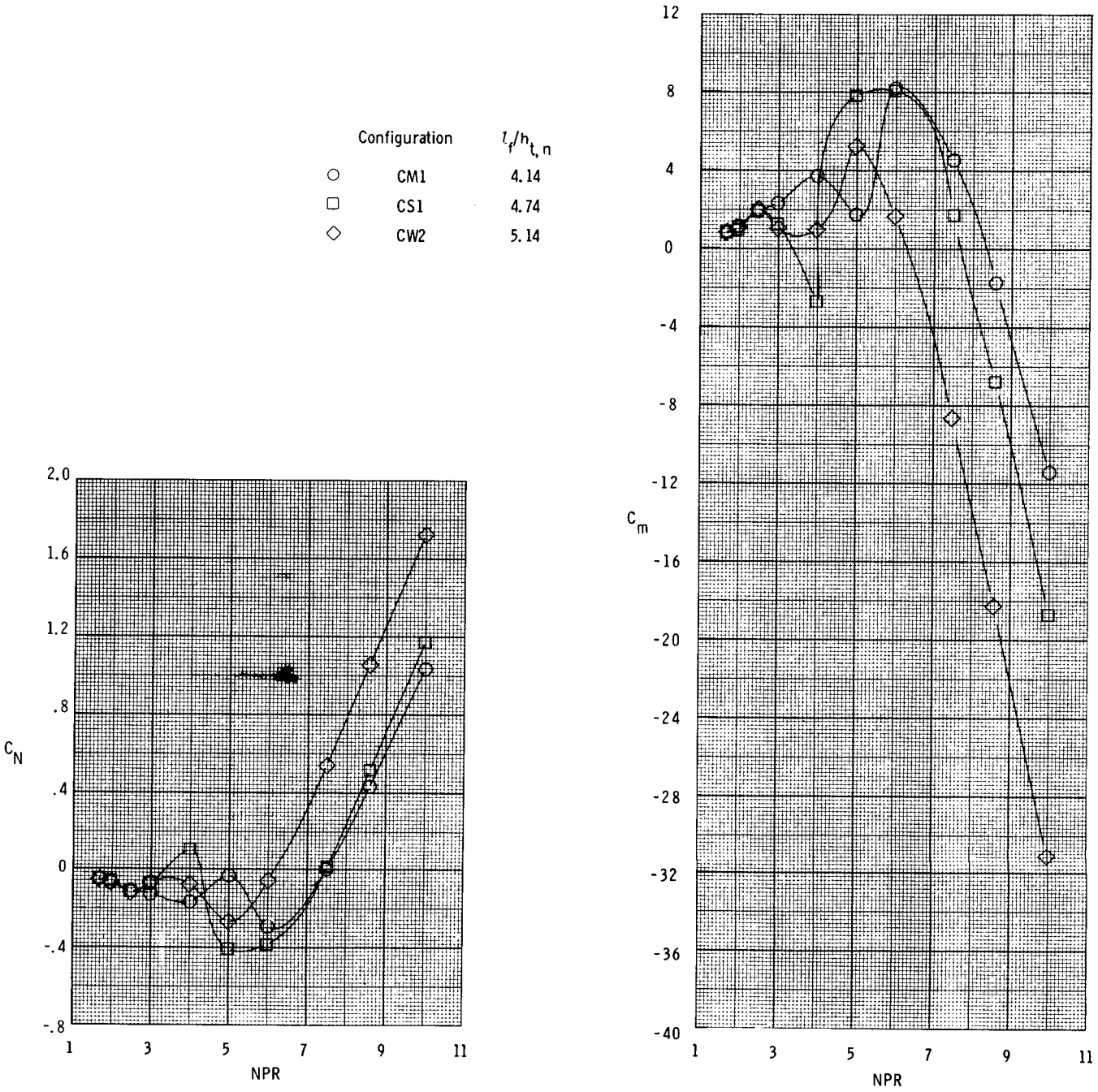

Figure C14. Effect of flap length on normal-force and pitching-moment coefficients for $\theta = 8.9°$, $\rho - \theta = 8.0°$, and $\beta = 21.0°$.

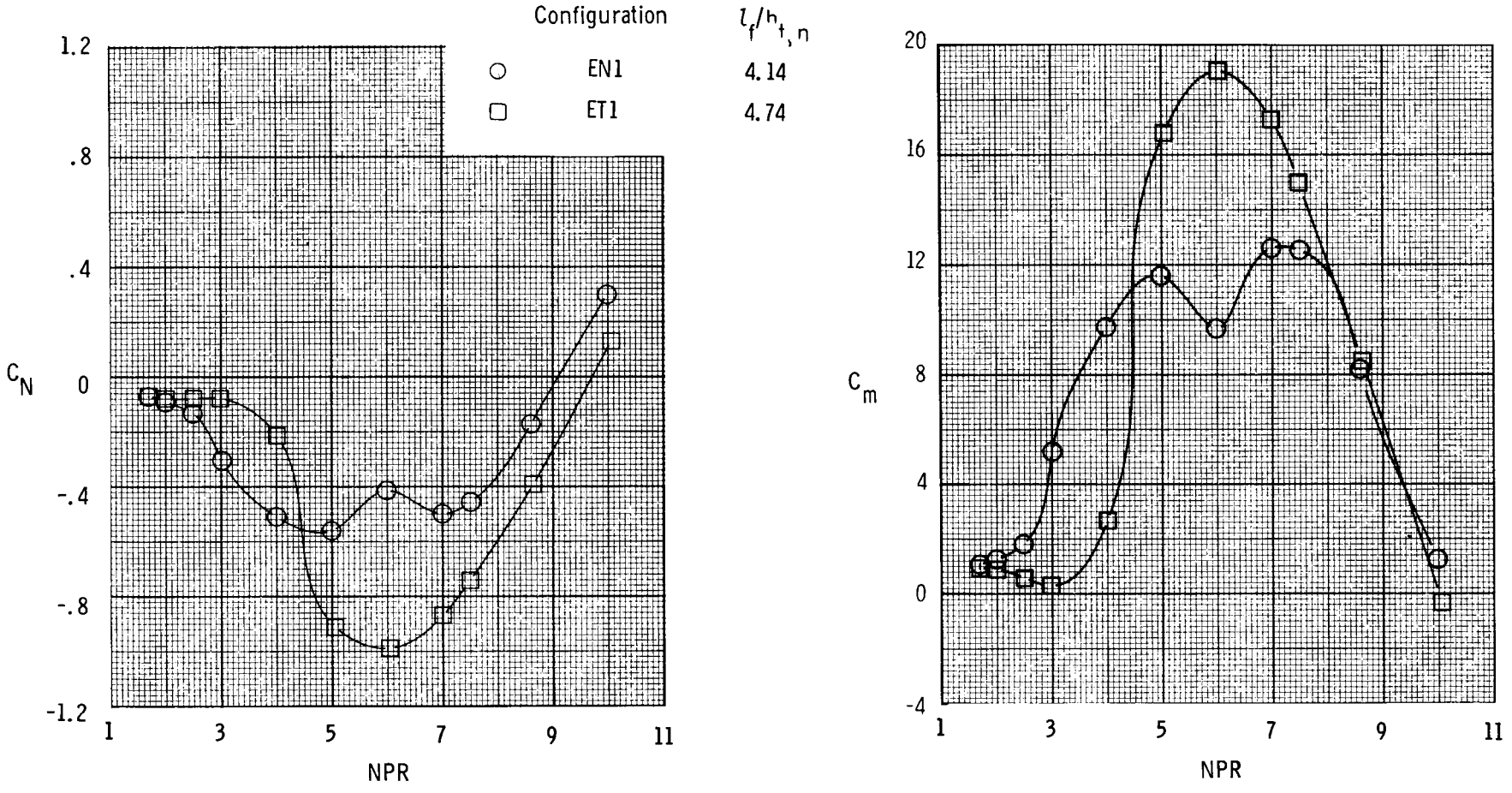

Figure C15. Effect of flap length on normal-force and pitching-moment coefficients for $\theta = 13.4°$, $\rho - \theta = 5.0°$, and $\beta = 22.5°$.

NASA
National Aeronautics and Space Administration

Report Documentation Page

1. Report No.	2. Government Accession No.	3. Recipient's Catalog No.
NASA TM-4112		

4. Title and Subtitle	5. Report Date
Static Internal Performance of Convergent Single-Expansion-Ramp Nozzles With Various Combinations of Internal Geometric Parameters	May 1989
	6. Performing Organization Code
7. Author(s)	8. Performing Organization Report No.
E. Ann Bare and Francis J. Capone	L-16535
9. Performing Organization Name and Address	10. Work Unit No.
NASA Langley Research Center Hampton, VA 23665-5225	505-68-91-06
	11. Contract or Grant No.
12. Sponsoring Agency Name and Address	13. Type of Report and Period Covered
National Aeronautics and Space Administration Washington, DC 20546-0001	Technical Memorandum
	14. Sponsoring Agency Code

15. Supplementary Notes

16. Abstract

An investigation has been conducted in the static test facility of the Langley 16-Foot Transonic Tunnel to determine the effects of five geometric design parameters on the internal performance of convergent single-expansion-ramp nozzles. The effects of ramp chordal angle, initial ramp angle, flap angle, flap length, and ramp length were determined. All nozzles tested had a nominally constant throat area and aspect ratio. Static pressure distributions along the centerlines of the ramp and flap were also obtained for each configuration. Nozzle pressure ratio was varied up to 10.0 for all configurations.

17. Key Words (Suggested by Authors(s))	18. Distribution Statement
Nonaxisymmetric nozzles Static internal performance Convergent single-expansion-ramp nozzles	Unclassified—Unlimited Subject Category 02

19. Security Classif. (of this report)	20. Security Classif. (of this page)	21. No. of Pages	22. Price
Unclassified	Unclassified	103	A06

For sale by the National Technical Information Service, Springfield, Virginia 22161-2171